Earth-Science Reviews 136 (2014) 59–95

Contents lists available at ScienceDirect

Earth-Science Reviews

journal homepage: www.elsevier.com/locate/earscirev

Tectono-stratigraphic framework of Neoproterozoic to Cambrian strata, west-central U.S.: Protracted rifting, glaciation, and evolution of the North American Cordilleran margin

W.A. Yonkee [a,*], C.D. Dehler [b], P.K. Link [c], E.A. Balgord [c,1], J.A. Keeley [c], D.S. Hayes [b], M.L. Wells [d], C.M. Fanning [e], S.M. Johnston [f]

[a] Department of Geosciences, Weber State University, Ogden, UT 84408, USA
[b] Department of Geology, Utah State University, Logan, UT 84332, USA
[c] Department of Geosciences, Idaho State University, Pocatello, ID 83209, USA
[d] Department of Geoscience, University of Nevada Las Vegas, Las Vegas, NV 89154, USA
[e] Research School of Earth Sciences, Australian National University, Canberra, ACT 0200, Australia
[f] Physics Department, Cal Poly at San Luis Obispo, San Luis Obispo, CA 94307, USA

ARTICLE INFO

Article history:
Received 17 October 2013
Accepted 8 May 2014
Available online 15 May 2014

Keywords:
Neoproterozoic stratigraphy
Rifting
Rodinia
Snowball Earth
Detrital zircon

ABSTRACT

Stratigraphic, geochronologic, and geochemical patterns of Neoproterozoic to Cambrian sedimentary and volcanic rocks in Utah, Nevada, and SE Idaho record a dynamically evolving landscape along the North American Cordillera margin, which included: (1) initial development of intracratonic basins with deposition of siliciclastic strata of the Uinta Mountain Group from ~770 to 740 Ma; (2) early rifting and volcanism along a N–S (present day geographic coordinates) basin system with deposition of diamictite-bearing strata of the Perry Canyon and related formations from ~720 to 660 Ma; (3) early, broad subsidence with deposition of mature siliciclastic strata of the lower Brigham and McCoy Creek groups from ~660 to 580 Ma; (4) final rifting, volcanism, and transition to drift with deposition of variably immature siliciclastic strata of the Prospect Mountain and correlative formations from ~570 to 520 Ma; and (5) regional subsidence along a passive margin with deposition of Middle Cambrian to Devonian carbonate-rich strata. The Uinta Mountain Group comprises fluvial to marine, feldspathic to quartzose sandstone, conglomerate, and mudstone, with detrital zircon (DZ) patterns recording a mix of local basement sources to the N and distal Laurentian sources to the SE. The lower Perry Canyon and related formations contain variably feldspathic sandstone, quartz-pebble diamictite deposited during an older glacial episode, and mudstone, with DZ patterns recording a mix of distal sources, local basement sources, and sediment recycling during early rifting. The upper Perry Canyon and related formations contain mafic volcanic rocks, polymict diamictite deposited during a younger glacial episode, volcaniclastic wacke, and mudstone, with DZ patterns recording local basement sources along an evolving rift margin and felsic volcanism from ~700 to 670 Ma. Mafic volcanic rocks and trachyte to rhyolite clasts in diamictite have geochemical signatures typical of continental rifting. The lower Brigham and McCoy Creek groups contain mostly mature quartz arenite deposited in shallow marine environments, with DZ patterns recording distal Laurentian sources. The base of the Prospect Mountain and correlative formations is marked by an influx of feldspathic, coarse-grained sediment derived from local basement sources and ~570–540 Ma basalt volcanism, which was followed by deposition of subfeldspathic strata with dominant 1.7–1.8 Ga DZ grains, recording sources from the SE rift margin and a marked decrease in distal sources during uplift of the Transcontinental Arch. Overlying carbonate-rich strata were deposited in shallow marine settings, with episodic influx of siliciclastic sediment derived from basement exposed during regressions. Stratigraphic thickness-age relations of Neoproterozoic to early Paleozoic strata are consistent with two episodes of rifting concentrated at *ca.* 700–670 Ma and 570–540 Ma along western Laurentia, leading to final development of a passive margin. Early rifting was incomplete with an estimated 25–40% extension of initially thick lithosphere that was weakened by igneous activity. Final rifting of previously thinned lithosphere involved an estimated 20–35% additional extension, renewed igneous activity, and thermal thinning of mantle lithosphere, with localized extension culminating in final separation along the continental margin. Stratigraphic, geochronologic, and available paleomagnetic data

* Corresponding author. Tel.: +1 801 626 7419.
E-mail address: ayonkee@weber.edu (W.A. Yonkee).
[1] Now at: Department of Geosciences, University of Arizona, Tucson, AZ 85721, USA.

http://dx.doi.org/10.1016/j.earscirev.2014.05.004
0012-8252/

are consistent with linkage of western Laurentia to Australia–East Antarctica within Rodinia, followed by protracted rifting and drift during Cambrian time.

Contents

1. Introduction

Thick successions of Neoproterozoic to early Paleozoic sedimentary and associated volcanic rocks in the west-central U.S. comprise a key part of the rifted western margin (present day geographic coordinates) of Laurentia and subsequent North American Cordilleran orogenic belt (Fig. 1). Although a general lithostratigraphic framework has been established for these rocks (Fig. 2; Crittenden et al., 1971; Stewart, 1972; Christie-Blick, 1982; Stewart, 1991; Link et al., 1993), depositional ages, spatial and temporal variations in provenance, and tectonic setting are incompletely understood. Thus, fundamental concepts of Cordilleran geology, such as rift timing, paleogeographic evolution of the margin, and influence of sedimentary architecture on subsequent deformation, remain debated. Furthermore, these successions include diamictite-bearing strata that record Cryogenian (635–850 Ma) glaciations (Crittenden et al., 1983; Link et al., 1993), which have been interpreted as being of global extent (Hoffman et al., 1998).

Neoproterozoic to Cambrian strata in the west-central U.S. were deposited during rifting of the supercontinent Rodinia, which was previously assembled from *ca.* 1300 to 900 Ma (Meert and Torsvik, 2003; Li et al., 2008). Rifting initiated between *ca.* 820 and 700 Ma along a number of zones (Li et al., 1999, 2003, 2008), including the western margin of Laurentia (Stewart, 1972; Bond et al., 1984; Levy and Christie-Blick, 1991; Ross, 1991; Karlstrom et al., 2001; Colpron et al., 2002; Lund et al., 2010). The temporal and spatial patterns of rifting that ultimately led to development of the Cordilleran passive margin, however, are controversial. Bond et al. (1984) interpreted rifting followed by a transition to drift at ~550–600 Ma based on subsidence patterns of early Paleozoic strata. In contrast, Ross (1991) interpreted earlier Neoproterozoic breakup of the margin and many paleogeographic reconstructions show separation and drift of western Laurentia prior to 720 Ma (e.g., Meert and Torsvik, 2003; Li et al., 2008; Hoffman and Li, 2009). Additionally, the nature of sedimentation and igneous activity varied along the margin, recording lateral changes in rift patterns (Hansen et al., 1993; Lund, 2008).

The Cryogenian Period was marked by profound climatic changes, which were partly related to enhanced chemical weathering and sedimentation during breakup of Rodinia (Goddéris et al., 2003;

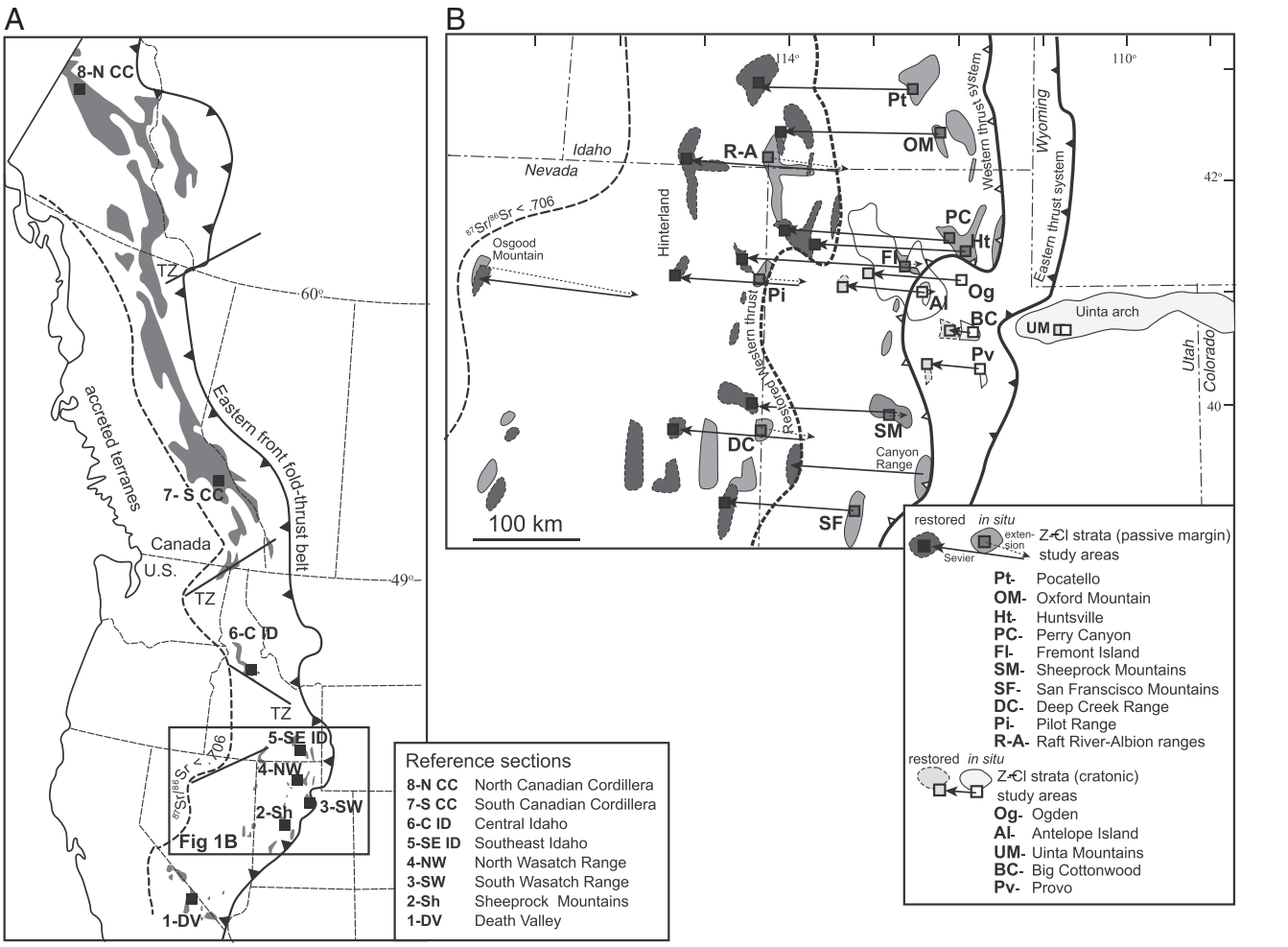

Fig. 1. A. Generalized map shows exposures of Neoproterozoic to early Cambrian strata (gray) along the North American Cordilleran margin. Locations of reference stratigraphic sections in Fig. 2 (solid squares), $^{87}Sr/^{86}Sr < 0.706$ line that approximates west edge of North American Precambrian crust (Armstrong et al., 1977; Elison et al., 1990), east front of Cordilleran thrust belt, interpreted transfer zones (TZ) between rift segments (Lund, 2008), and location of Fig. 1B are indicated. B. Regional geologic map shows *in situ* and palinspastically restored (for Neogene extension and Sevier shortening) locations of study areas and exposures of Neoproterozoic to early Cambrian strata in Utah, Nevada, and Idaho. Frontal trace of the eastern thrust system, *in situ* and restored positions of the leading edge of the western thrust system that carries thick passive margin strata, and $^{87}Sr/^{86}Sr < 0.706$ line are indicated. Note, Uinta arch in the foreland is nearly autochthonous.

Donnadieu et al., 2004). Two major intervals of glaciation, correlated with the Sturtian and Marinoan successions in Australia, are proposed to have occurred respectively between 660–720 Ma and 635–650 Ma (Hoffman and Li, 2009). The "Sturtian" and "Marinoan" intervals, however, may have included multiple glacial episodes, and precise timing and extent of glaciations remain problematic (Allen and Etienne, 2008; Keeley et al., 2013). According to the Snowball Earth model the planetary surface was frozen during these intervals (Kirschvink, 1992; Hoffman et al., 1998; Evans, 2000). Predictions of this model include glacial deposits of the same age worldwide, long duration (~10 m.y.) glacial episodes, disruption of geochemical cycles, and rapid changes to greenhouse conditions with deposition of cap carbonates at the ends of glacial episodes (Hoffman and Schrag, 2002; Donnadieu et al., 2004; Halverson et al., 2005; Hoffman, 2011). In contrast, others have proposed that many diamictites were deposited by mass-movement flows and that glaciations were diachronous and of local extent, perhaps related to progressive uplift along propagating rift margins (Eyles and Januszczak, 2004).

To better understand the history of rifting and glaciation along the Cordilleran margin, integrated stratigraphic, geochronologic, and geochemical analyses of Neoproterozoic to Cambrian sedimentary and volcanic rocks in Utah, Nevada, and Idaho were completed. Systematic U–Pb detrital zircon (DZ) analysis, in concert with measurement of detailed stratigraphic sections, provided extensive new data to bracket maximum depositional ages and constrain changing provenance during uplift of different basement blocks that have distinctive zircon age signatures (Gehrels and Pecha, 2014). Geochemical analysis of associated volcanic rocks provided new data to interpret tectonic settings. Results of these analyses are used to address the following questions:

(1) What is the chronostratigraphic framework of Neoproterozoic to early Paleozoic strata along the west-central North American Cordillera?
(2) How did the paleogeography and sediment sources of the basin system evolve over this time?
(3) What were the spatial and temporal patterns of subsidence and relations to rift processes?
(4) What were relations of rift patterns to the breakup of Rodinia?
(5) What were the relations of diamictite-bearing strata to proposed snowball Earth glaciations?

2. Geologic setting

The west-central U.S. experienced a complex geologic history during evolution of the Cordilleran margin. This history included: (i) formation of Archean to Paleoproterozoic basement rocks; (ii) rifting, development

of a passive margin, and deposition of Neoproterozoic to Jurassic sedimentary rocks; (iii) Cretaceous to Paleogene contractional deformation during the Sevier orogeny; and (iv) Neogene extensional deformation during development of the Basin-and-Range province (DeCelles, 2004).

Basement rocks in the region comprise various blocks that influenced rift patterns and were sediment sources for younger strata. These blocks include the Archean Wyoming province, Neoarchean Grouse Creek block, evolved Paleoproterozoic Farmington zone and Mojave province, and juvenile Paleoproterozoic Yavapai and Mazatzal provinces (Fig. 3; Foster et al., 2006; Whitmeyer and Karlstrom, 2007). The Wyoming province contains 2.8–3.0 Ga gneisses with older inherited zircon grains and 2.6–2.7 Ga granitic plutons and supracrustal belts (Frost et al., 2006; Mueller and Frost, 2006). The Grouse Creek block, best exposed in NW Utah, contains 2.5–2.6 Ga leucogranite intruded into schist and amphibolite, which were overprinted by 1.7 Ga metamorphism (Strickland et al., 2011; Isakson, 2012). Basement rocks at the base of the Willard thrust sheet in northern Utah, referred to as the Facer Formation, also contain 2.5–2.6 Ga leucogranite, metaquartzite, and minor amphibolite with ~1.6 Ga cooling ages (Crittenden and Sorensen, 1980; Balgord, 2011). The Farmington zone contains granitic orthogneiss with distinctive 2.45 Ga zircon grains, along with paragneiss, schist, and metaquartzite containing a mix of 1.7–2.7 Ga metamorphic and inherited zircon grains (Bryant, 1988; Mueller et al., 2011; Nelson et al., 2011; Yonkee et al., 2013). The Mojave province to the S also contains granitic gneiss and paragneiss with 1.7–2.7 Ga zircon grains (Shufeldt et al., 2010). The Selway terrane to the N has mostly 1.7–1.9 Ga zircon grains (Mueller et al., 2005) and intersects with the ~1.9 Ga Great Falls zone (Mueller et al., 2002); the 1.8–2.1 Ga Trans-Hudson province is present farther N in Canada. The Yavapai and Mazatzal provinces contain 1.6–1.8 Ga volcanic arc rocks with juvenile isotopic signatures (Bickford et al., 2008). Additional sediment sources include the mid-continent granite province and associated 1.3–1.5 Ga granitic plutons in the SW U.S. (Bickford et al., 1986), and the Grenville-Llano province to the E and SE with a range of 1.0–1.3 Ga zircon ages and associated 1.1 Ga granitic plutons in the SW U.S. (Fig. 3; Eriksson et al., 2003). The intracratonic Mesoproterozoic Belt basin contains up to 15 km of strata and volcanic rocks deposited across W Montana to central Idaho, with abundant reworked ~1.7–1.8 Ga, local 1.55 Ga, and some syndepositional ~1.4 Ga zircon grains (Link et al., 2007).

Neoproterozoic to Jurassic strata in Utah, Nevada, and SE Idaho comprise different tectono-stratigraphic packages (stages) marked by changes in tectonic setting, lithologies of sedimentary and volcanic rocks, DZ signatures, basin geometry, and subsidence patterns. Stages include: (1) a basal package of Neoproterozoic siliciclastic strata deposited in intracratonic basins (Uinta Mountain Group and correlatives); (2) a lower package of Neoproterozoic diamictite-bearing strata and volcanic rocks deposited during early rifting (Perry Canyon and related formations); (3) a middle package of later Neoproterozoic mature siliciclastic strata deposited during early subsidence (lower Brigham and McCoy Creek groups); (4) an upper package of late Ediacaran to Early Cambrian variably immature siliciclastic strata and minor volcanic rocks deposited during final rifting and transition to drift (Prospect Mountain and related formations); (5) a carbonate-rich package of Middle Cambrian to Devonian, westward-thickening strata deposited along a passive margin; and (6) Mississippian to Jurassic strata deposited in a mix of environments as the margin was disrupted (Fig. 2; Oldow et al., 1989; Poole et al., 1992; Link et al., 1993). A hinge zone marks the transition between thick strata that accumulated on rifted crust to the west and thinner strata that accumulated on cratonic crust to the east (Fedo and Cooper, 2001; Hintze and Kowallis, 2009).

These strata were subsequently deformed and thrust eastward during the Cretaceous to Paleogene Sevier orogeny (Royse, 1993; DeCelles, 2004). The Sevier belt comprises: (i) a hinterland where mid-crustal rocks are exposed in metamorphic core complexes; (ii) a western region that includes the Willard–Paris–Meade and Sheeprock-Canyon Range thrust sheets that carried thick passive-margin strata; and (iii) an eastern region with smaller thrust sheets that carried thinner cratonic strata (Fig. 4). The hinterland experienced complex contractional and extensional deformation, complicating interpretation of primary stratigraphic relations (Wells, 1997). Aerially extensive thrust sheets in the western region were transported 50 to 100 km eastward relative to their footwalls above a basal decollement in Neoproterozoic strata (Crittenden, 1972; Yonkee, 2005; DeCelles and Coogan, 2006). Thrust sheets in the eastern region were mostly transported above a regional decollement in Cambrian shale. Farther east, the Uinta-Cottonwood arch was uplifted.

The Sevier belt was subsequently extended by Neogene normal faults during development of the Basin and Range province. Uplift and erosion in footwalls of normal faults exposed a wide range of structural levels. Although deformed, stratigraphic sections have been restored by careful structural analysis (Fig. 4).

3. Methods

Integrated studies were completed to determine stratigraphic relations, provenance, maximum depositional ages, and tectonic settings of Neoproterozoic to Cambrian sedimentary and volcanic rocks exposed in Utah, Nevada, and Idaho (Fig. 4). Fieldwork involved description of sedimentary features including paleocurrent indicators, clast counts in diamictite, and collection of samples for petrographic, geochronologic, and geochemical analyses. Petrographic point counts (300 per thin section) were completed to estimate volume fractions of quartz, feldspar, lithic fragments, and matrix (<50 μm grains).

U–Pb zircon geochronology was completed for 101 samples, with 100 grains typically analyzed per sample. Zircon grains were extracted from samples by traditional methods of crushing, followed by Wilfley table, heavy-liquid, and magnetic separation. Representative splits of zircon fractions, along with fragments of zircon standards, were incorporated into epoxy mounts that were polished and imaged prior to isotopic analysis. U–Pb analysis for the majority of samples was done using laser ablation-inductively coupled plasma mass spectrometry (LA-ICPMS) at the Arizona LaserChron Center following procedures given by Gehrels et al. (2006, 2008); five samples were analyzed using LA-ICPMS at Washington State University. Samples with abundant young zircon grains (<750 Ma) and volcanic clasts were targeted for SHRIMP analysis at the Research School of Earth Sciences, The Australian National University, following procedures given by Williams (1998). U–Pb data were plotted on concordia diagrams and age-probability diagrams using the software package Isoplot (Ludwig, 2008). The $^{206}Pb/^{207}Pb$ age was used for grains older than 900 Ma and the $^{206}Pb/^{238}U$ age was used for younger grains. Analyses >10% discordant or >5% reverse discordant based on comparison of $^{206}Pb/^{238}U$ and $^{206}Pb/^{207}Pb$ ages were not plotted. Analytical uncertainties were typically less than ±1% at a one sigma level (±20 Ma for a 2000 Ma grain). Zircon U–Pb age data are given in Table SM1 in the Supplementary materials.

Geochemical characteristics of igneous rock and volcanic clasts were determined by X-ray fluorescence mass spectrometry (XRF) at the University of Wisconsin-Eau Claire. Major element data for less altered samples were plotted on standard diagrams to distinguish igneous rock types. Trace element ratios, which are unlikely to have been modified during alteration, were used to interpret tectonic setting (Pearce and Cann, 1973; Pearce and Norry, 1979). Geochemical data are given in Table SM2 in the Supplementary materials.

4. Characteristics of tectono-stratigraphic packages

Stratigraphic sections exposed across the study region, after palinspastic restoration, span an E–W distance >300 km, and a N–S distance >400 km across the Cordilleran margin (Fig. 4). Lithologic characteristics, DZ patterns, and geochemical data are described for

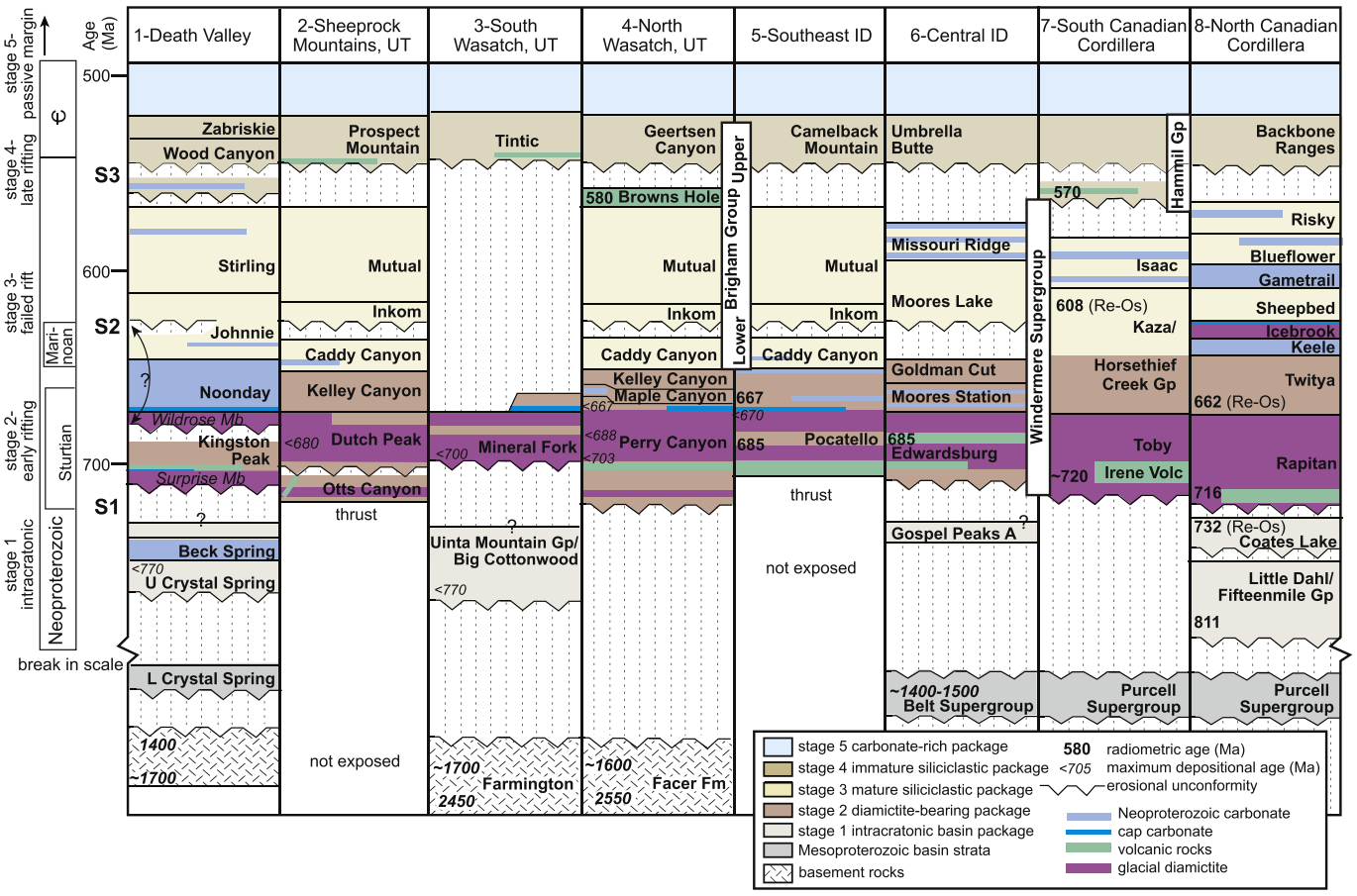

Fig. 2. Reference stratigraphic sections and published age constraints (including results in this paper) for Neoproterozoic to Cambrian strata along the Cordilleran margin (see Fig. 1A for locations of sections). Stratigraphic sections include: basement rocks; Mesoproterozoic basin strata; Neoproterozoic intracratonic basin strata (stage 1); Neoproterozoic diamictite-bearing strata and volcanic rocks deposited during early rifting (stage 2); later Neoproterozoic mature siliciclastic strata (stage 3); Ediacaran to Early Cambrian variably immature strata and volcanic rocks deposited during final rifting and transition to drift (stage 4); and Middle to late Cambrian carbonate-rich strata deposited along a passive margin (stage 5). Major sequence boundaries S1 to S3 indicated. Data from: 1—Death Valley (Prave, 1999; Petterson et al., 2011; Macdonald et al., 2013; Mahon et al., 2014); 2—Sheeprock Mountains (Christie-Blick, 1982; this study); 3—southern Wasatch (Christie-Blick, 1983; this study); 4—northern Wasatch (Blick, 1979; Crittenden et al., 1983; Balgord et al., 2013; this study); 5—southeast Idaho (Link, 1982; Fanning and Link, 2004; Keeley et al., 2013; this study); 6—central Idaho (Lund et al., 2003, 2010); 7—South Canadian Cordillera (Devlin et al., 1988; Ross et al., 1995; Colpron et al., 2002); 8—North Canadian Cordillera (Rainbird et al., 1996; Macdonald et al., 2010; Rooney et al., 2014). Ages of Icebrook and upper Kingston Peak formations are uncertain and could correlate with late Sturtian or Marinoan glacial episodes (Prave, 1999; Macdonald et al., 2013). Major sequence boundaries (S1 to S3) from Link et al. (1987) indicated.

the following areas: the Big Cottonwood-Provo and Antelope Island areas in the eastern region; the Sheeprock-San Francisco, Perry Canyon-Fremont Island, and Pocatello-Oxford Mountain areas in the western region; and the Deep Creek and Raft River–Albion areas in the hinterland. Relations are described for five stages and associated tectono-stratigraphic packages: stage 1—basal siliciclastic package; stage 2—lower diamictite-bearing and volcanic package; stage 3—middle mature siliciclastic package; stage 4—upper variably immature siliciclastic and volcanic package; and stage 5—carbonate-rich package. Stratigraphic columns and DZ spectra for study areas are shown in Fig. 6A to G. Compilations of DZ spectra, thin section point count data, and paleocurrent directions are shown in Fig. 7. Diamictite clast count data are summarized in Fig. 8.

4.1. Stage 1—basal siliciclastic package

The basal package includes the Uinta Mountain Group (UMG) and correlative Big Cottonwood Formation (BCF), which are exposed along the E–W trending Uinta-Cottonwood arch (UCA; Fig. 4). The UMG consists of feldspathic to quartzose sandstone, conglomerate, and mudstone deposited in fluvial to shallow marine environments (Fig. 5A; Hansen, 1965; Dehler et al., 2010; Kingsbury-Stewart et al., 2013). The BCF, interpreted to be a finer-grained equivalent of the UMG, consists mostly of quartzose sandstone and mudstone also deposited in fluvial to shallow marine environments (Link et al., 1993; Ehlers and Chan, 1999). Total thickness of the package is >5 km along the depocenter of the intracratonic UMG basin, which was bounded on the north by an E–W trending normal fault system subparallel to a crustal boundary between Archean and Paleoproterozoic basement rocks (Fig. 3); the basin was subsequently inverted to form the UCA during mostly Paleogene deformation (Bradley and Bruhn, 1988). Correlative strata thin significantly to the south and are absent north of the UCA. The UMG basin may have been connected to the Chuar and Pahrump basins to the SW (Dehler et al., 2010), which had a different geometry from the ensuing regional rift system.

DZ patterns vary with stratigraphic level and rock type, recording varying sediment sources (Dehler et al., 2010). Feldspathic sandstone contains abundant Archean DZ grains sourced from uplifted basement rocks of the Wyoming province to the N (samples 91PL05, 69PL05, 90PL05; Fig. 6A). Quartzose sandstone contains abundant 1.0–1.3 Ga and 1.3–1.5 Ga grains likely sourced from the distal Grenville–Llano and mid-continent granite provinces and fewer 1.6–1.8 Ga grains sourced from the Yavapai–Mazatzal provinces (73PL05, 112DH12, 111DH12, 122PL02; Fig. 6A). Incorporation of distal source material is interpreted to record long distance sediment transport via a transcontinental river system (Dehler et al., 2010), along with possible recycling of material from the Grenvillian clastic wedge (Rainbird et al., 2012). The lower part of the UMG contains rare young (766 ± 5 Ma) zircon grains

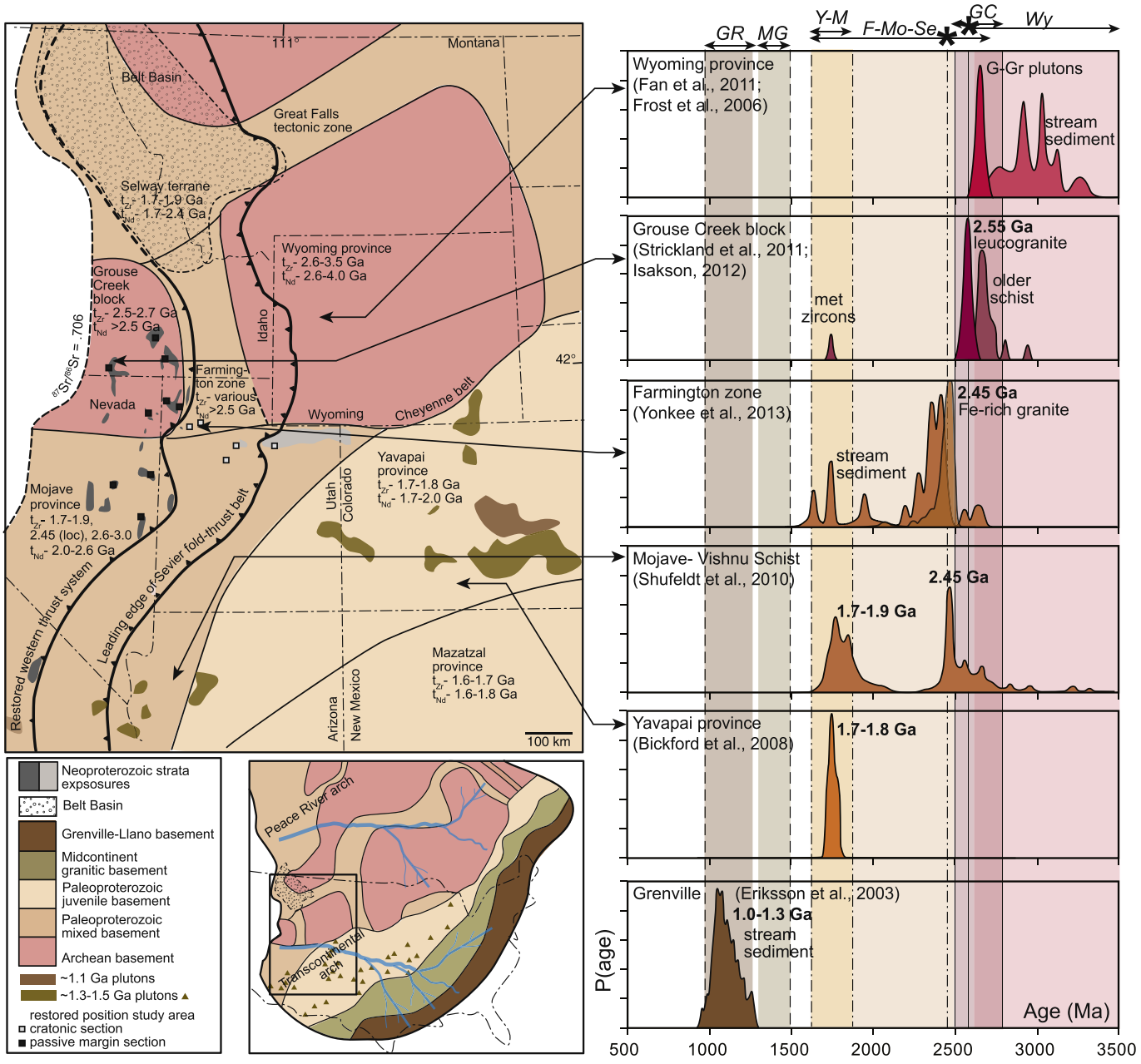

Fig. 3. Generalized map of basement provinces shows local sediment sources for Neoproterozoic to Cambrian strata. Leading edge of Sevier fold-thrust belt, restored positions of study areas, and Nd model ages (tNd) of provinces (Bennett and DePaolo, 1987) are indicated. Inset map of Laurentia shows locations of distal sediment sources. Zircon spectra from different basement sources have distinctive patterns: Wyoming province (Wy) has range of 2.6–3.0 Ga grains (Frost et al., 2006; Fan et al., 2011); Grouse Creek block (GC) has prominent 2.55 Ga peak (asterisk) (Strickland et al., 2011; Isakson, 2012); Farmington zone, Mojave province, and Selway terrane (F-Mo-Se) have a mix of 1.7–1.9 Ga metamorphic grains, 2.45 Ga grains from local Fe-rich granitic plutons (asterisk), and reworked Archean grains (Shufeldt et al., 2010; Mueller et al., 2011; Yonkee et al., 2013); Yavapai and Mazatzal provinces (Y-M) have 1.7–1.8 Ga peak (Bickford et al., 2008); mid-continent granite (MG) and A-type granite intrusions in the SW U.S. have 1.3–1.5 Ga grains; and Grenville-Llano province (GR) has range of 1.0–1.3 Ga grains with multiple subpeaks (Eriksson et al., 2003), along with ~1.1 Ga late granite intrusions in the SW U.S. Modified from Whitmeyer and Karlstrom (2007) and Balgord et al. (2013).

that define maximum depositional age (91PL05, SCUMG-9; Fig. 6A). The Red Pine Shale in the upper UMG contains the microfossils *Chuaria* and *Melanocyrillium* (Dehler et al., 2010), which are correlative with microfossils in the upper Chuar Group that contains a 742 ± 6 Ma tuff (Karlstrom et al., 2000; Dehler et al., 2001).

4.2. Stage 2—lower diamictite-bearing and volcanic package

This package is represented by the locally deposited Mineral Fork Formation in the eastern region, the Perry Canyon Formation and related strata in the western region, and complexly deformed strata in the hinterland (Fig. 4). Strata display distinct vertical changes in lithology and are subdivided into: stage 2A—feldspathic to quartzose strata (Fig. 5B) and pebbly diamictite (Fig. 5C) deposited during initial extension and an older glacial episode; stage 2B—mafic volcanic rocks (Fig. 5D), polymict diamictite (Fig. 5E), cap carbonate (Fig. 5F), and volcaniclastic wacke deposited during regional extension and a younger glacial episode; and stage 2C—argillite to fine-grained quartzite deposited during onset of regional subsidence (Condie, 1967; Christie-Blick, 1982, 1983; Crittenden et al., 1983; Balgord et al., 2013). Strata deposited during stage 2B contain young (~670–700 Ma) zircon grains related to felsic volcanism, whereas stage 2A strata typically lack young grains. Relations are described separately for each study area due to lateral variability.

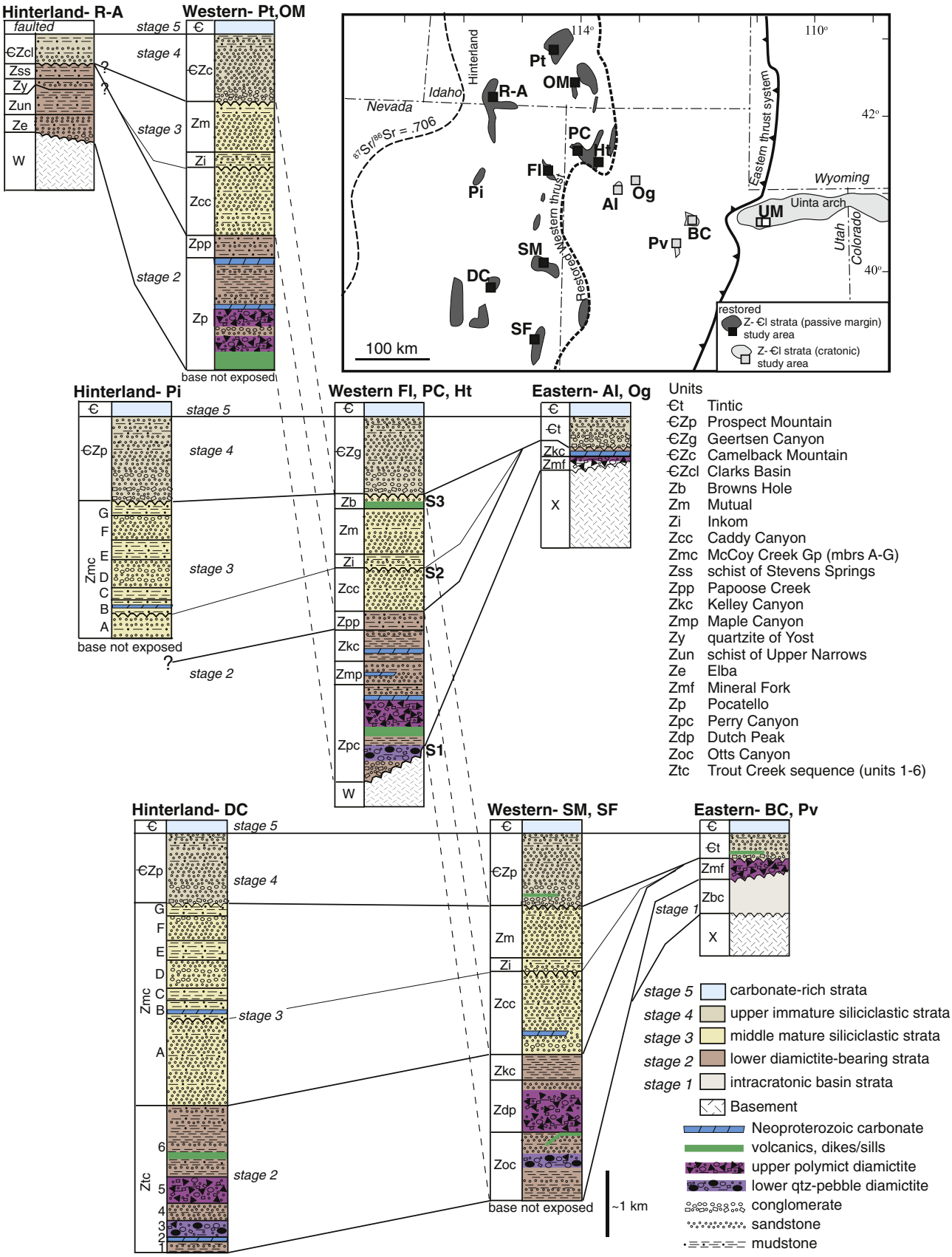

Fig. 4. Generalized stratigraphic columns shown for: Uinta Mountains (UM) in the Laramide foreland; Big Cottonwood (BC), Provo (Pv), Antelope Island (AI), and Ogden (Og) areas that have thin cratonic strata in the eastern thrust system; Sheeprock Mountains (SM), San Francisco Mountains (SF), Huntsville (Ht), Perry Canyon (PC), Fremont Island (Fl), Oxford Mountain (OM), and Pocatello (Pt) areas that have thick passive-margin strata in the western thrust system; and Deep Creek Range (DC), Pilot Range (Pi), and Raft River–Albion ranges (R–A) in the hinterland. Strata are correlated by stages 1 to 5. Major sequence boundaries (S1 to S3) from Link et al. (1987) also indicated. Inset map shows restored locations of study areas.

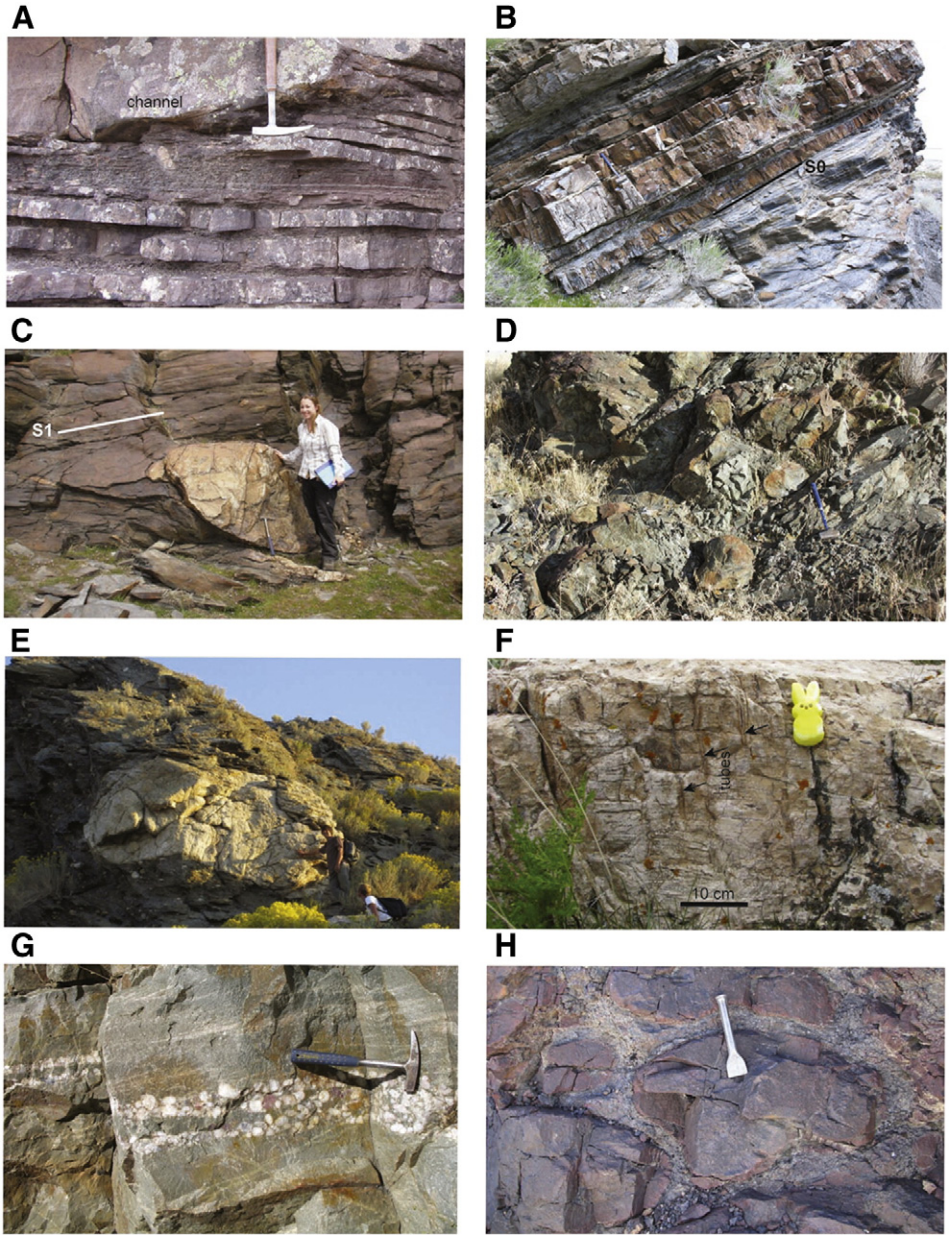

Fig. 5. Outcrop characteristics of key rock types. A. Interbedded feldspathic sandstone and mudstone is cut by channel with pebbly sandstone. From the Uinta Mountain Group. Hammer for scale. B. Upward-fining layers of quartzite to argillite represent medial to distal turbidites. From quartzite-grit member of Perry Canyon Formation. Hammer for scale. C. Quartzite boulder interpreted to be a lonestone lies in a pebbly mudstone matrix. The matrix displays slaty foliation (S1). From pebbly slate member of Perry Canyon Formation. D. Basalt, now altered to greenstone, displays pillows with fine-grained rims and fragmented interpillow material. From volcanic member of Perry Canyon Formation. Hammer for scale. E. Polymict diamictite contains large clasts, including 4-m leucogranite boulder, that sit in a sandy to micaceous matrix. From diamictite member of Perry Canyon Formation. F. Laminated dolostone displays cap-like features, including sheet crack cements and tubes (arrows). The dolostone overlies diamictite of the Mineral Fork Formation at Antelope Island. G. Subfeldspathic quartz arenite contains quartz-pebble layers and displays cross beds. From lower Prospect Mountain Formation. Hammer for scale. H. Basalt flow displays pillows with altered rims, separated by fragmental material. From lower Prospect Mountain Formation. Chisel for scale.

4.2.1. Eastern region: Big Cottonwood–Provo area

The package here is represented by interstratified polymict diamictite, sandstone, and mudstone of the Mineral Fork Formation. The formation is generally <100 m thick, but locally fills paleovalleys up to 800 m deep carved into underlying strata along Big Cottonwood Canyon (Ojakangas and Matsch, 1980; Christie-Blick, 1983; Young, 2002). Diamictite is typically massive and consists of pebble to boulder (up to ~3 m) clasts that sit in a sandy to micaceous matrix. Clast types include orthoquartzite, carbonate, granite/gneiss, and rare volcanic rocks (Fig. 8). Quartzite clasts are lithologically similar to and likely derived from the underlying BCF and UMG. Carbonate clasts may have been eroded from strata originally overlying the BCF, or from carbonate units located farther SW. Granitic clasts were likely sourced from local basement rocks. Sandstone is subfeldspathic to quartzose and includes laminated and cross-bedded facies that record W- to NW-directed paleoflow (Christie-Blick, 1983). Mudstone contains rare dropstones, Fe-rich layers similar to glaciogenic ironstones (Young, 2002), and carbonaceous layers with microfossils (Knoll et al., 1981). Repeated layers of upward-fining quartzite to mudstone are interpreted to represent turbidites. Interlayering of diamictite, cross-bedded sandstone, mudstone with dropstones, and turbidites suggests a dynamic glaciomarine setting with episodes of locally open marine conditions (Blick, 1979).

DZ patterns for diamictite and sandstone display a mixed signature of Mesoproterozoic, Paleoproterozoic, and Archean grains (samples 50CD10, 44CD10, 43CD10, 21CD10; Fig. 6A). Patterns are similar to DZ spectra of quartzose strata in the BCF and UMG, consistent with the

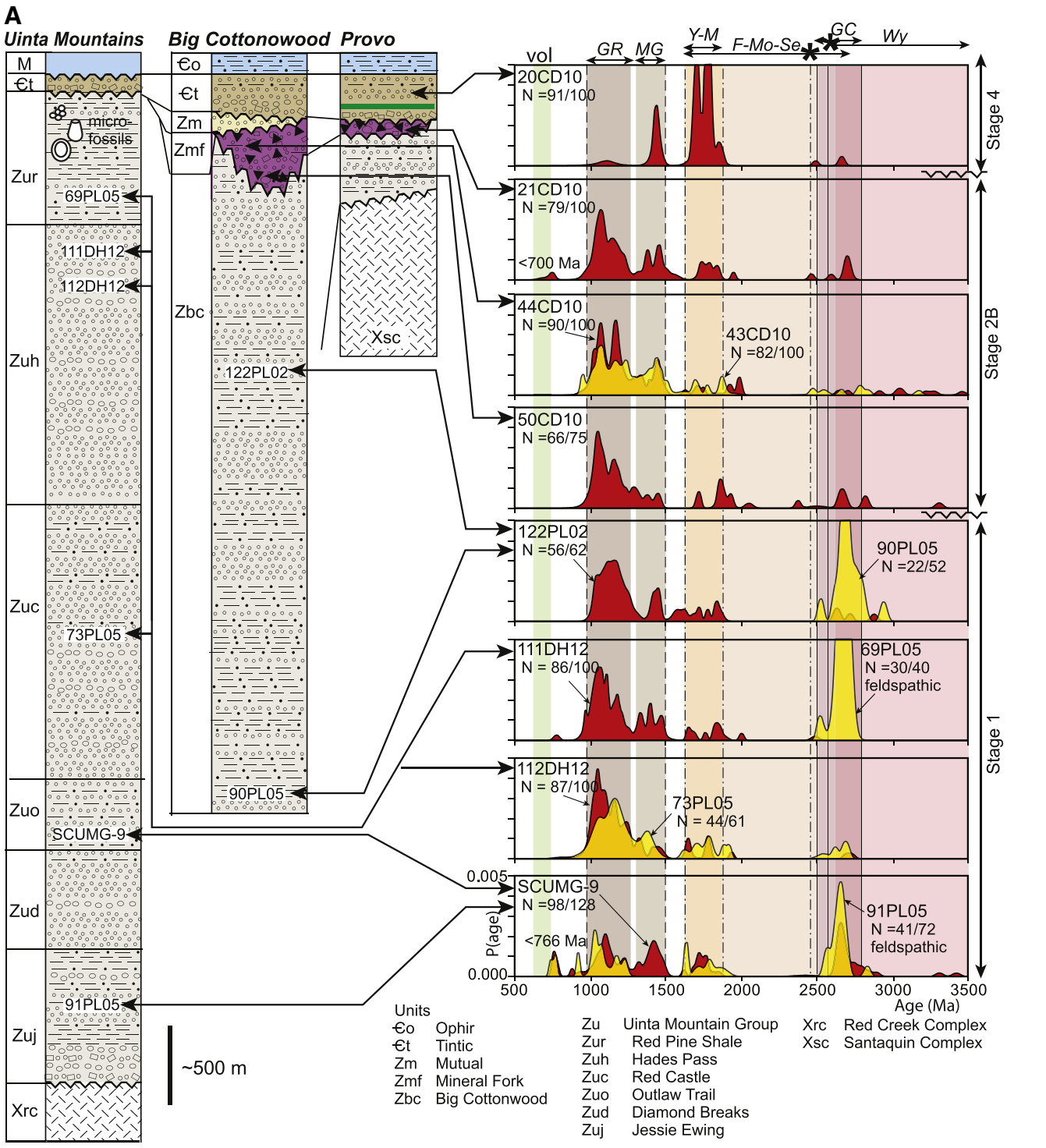

Fig. 6. Generalized stratigraphic columns and detrital zircon spectra (probability density distributions) for the study areas. Sample names and number of grains (N) >90% concordance/total grains analyzed are listed. Expected ages for different sediment sources from Fig. 3 are: Wy—Wyoming province; GC—Grouse Creek block with 2.55 Ga leucogranites (asterisk); F–Mo–Se—Farmington zone, Mojave province, and Selway terrane, with 2.45 Ga Fe-rich granites (asterisk); Y–M—Yavapai and Mazatzal provinces; MG—mid-continent granite province and associated plutons; GR—Grenville-Llano province; vol- syndepositional volcanic rocks. Lithologic symbols same as in Fig. 4. A. Uinta Mountains, Big Cottonwood, and Provo areas. B. Antelope Island and Ogden areas. C. Sheeprock and San Francisco Mountains in central Utah. D. Huntsville, Perry Canyon, and Fremont Island-Promontory areas along the northern Wasatch front. E. Pocatello and Oxford Mountain areas in SE Idaho. Ages of tuffaceous layers (i) and (ii) are respectively from Keeley et al. (2013) and Fanning and Link (2004). F. Deep Creek Range and nearby areas in W Utah to E Nevada. G. Raft River–Albion Ranges in NW Utah to S Idaho. DZ spectra from Strickland et al. (2011) shown in gray.

presence of reworked orthoquartzite clasts. A sample from the Provo area (21CD10) has rare *ca.* 700 Ma zircon grains that define maximum depositional age and indicate deposition during the younger glacial episode.

4.2.2. Eastern region: Antelope Island area

The package here is represented by a <30-m-thick unit of diamictite that overlies basement rocks of the Farmington zone (Fig. 6B; Yonkee et al., 2000). Diamictite is typically massive and contains pebble to

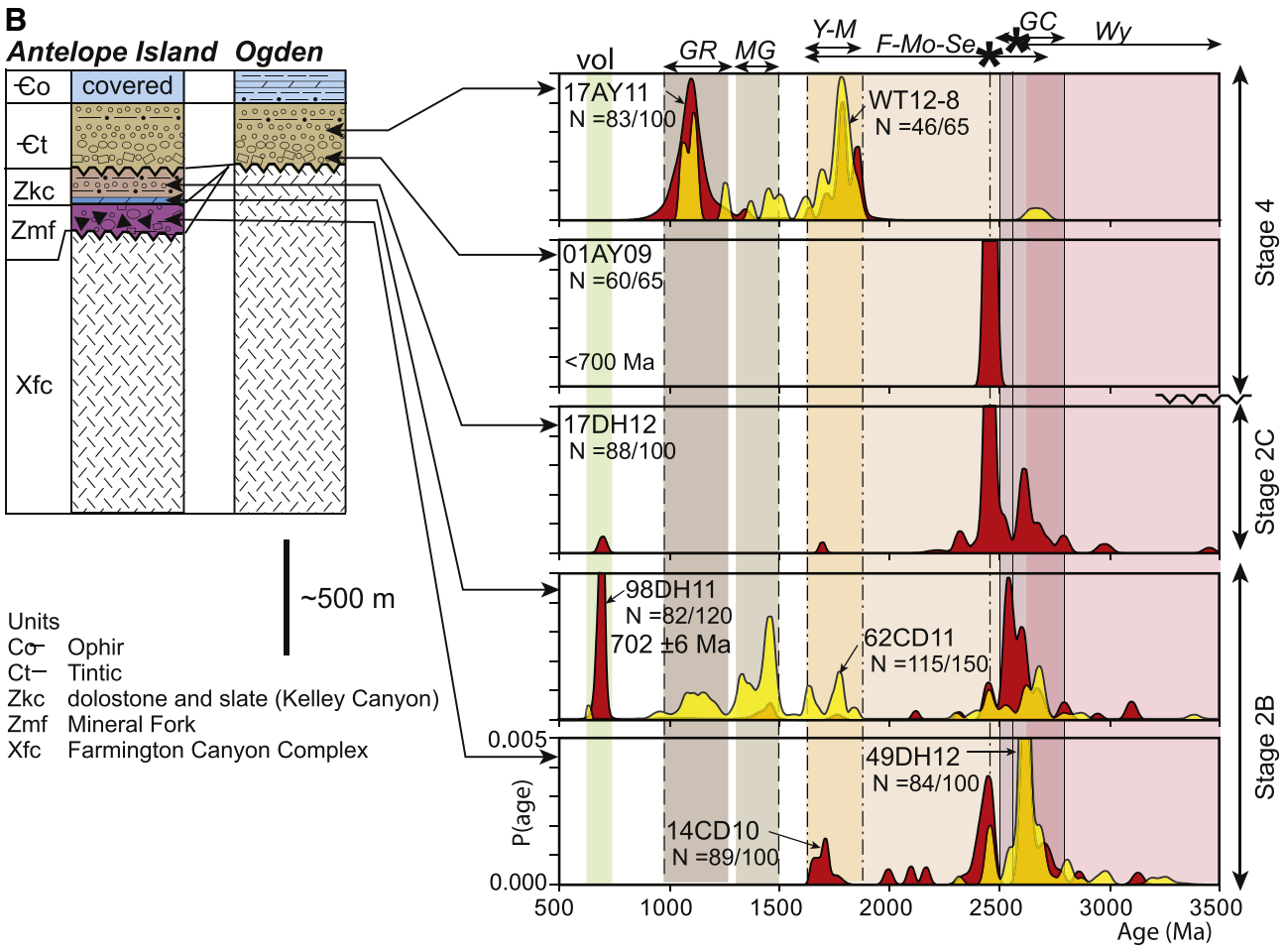

Fig. 6 (*continued*).

boulder (up to 4 m) clasts that sit in sandy to micaceous matrix; stratified wacke to mudstone with dropstones is also locally present. Most clasts are Fe-rich granites that are geochemically similar to granitic orthogneiss of the Farmington zone, along with lesser amounts of paragneiss and quartzite (Yonkee et al., 2013). Diamictite is overlain by a ~10-m-thick unit of laminated pink dolostone that displays tube structures and sheet crack cements, negative $\delta^{13}C$ values characteristic of cap carbonates, and disrupted beds of quartzose sandstone and siltstone (Fig. 5 F; Hayes, 2013). Dolostone is overlain by interbedded argillite and ferroan dolostone, grading upward into fine-grained quartzite.

DZ patterns from the diamictite have distinctive peaks at 2.45 and 2.6–2.8 Ga, along with some 1.7–1.8 Ga grains (14CD10, 17DH12; Fig. 6B), consistent with sources from the Farmington zone and Wyoming province. Disrupted sandy beds in the cap dolostone contain 2.45 and 2.6–2.8 Ga DZ grains, along with distinctive 2.55 Ga and young grains that give a mean (maximum depositional) age of 702 ± 6 Ma (98DH11, Fig. 6B). The 2.55 Ga and ~700 Ma grains are unusual for eastern areas, but are common in areas to the west and may record reworking and redeposition of glacial deposits during rapid sea level rise. A sandstone dike in the dolostone (62CD11, Fig. 6B) contains 2.45 and 2.6–2.8 Ga DZ grains, along with Mesoproterozoic grains that may have been recycled from UMG to the south. Overlying fine-grained quartzite (17DH12; Fig. 6B) has a similar DZ pattern to the diamictite.

4.2.3. Western region: Sheeprock–San Francisco area

The package here includes the: Otts Canyon Formation with lower slate, pebbly diamictite, and upper quartzite members; mafic intrusive rocks; Dutch Peak Formation with conglomerate, diamictite, and greywacke members; and Kelley Canyon Formation (Fig. 6C; Blick, 1979; Christie-Blick, 1982). These rocks were metamorphosed at greenschist facies, internally strained, and translated eastward in the Sheeprock thrust sheet (Mukul and Mitra, 1998). The lower member of the Otts Canyon Formation consists of ~500 m of upward-fining layers of quartzose to subfeldspathic sandstone to mudstone (now slate), interpreted to be distal turbidites deposited during early subsidence. The middle member contains pebbly diamictite with quartzite and minor granitic clasts that sit in a micaceous matrix (Fig. 8). The member is typically <100 m thick and is interpreted to record the older glacial episode (Christie-Blick, 1982). The upper member contains fine- to medium-grained quartzite and slate interpreted to represent turbidites. The member thickens to the SE from 200 to 800 m, likely reflecting syndepositional faulting. Diabase dikes, altered to greenstone consisting of albite, epidote, actinolite, and chlorite, cut the upper Otts Canyon Formation.

The base of the overlying Dutch Peak Formation is marked by a <100-m-thick unit of poorly sorted conglomerate with abundant basalt clasts, indicating volcanic rocks were present prior to erosion, along with laminated quartzite containing dropstones interpreted to mark the onset of the younger glacial episode (Christie-Blick, 1982). The main part of the formation comprises the diamictite and greywacke members that thicken to the SE from 500 to 700 m. Diamictite is massive to crudely stratified and contains polymict pebble to boulder (up to 3 m) clasts that sit in sandy to micaceous matrix. Clasts are mostly granitic, along with lesser amounts of quartzite, reworked sedimentary rocks, and volcanic basalt, trachyte, and rhyolite (Fig. 8). The greywacke member consists of poorly sorted, volcaniclastic to feldspathic wacke deposited as turbidites, diamictite lenses redeposited by mass flows, and moderately sorted quartzose sandstone.

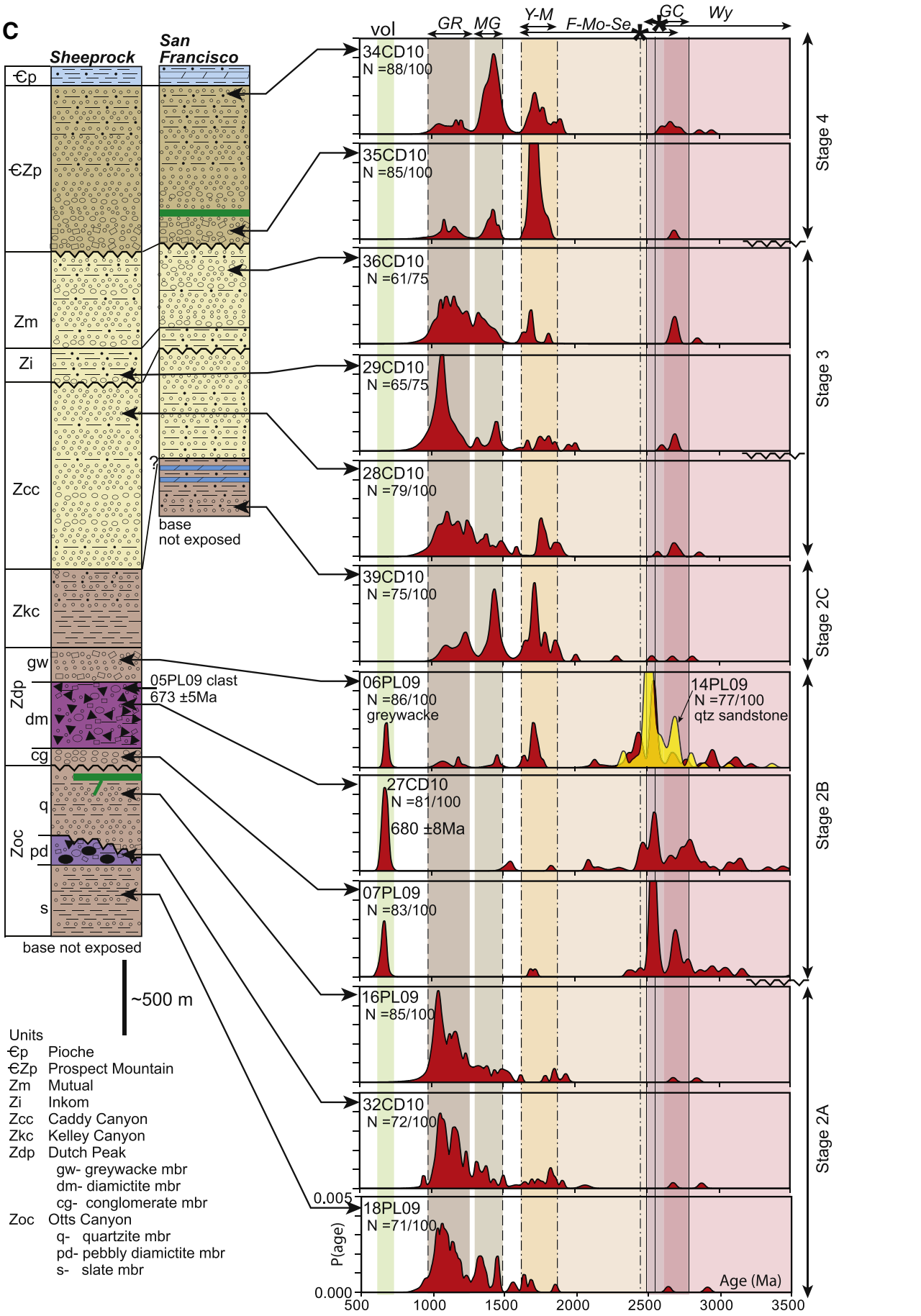

Fig. 6 (*continued*).

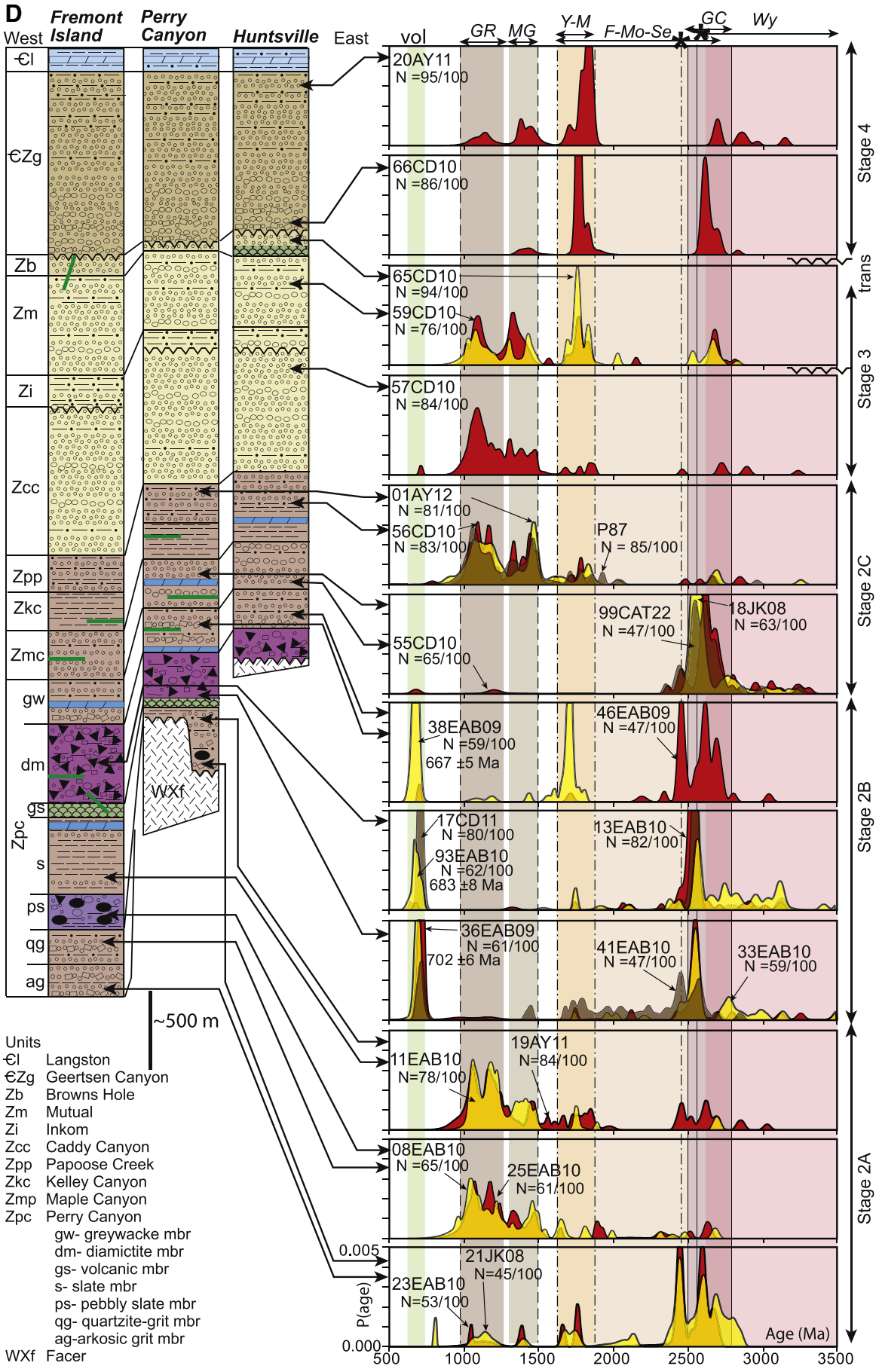

Fig. 6 (*continued*).

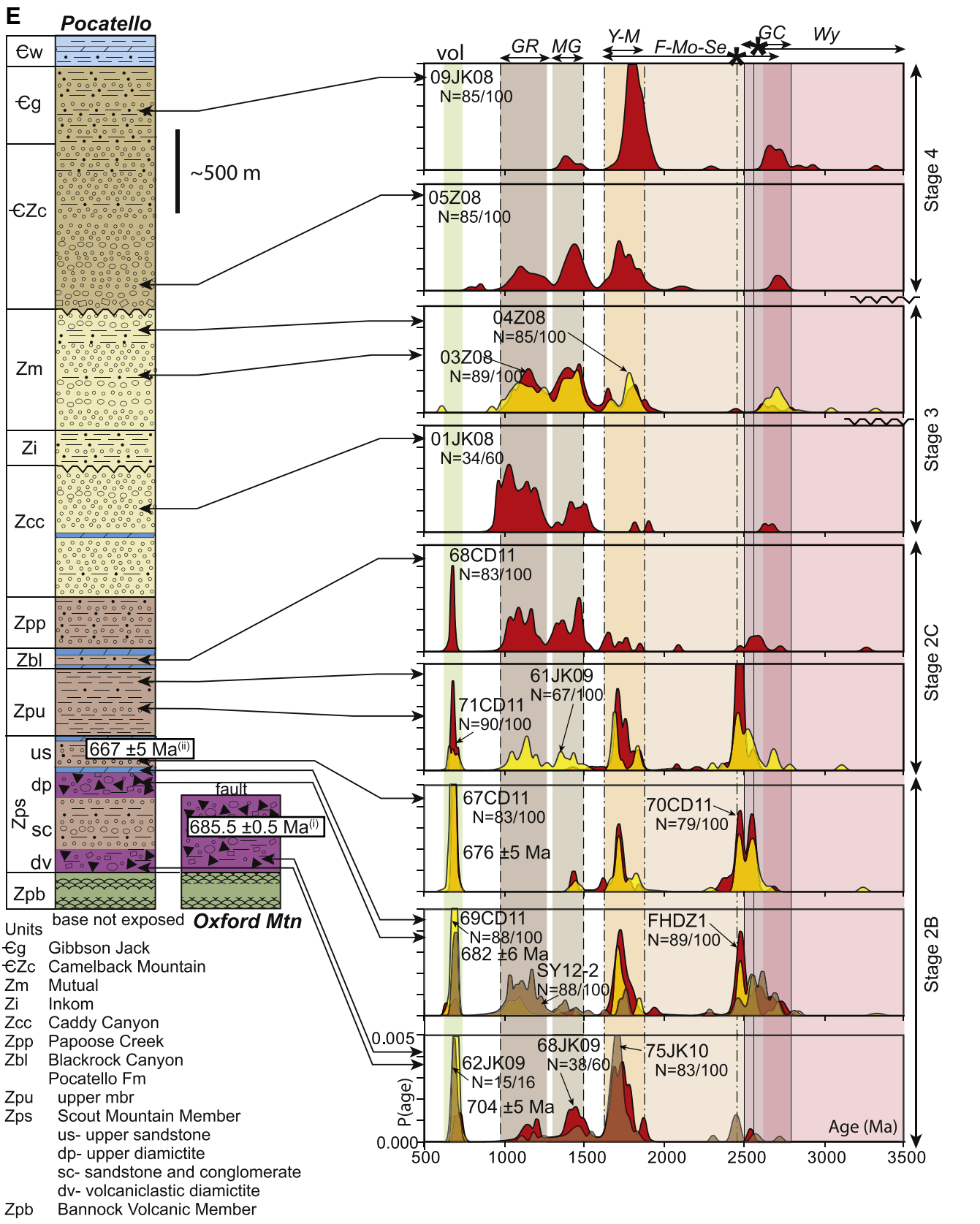

Fig. 6 (*continued*).

The overlying Kelley Canyon Formation consists of argillite with silty laminations and fine-grained quartzite. Strata have a total thickness of 300–500 m and were likely deposited from suspension and as distal turbidites in relatively deep water. The upper part of the formation contains wavy laminated quartzite and siltstone with sedimentary dikes and syneresis cracks, recording shallower water

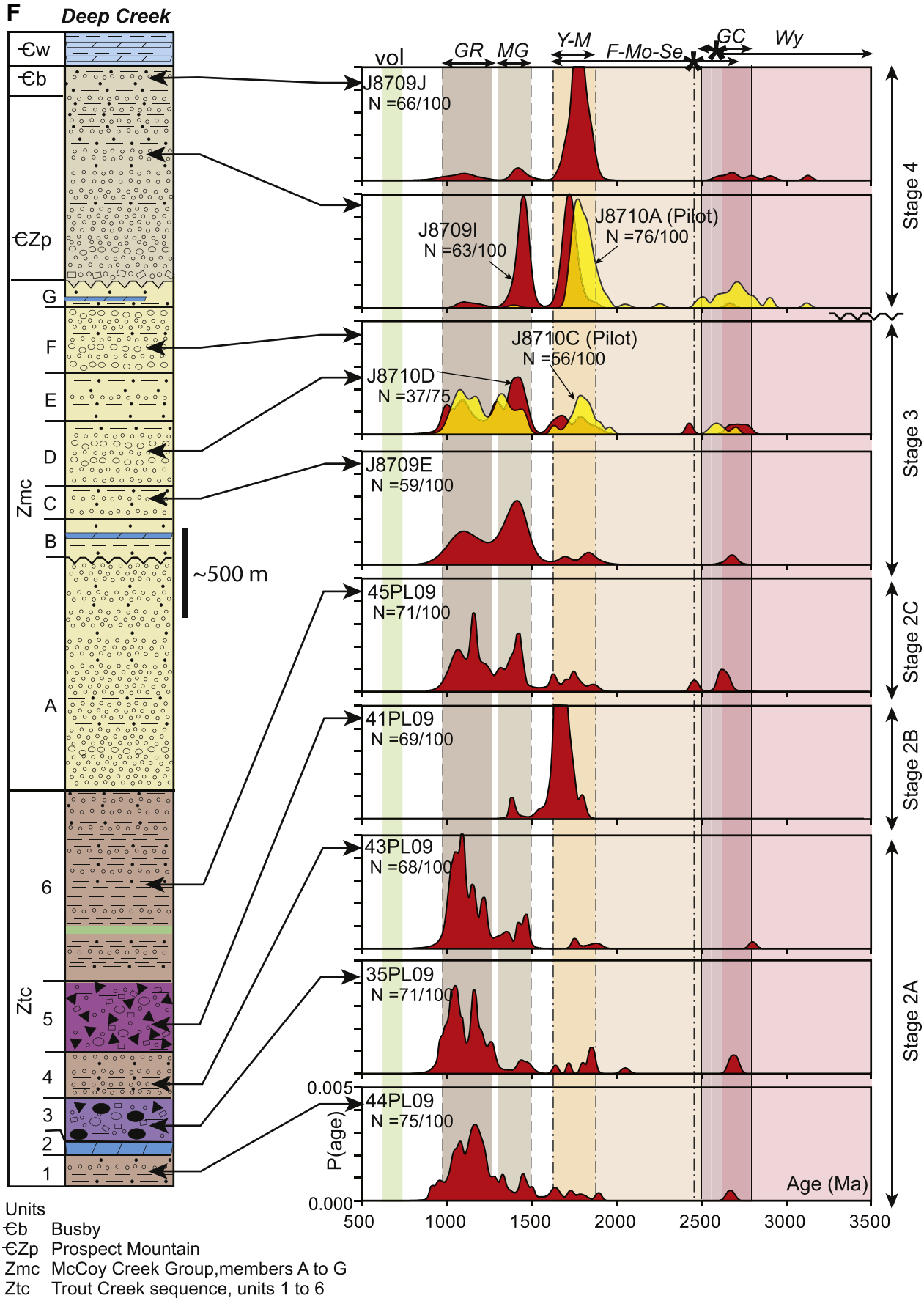

Fig. 6 (*continued*).

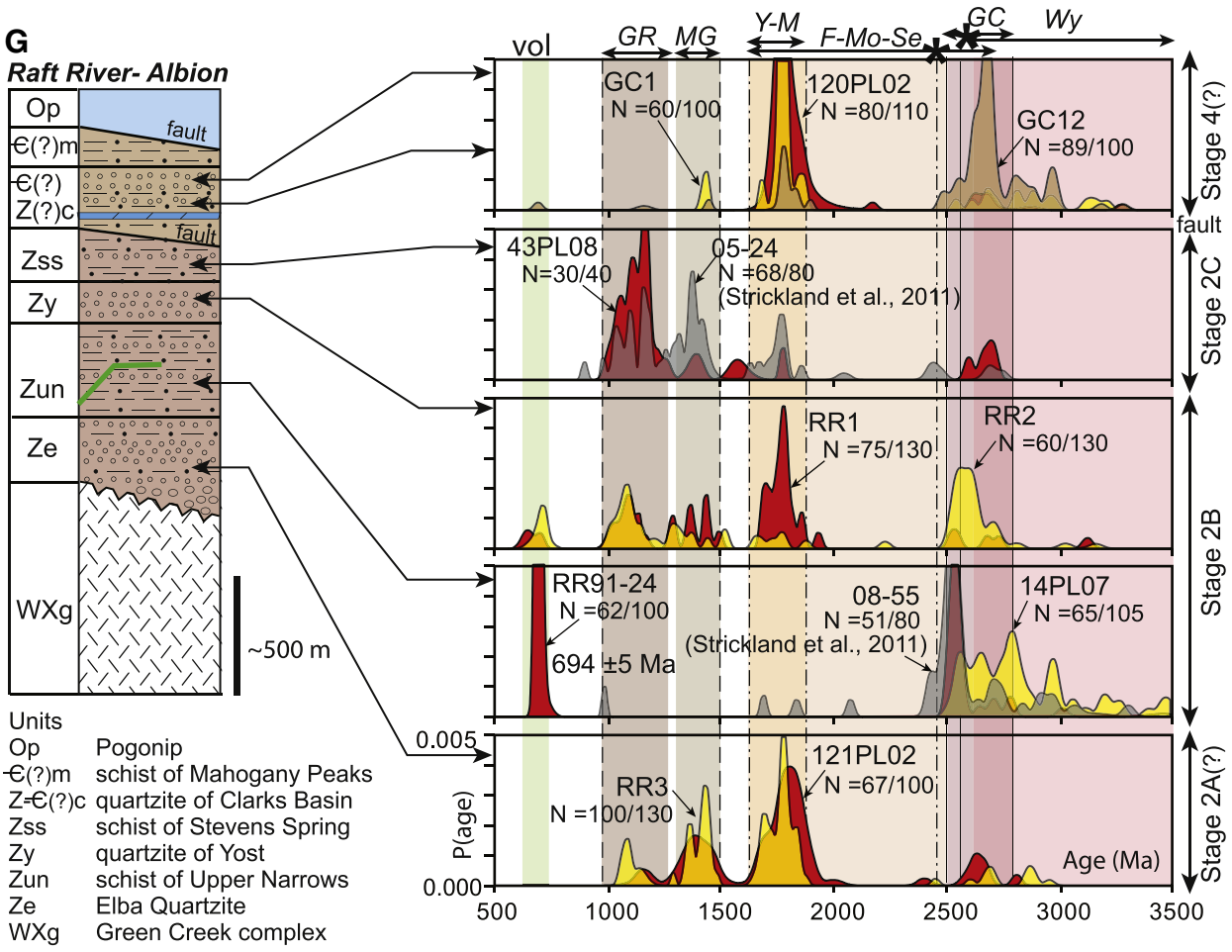

Fig. 6 (*continued*).

depths and transition into the overlying Brigham Group. In the San Francisco Mountains (Fig. 1), a ~700-m-thick unit of quartzite, argillite, and minor carbonate has been mapped as the "Pocatello Formation and Blackrock Canyon Limestone" (Hintze and Davis, 2002). However, continuation of these formation names from Idaho to central Utah is problematic; rather these strata likely reflect a facies change in the Kelley Canyon to lower Caddy Canyon formations (Christie-Blick, 1982).

DZ patterns for the Otts Canyon Formation show abundant 1.0–1.3 Ga and 1.3–1.5 Ga grains, interpreted to record distal sources from the Grenville–Llano and mid-continent granite provinces with sediment delivered via a transcontinental river system, along with possible recycling from the UMG (18PL09, 32CD10, 16PL09; Fig. 6C). DZ patterns for the Dutch Peak Formation show a distinct change marked by abundant Archean grains with peaks at 2.55 Ga and 2.6–3.0 Ga, consistent with sources from the Grouse Creek block and Wyoming province, along with young (670–700 Ma) grains (07PL09, 27CD10, 06PL09, 14PL09; Fig. 6C). Abundant young grains in volcaniclastic diamictite (27CD10) have a mean (maximum depositional) age of 680 ± 8 Ma and a reworked rhyolite clast near the top of the formation (05PL09) has an age of 673 ± 5 Ma (Fig. 6C). Interbedded quartzite and argillite in the San Francisco Mountains, interpreted as correlative to the upper Kelley Canyon Formation, contain Paleoproterozoic and Mesoproterozoic DZ grains that record increased input from the Yavapai province and distal sources (39CD10; Fig. 6C).

4.2.4. Western region: Perry Canyon–Fremont Island area

In northern Utah, diamictite-bearing strata are exposed along a 50-km W–E transect that reveals stratigraphic variations during early rifting (Fig. 6D). Strata comprise the: Perry Canyon Formation with basal arkosic grit, quartzite-grit, pebbly slate, slate, volcanic, diamictite, and greywacke members; Maple Canyon Formation; and Kelley Canyon Formation (Condie, 1967; Blick, 1979; Crittenden et al., 1983; Balgord et al., 2013). These rocks were metamorphosed at greenschist facies, internally strained, and translated eastward in the Willard thrust sheet (Crittenden, 1972; Yonkee, 2005).

The arkosic grit and quartzite-grit members were deposited to the west in the Fremont Island area where they are >300 m thick. The basal member consists of upward-fining layers of pebbly conglomerate, feldspathic wacke, and mudstone (now slate) deposited as proximal turbidites. The overlying member contains upward-fining layers of medium-grained quartzite to mudstone deposited as medial turbidites, along with coarser layers containing feldspathic wacke similar in character to the basal member. Textural and mineralogical maturity increase upwards.

The pebbly slate and slate members vary in thickness and lithology between areas, interpreted to reflect syndepositional faulting. In the western Fremont Island area, the pebbly slate member contains outsized quartzite boulders interpreted to be glacial dropstones (Fig. 5C; Crittenden et al., 1983). The overlying member contains interbedded slate and fine-grained quartzite partly deposited as distal turbidites as the basin subsided. A 5-m-thick dolostone unit with positive $\delta^{13}C$ is present at the top of the member (Dehler et al., 2012). In the central Perry Canyon area, a <100-m-thick interval of graphitic slate rests nonconformably on basement rocks of the Facer Formation, which may have formed an uplifted block (Fig. 6D). Slate and pebbly slate thicken locally eastward, but are absent farther E in the Huntsville area.

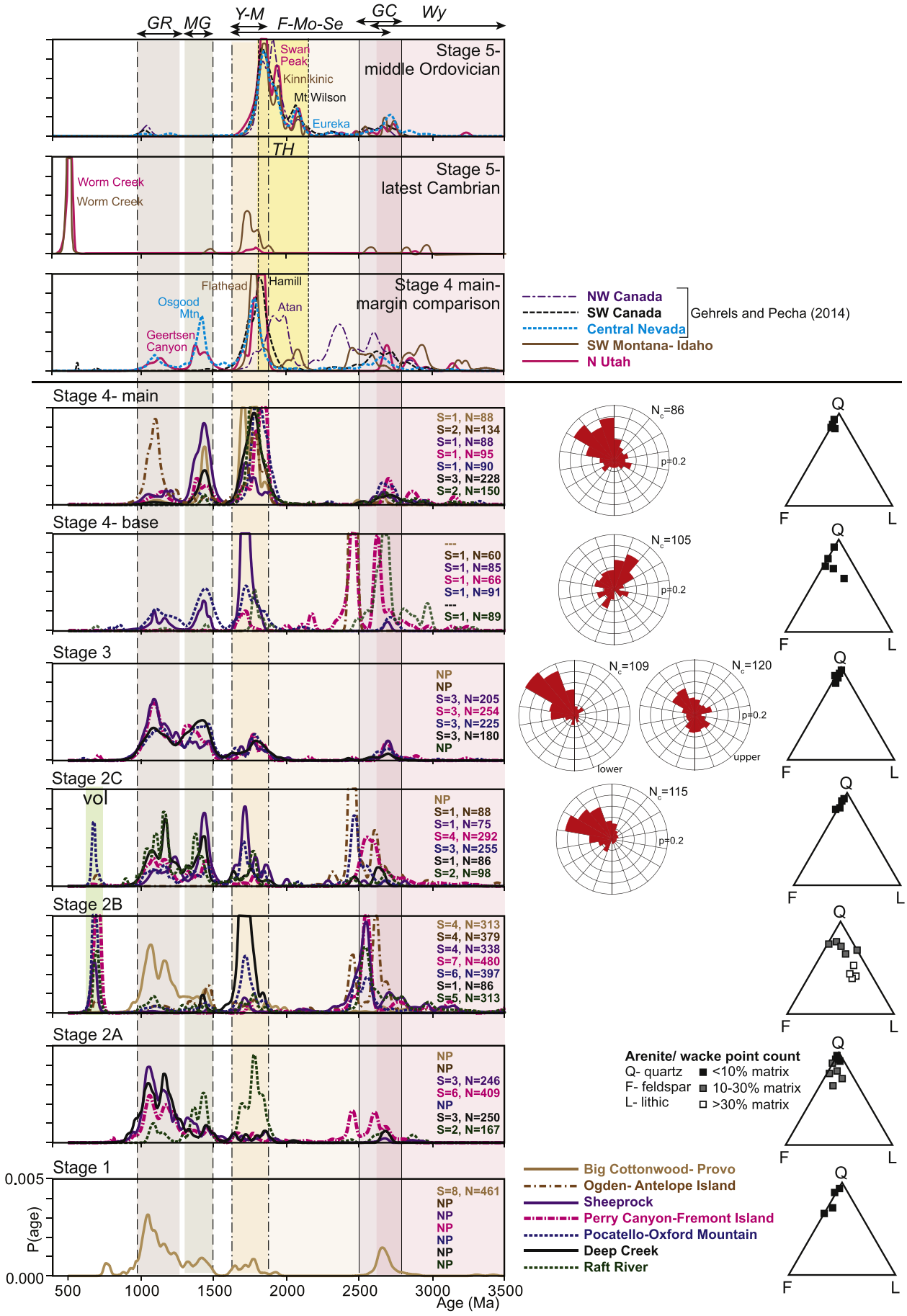
GR
MG
Y-M
F-Mo-Se
GC
Wy
Stage 5- middle Ordovician
Swan Peak
Kinnikinic
Mt Wilson
Eureka
TH
Stage 5- latest Cambrian
Worm Creek
Worm Creek
Stage 4 main-margin comparison
Flathead
Hamill
Osgood Mtn
Atan
Geertsen Canyon
NW Canada
SW Canada
Central Nevada
SW Montana- Idaho
N Utah
Gehrels and Pecha (2014)
Stage 4- main
S=1, N=88
S=2, N=134
S=1, N=88
S=1, N=95
S=1, N=90
S=3, N=228
S=2, N=150
Stage 4- base

S=1, N=60
S=1, N=85
S=1, N=66
S=1, N=91

S=1, N=89
Stage 3
NP
NP
S=3, N=205
S=3, N=254
S=3, N=225
S=3, N=180
NP
Stage 2C
vol
NP
S=1, N=88
S=1, N=75
S=4, N=292
S=3, N=255
S=1, N=86
S=2, N=98
Stage 2B
S=4, N=313
S=4, N=379
S=4, N=338
S=7, N=480
S=6, N=397
S=1, N=86
S=5, N=313
Stage 2A
NP
NP
S=3, N=246
S=6, N=409
NP
S=3, N=250
S=2, N=167
Stage 1
S=8, N=461
NP
NP
NP
NP
NP
NP
0.005
P(age)
0.000
500
1000
1500
2000
2500
3000
3500
Age (Ma)
Nc=86
p=0.2
Nc=105
p=0.2
Nc=109
lower
Nc=120
p=0.2
upper
Nc=115
p=0.2
Q
F
L
Arenite/ wacke point count
Q- quartz
F- feldspar
L- lithic
<10% matrix
10-30% matrix
>30% matrix
Big Cottonwood- Provo
Ogden- Antelope Island
Sheeprock
Perry Canyon-Fremont Island
Pocatello-Oxford Mountain
Deep Creek
Raft River

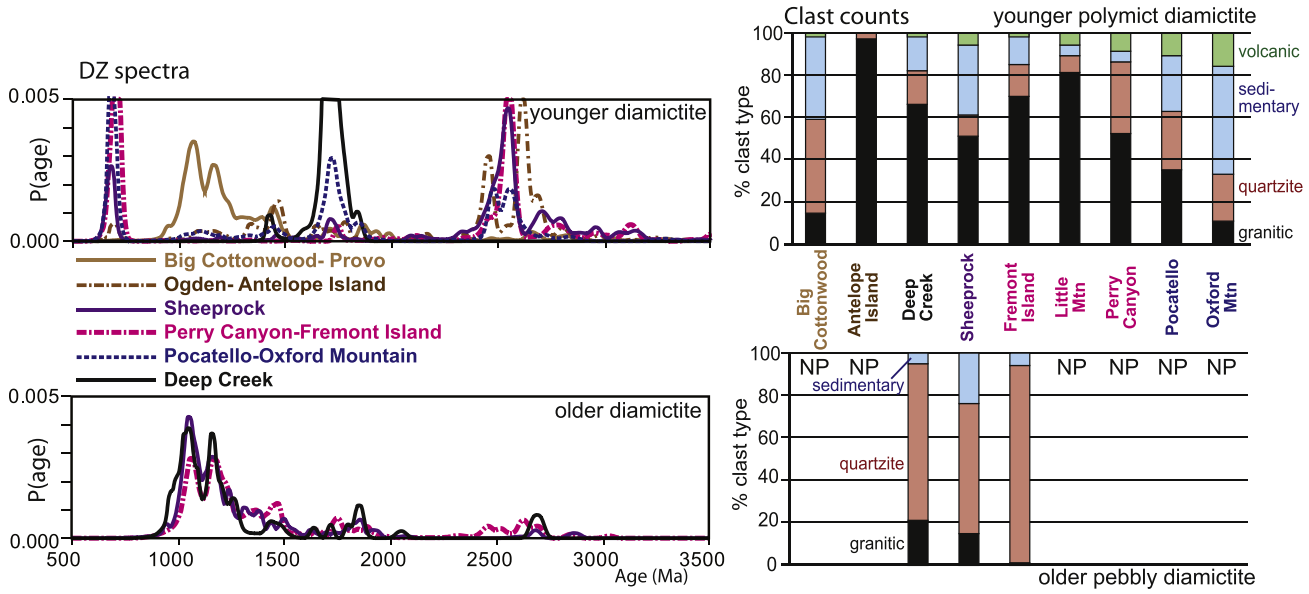

Fig. 8. Clast count and DZ spectra for older and younger diamictites. Clast counts include data from Blick (1979). Clast compositions and DZ patterns are distinctly different between pebbly diamictite of the older glacial episode and polymict diamictite of the younger glacial episode. NP- not present.

The volcanic member includes pillow basalts, agglomerate, and intrusive rocks (Fig. 5D), which are altered to greenstone consisting of albite, epidote, chlorite and actinolite. Pillow basalts and hyaloclastic material record submarine eruptions. Dikes and sills intrude pillow basalts and parts of the overlying diamictite. Geochemical characteristics of igneous rocks are described later. The diamictite member varies from >400 m thick at Fremont Island, to <100 m thick farther E in the Huntsville area. Diamictite consists of pebble to boulder (up to 5 m) clasts that sit in a sandy to micaceous matrix (Fig. 5E). Clasts include Fe-poor granites that are geochemically similar to leucogranite of the Grouse Creek block (Yonkee et al., 2013), along with subordinate quartzite and reworked sedimentary clasts (Fig. 8; Blick, 1979; Balgord et al., 2013). Lenses of volcaniclastic diamictite contain basalt, trachyte, and rhyolite clasts. Diamictite is typically massive, but stratified intervals of conglomerate, wacke, and mudstone are locally present, likely recording episodes of open water or deposition below non-grounded sea ice.

The greywacke member consists of volcaniclastic to feldspathic wacke, argillite, and minor carbonate, and has a thickness of ~200 m. Laminated pink dolostone with negative $\delta^{13}C$ characteristic of cap carbonates is exposed above diamictite north of Fremont Island, and a thin layer of laminated limestone is present near the base of the member in the Perry Canyon area (Dehler et al., 2012). Upward-fining layers of wacke to argillite display climbing-ripple cross-stratification and flame structures, which are interpreted to record rapid deposition as turbidites. The overlying Maple Canyon Formation consists mostly of subfeldspathic sandstone and has a thickness up to ~300 m. Sandstone displays low-angle tabular and trough cross beds that indicate overall W- to NW-directed paleoflow (Fig. 7). A ~20-m-thick unit of sandy limestone near the top of the formation in the Perry Canyon area records a transition to positive $\delta^{13}C$ values.

The overlying Kelley Canyon Formation consists of argillite and interbedded fine-grained quartzite that were deposited from suspension and as distal turbidites, and have a total thickness of 300–500 m. Quartzite increases in abundance upwards; the upper part of the formation contains siltstone and quartzite with syneresis cracks and is locally mapped as the Papoose Creek Formation (Crittenden, 1988). Mafic to ultramafic dikes crosscut the upper Perry Canyon to Kelley Canyon formations, recording waning stages of igneous activity.

DZ patterns vary with stratigraphic level and location. The basal arkosic grit displays DZ peaks at 2.45 Ga and 2.6–2.8 Ga, recording local sources from the Farmington zone and Wyoming province (23EAB10; Fig. 6D). The overlying pebbly slate and slate members (08EAB10, 11EAB10; Fig. 6D) contain abundant 1.0–1.3 Ga and 1.3–1.5 Ga DZ grains that record distal Laurentian sources and possible recycling from the UMG. Interbedded quartzite and slate farther E display a mix of Mesoproterozoic, 2.45 Ga, and 2.6–2.8 Ga grains that record a mix of distal and local sources (21JK08, 19AY11; Fig. 6D). DZ spectra for the diamictite member show a distinct change with prominent 2.55 Ga grains (41EAB10, 36EAB09, 17CD11, 13EAB10, 93EAB10; Fig. 6D), consistent with sources from ice sheets that flowed across the Grouse Creek block. Diamictite also contains young zircon grains related to felsic volcanism (Fig. 9E), which give maximum depositional ages of 702 ± 6 Ma and 683 ± 10 Ma respectively for lower and middle parts of the member (36EAB09, 93EAB10; Fig. 6D). Overlying volcaniclastic wacke contains abundant young grains that give a maximum depositional age of 667 ± 5 Ma (38EAB09; Fig. 6D). Ages of young grains decrease stratigraphically upward, suggestive that although reworked, these grains closely bracket depositional ages. The Maple Canyon Formation contains 2.6–2.8 Ga DZ grains, but lacks Paleoproterozoic grains, consistent with sources from the Wyoming province (18JK08, 55CD10, 99CAT22; Fig. 6D). Quartzite in the upper Kelley Canyon Formation contains abundant 1.0–1.3 Ga and 1.3–1.5 Ga grains that record a transition to distal Laurentian sources (01AY12, 56CD10, P87; Fig. 6D). The increase in distal sources, compositional maturity, and aerial extent of deposition are interpreted to reflect regional subsidence and reduced topography following cessation of early rifting.

4.2.5. Western region: Pocatello–Oxford Mountain area

Within SE Idaho, the interval includes the Bannock Volcanic, Scout Mountain, and upper members of the Pocatello Formation (Fig. 6E;

Fig. 7. Plots of combined DZ spectra for samples grouped by stage for each study area. Composite DZ spectra for different areas are similar for each stage and vary between stages. Number of samples (S) and total grains (N) for each composite spectra are listed. Paleocurrent data grouped by stage are shown in the rose diagrams (N_c is total number of directional data per plot). Point count data are shown on ternary plots. The top three plots compare DZ patterns along the length of the Cordillera margin and include samples from Gehrels and Pecha (2014) with names of stratigraphic units listed; TH—Trans-Hudson source area for early Cambrian strata in NW Canada and for middle Ordovician strata.

Link, 1982, 1987; Keeley et al., 2013). The Bannock Volcanic Member includes pillow lava, agglomerate, mafic dikes, and minor intercalated sandstone. The member is >200 m thick, but the base is covered and the nature of underlying strata is uncertain. Mafic rocks are altered to greenstone consisting of albite, epidote, actinolite, and chlorite, similar to the volcanic member of the Perry Canyon Formation. Near Pocatello, the Scout Mountain Member is ~600 m thick and includes volcaniclastic diamictite, sandstone and conglomerate, polymict diamictite, cap dolostone, and upper sandstone units (Fig. 6E; Link, 1987). Volcaniclastic diamictite contains a mix of reworked volcanic, sedimentary, quartzite, and granitic clasts, which sit in a chloritic matrix. Overlying sandstone is feldspathic, moderately to poorly sorted, and forms upward fining beds interpreted to be turbidites; conglomerate contains rounded quartzite, granitic, and volcanic basalt, trachyte, and rhyolite clasts. Polymict diamictite contains a mix of clast types (Fig. 8), some of which display facets and glacial striations, similar to the diamictite member of the Perry Canyon Formation. Diamictite is overlain by a 1- to 20-m-thick cap carbonate that consists of pink laminated, variably sandy dolostone with negative $\delta^{13}C$ (Dehler et al., 2011). The cap carbonate grades upwards into moderately to poorly sorted, volcaniclastic wacke to arenite, similar to the greywacke member of the Perry Canyon Formation, that is interbedded with limestone containing relict aragonite fans and negative $\delta^{13}C$ values (Lorentz et al., 2004). The upper member of the Pocatello Formation consists of 300–500 m of argillite and interlayered fine-grained quartzite, similar to the Kelley Canyon Formation, recording regionally extensive transgression. The overlying Blackrock Canyon Limestone contains micritic, oolitic, and sandy carbonate that have positive $\delta^{13}C$ values and record a return to shallow water conditions (Corsetti et al., 2007). The Papoose Creek Formation contains abundant quartzite with syneresis cracks that marks the transition to the Brigham Group. Only the Bannock Volcanic and lower part of the Scout Mountain Member are exposed at Oxford Mountain; the upper contact here is a detachment fault (Keeley et al., 2013).

DZ patterns for the Scout Mountain Member show a mix of 1.7–1.8 Ga, 2.45 Ga, 2.55 Ga, and 2.6–2.8 Ga grains reflecting sources from the Farmington zone, Grouse Creek block, and Wyoming province. Samples also contain young zircon grains with mean (maximum depositional) ages of 704 ± 5 Ma for the volcaniclastic diamictite (62JK09), 682 ± 6 Ma for the polymict diamictite (69CD11), and 676 ± 5 Ma for the upper sandstone unit (70CD11; Fig. 6E), close to a SHRIMP age of 667 ± 5 Ma for a nearby volcaniclastic bed (Fanning and Link, 2004). Mean ages decrease stratigraphically upward, similar to patterns in the Perry Canyon Formation, suggestive that young grains closely bracket depositional ages. However, zircon grains are reworked and subpopulations with age differences <10 Ma are not resolvable with LA-ICPMS or SHRIMP methods (Condon and Bowring, 2011). High-precision TIMS dating of zircon from volcanic diamictite at Oxford Mountain revealed 685.5 ± 0.4 Ma syndepositional grains, along with reworked grains having ages of 690–713 Ma (Keeley et al., 2013). Reworked volcanic clasts in conglomerate and diamictite have ages of 692 to 717 Ma (Fig. 6E; Fanning and Link, 2004; Keeley et al., 2013), which combined with ages of young zircon grains, indicate regional igneous activity spanned ~710–670 Ma. The upper member of the Pocatello Formation and Blackrock Canyon Limestone contain more abundant Mesoproterozoic DZ grains, reflecting increasing distal sources (71CD11, 61JK09, 68CD11; Fig. 6E).

4.2.6. Hinterland: Deep Creek area

Limited exposures of diamictite-bearing strata here are represented by units 1 to 6 of the Trout Creek sequence (Fig. 6F; Misch and Hazzard, 1962). These rocks were metamorphosed to amphibolite facies and penetratively deformed, such that primary sedimentary textures are obscured (Rodgers, 1984). Total structural thicknesses of the Trout Creek sequence is ~2000 m. Unit 1 consists of schist and interbedded quartzite, similar to the basal slate member of the Otts Canyon Formation exposed to the E in the Sheeprock Mountains. Carbonate and interbedded quartzite of unit 2 overlie the schist. Unit 3 contains pebbly diamictite with mostly quartzite clasts and minor granite cobbles, similar to the pebbly diamictite member of the Otts Canyon Formation (Fig. 8). Unit 4 contains interbedded quartzite and schist, and has an upper contact marked by laminated siltstone with dropstones, recording onset of the younger glacial episode. Unit 5 contains polymict diamictite with large granitic clasts (up to 3 m) that sit in a sandy to micaceous matrix, similar to the diamictite member of the Dutch Peak Formation (Fig. 8). Unit 6 consists of phyllite with thin beds of fine-grained quartzite, similar to the Kelley Canyon Formation, and is locally cut by mafic dikes and sills. Quartzite and phyllite with syneresis cracks in the upper part of unit 6 mark the transition into the McCoy Creek Group.

Schist and pebbly diamictite of units 1 to 3 have similar DZ patterns with abundant 1.0–1.3 Ga and 1.3–1.5 Ga grains, interpreted to reflect distal sources, along with possible recycling from the UMG (44PL09, 35PL09, 43PL09; Fig. 6F). Polymict diamictite of unit 5 has a distinctly different DZ pattern with mostly 1.6–1.8 Ga grains (41PL09; Fig. 6F), interpreted to reflect sources from ice sheets that flowed across the Yavapai–Mazatzal provinces. Nd isotopic values for part of the Trout Creek sequence also record input from Paleoproterozoic basement to the east (Farmer and Ball, 1997). Fine-grained quartzite and phyllite of unit 6 have a mixed DZ signature with more 1.0–1.3 Ga and 1.3–1.5 Ga grains and fewer Paleoproterozoic and Archean grains, recording an increase in distal sources (45PL09; Fig. 6F).

4.2.7. Hinterland: Raft River–Albion area

Strata in this area were overprinted by high-grade metamorphism and deformation, including thrusting along the Basin-Elba fault that was later reactivated during extension (Hodges and Walker, 1992) and omission of strata across low-angle normal faults (Wells, 1997). The Basin-Elba hanging wall exposes strata correlated with the McCoy Creek Group as described under stage 3 (Miller, 1983). Within the Basin-Elba footwall, Archean basement is overlain by the Elba Quartzite, schist of Upper Narrows, quartzite of Yost, schist of Stevens Spring, and quartzite of Clarks Basin (Fig. 6G; Compton, 1972). These strata have alternatively been interpreted as Paleoproterozoic, Neoproterozoic, and Cambrian (Armstrong, 1968; Compton et al., 1977; Wells et al., 1998); a Neoproterozoic age for the succession is indicated by the DZ data presented here. The Elba Quartzite includes a local basal quartz-cobble conglomerate that sits on aluminous material interpreted to be a fossil weathering zone. The main part of the formation consists of quartzose to subfeldspathic quartzite with thin schistose interbeds. The schist of Upper Narrows contains schist and subordinate feldspathic quartzite, meta-tuffaceous layers, and metadiabase (Compton et al., 1977). The quartzite of Yost contains subfeldspathic to micaceous quartzite with interbedded hematitic schist. The schist of Stevens Spring contains variably graphitic schist with interlayers of micaceous quartzite and amphibolite, and is lithologically similar to the Kelley Canyon Formation. The quartzite of Clarks Basin contains abundant micaceous to subfeldspathic quartzite, along with two thin carbonate layers having positive $\delta^{13}C$ (Wells et al., 1998).

The Elba Quartzite contains 1.7–1.8 Ga and Mesoproterozoic DZ grains that record input from distal Laurentian sources (RR3, 121PL02; Fig. 6G). The schist of Upper Narrows contains abundant Neoarchean grains, consistent with a source from the Grouse Creek block (14PL07; Fig. 6G), and includes a tuffaceous layer with euhedral zircon grains that give a mean (maximum depositional) age of 694 ± 5 Ma (RR91-24). The quartzite of Yost also contains Neoarchean and minor young (650–700 Ma) grains, along with 1.7–1.8 Ga and Mesoproterozoic grains (RR1, RR2; Fig. 6G). These units may be correlative with the diamictite and greywacke units of the Perry Canyon and Pocatello formations that have similar DZ patterns. However, diamictite is not found in the Raft River–Albion area, which may have been located on an uplifted block or distal to the ice-grounding line. The schist of Stevens Spring contains abundant Mesoproterozoic and lesser amounts of 1.7–1.8 DZ grains

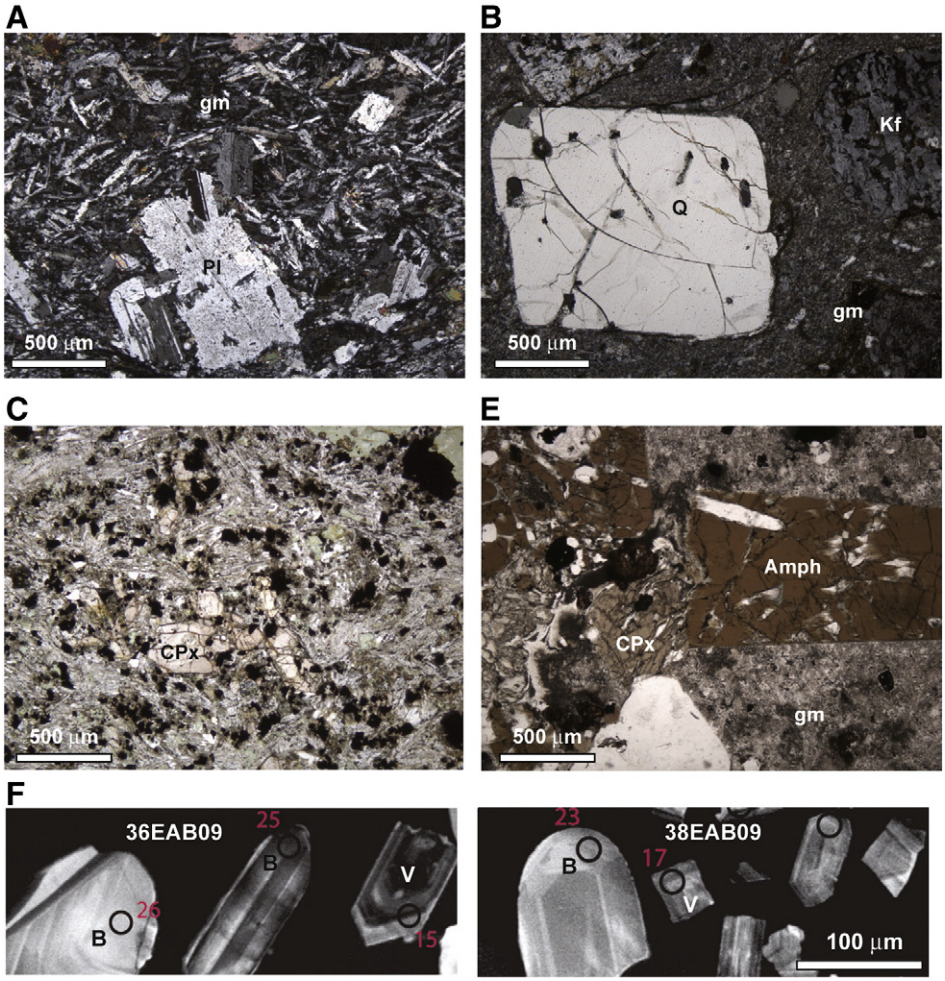

Fig. 9. Photomicrographs of igneous rocks and cathodoluminescence images of zircon grains. A. Greenstone from Perry Canyon Formation contains plagioclase phenocrysts (pl, altered to albite) that sit in groundmass (gm) of fine-grained albite, epidote, actinolite, and chlorite. B. Rhyolite volcanic clast from diamictite member of Perry Canyon Formation contains alkali feldspar (Kf) and partly resorbed quartz (Q) phenocrysts that sit in albite-rich groundmass (gm). C. Basalt from Browns Hole Formation contains plagioclase (altered to albite) and clinopyroxene (CPx) phenocrysts that sit in a fine-grained matrix. D. Trachyte clast from agglomerate in Browns Hole Formation with alkali hornblende (Amph) and titaniferous clinopyroxene phenocrysts. E. Cathodoluminescence images for samples 36EAB09 and 38EAB09 illustrate typical morphologies of detrital volcanic zircon grains (V, euhedral, simple zoning) and detrital basement grains (B, rounded, truncated and complex zoning).

(43PL08; Fig. 6G), broadly similar to the Kelley Canyon Formation. The quartzite of Clarks Basin shows a different pattern with abundant Neoarchean grains in the lower part and 1.7–1.8 Ga DZ grains in the upper part of the formation (GC-12, GC-1, 120PL02; Fig. 6G), similar to strata of stage 4, as described later.

4.3. Early rift-related igneous geochemistry

Igneous rocks of stage 2 include: basalt, agglomerate, and associated mafic dikes and sills altered to greenstone (Fig. 9A) that lie below and are locally interlayered with diamictite; basalt, trachyte, and rhyolite clasts within diamictite (Fig. 9B); and ultramafic to mafic dikes in the upper part of the interval. Greenstone samples from SE Idaho, northern Utah, and central Utah have subalkaline basaltic compositions based on major elements and display a tholeiitic trend (Fig. 10A). However, alkali contents may have been altered during metamorphism, and thus trace element ratios are also used to interpret rock types and tectonic setting. Zr/Ti and Nb/Y ratios confirm greenstone samples are mostly subalkaline to alkaline basalts (Fig. 10B). Most samples plot in fields related to intra-plate rift settings on tectonic discrimination diagrams (Fig. 10C). Rare earth element patterns for the Bannock Volcanic Member in SE Idaho also indicate an intra-plate rift setting (Harper and Link, 1986).

Reworked volcanic clasts in diamictite provide a broad sampling of associated igneous activity. Clast types include plagioclase-phyric basalt (similar to greenstone), trachyte with alkali feldspar phenocrysts, and rhyolite with partly resorbed quartz phenocrysts (Fig. 9B). Clasts display a range of silica contents and typically have high total alkali contents (Fig. 10A). Zr/Ti and Nb/Y indicate a range of rock types from alkali basalt to trachyte and alkali rhyolite (Fig. 10B), consistent with a rift setting. Hf isotopic ratios of reworked volcanic zircon grains indicate significant crustal contamination (Balgord et al., 2013; Keeley et al., 2013).

Ultramafic to mafic dikes that cross cut the upper Perry Canyon to Kelley Canyon formations in northern Utah record waning igneous activity and contain abundant chlorite and actinolite, rare biotite, and varying amounts of carbonate. Some dikes have <40 wt.% SiO_2, low alkali contents, and >10 wt.% volatiles, possibly related to carbonate metasomatism, (Fig. 10A).

4.4. Stage 3—middle mature siliciclastic package

This package is represented by the lower Brigham Group in the western region and McCoy Creek Group in the hinterland, but is generally absent to the east (Fig. 4; Crittenden et al., 1971; Stewart, 1972; Link et al., 1987, 1993). This package contains laterally consistent lithologies with similar DZ patterns (Fig. 7).

4.4.1. Eastern region

The interval is absent here except for a local unit of quartzite in the south-central Wasatch Range (Fig. 6A). This quartzite is <200 m thick and lies above an erosional unconformity on diamictite of the Mineral Fork Formation and below an unconformity at the base of Cambrian arkosic strata. The unit was originally identified as the Mutual Formation by Crittenden et al. (1952), but detailed correlation to the thicker strata exposed in the western region is uncertain (Christie-Blick, 1982).

4.4.2. Western region

The package here includes the Caddy Canyon, Inkom, and Mutual formations (Fig. 2). The Caddy Canyon Quartzite consists of mostly medium-grained, moderately to well-sorted, well-cemented quartz arenite, with subordinate pebbly quartzite, argillite, and rare carbonate having positive $\delta^{13}C$ (Smith et al., 1994). Tabular to trough cross beds record mostly W- to NW-directed paleoflow in shallow marine environments (Fig. 7). The formation thickens to the W from ~500 to 900 m in northern Utah and from ~600 to 1000 m in SE Idaho. In central Utah, the formation is ~1200 m thick in the Sheeprock Range (Fig. 4). In the San Francisco Mountains, a ~300 m-thick unit of quartz arenite mapped as the Caddy Canyon Quartzite, is underlain by a ~700-m-thick unit of interbedded quartzite, argillite, and minor carbonate, interpreted to reflect a facies change in the lower Caddy Canyon to upper Kelley Canyon formations (Christie-Blick, 1982).

Paleovalleys near the base of the Inkom Formation, which are up to 60 m deep and filled with pebble conglomerate, are interpreted to represent a sequence boundary related to incision during Marinoan (635–650 Ma) glaciation and sea level drawdown (Levy et al., 1994). The Inkom Formation is 100–200 m thick and consists of laminated to thin-bedded, silty to micaceous argillite and fine-grained quartzite that forms a distinctive regional marker. The Inkom records deposition in predominantly low-energy marine environments, possibly during sea level rise after glaciation. Sorensen and Crittenden (1979) reported possible tuffaceous beds in northern Utah, but petrographic examination failed to reveal volcaniclastic material.

The Mutual Formation contains mostly grayish-red, medium- to coarse-grained, moderately sorted, quartzose to subfeldspathic arenite, with subordinate argillite and conglomerate containing quartzite and red chert pebbles. Trough cross beds record variable paleocurrent directions in fluvial and shallow marine environments (Fig. 7; Link et al., 1987). The formation thickens to the W from ~300 to 600 m in central and northern Utah, and from ~400 to 800 m in SE Idaho. The upper part of the formation in SE Idaho includes a unit of hematite-rich argillite and sandstone, interpreted to be correlative with the volcanic member of the Browns Hole Formation in northern Utah that marks the transition to stage 4. In the Promontory area, the Mutual Formation is intruded by mafic dikes that are truncated by an unconformity at the top of the formation, recording erosion during transition to stage 4.

The Caddy Canyon to Mutual formations in central Utah (28CD10, 36CD10; Fig. 6C), northern Utah (57CD10, 59CD10; Fig. 6D), and SE Idaho (01JK08, 03Z08, 04Z08; Fig. 6E), have similar DZ spectra with abundant 1.0–1.3 and 1.3–1.5 Ga grains that record distal sources from the Grenville-Llano and mid-continent granite provinces, along with possible sediment recycling. The prominence of distal DZ sources, regionally extensive deposition of mature siliciclastic strata, and lack of volcanic rocks are interpreted to reflect sediment delivery into a broad basin undergoing subsidence following early rifting. Slight increases in 1.7–1.8 Ga and Archean DZ grains in the upper Mutual (04Z08; Fig. 6E) and Browns Hole (65CD10; Fig. 6D) formations record increased input from local sources during transition to stage 4.

4.4.3. Hinterland

The package here includes members A to H of the McCoy Creek Group (Misch and Hazzard, 1962; Woodward, 1963, 1967), which is interpreted to be an overall finer-grained correlative to the lower Brigham Group. Member A contains fine- to medium-grained, moderate- to well-sorted quartzite with subordinate phyllite, lithologically similar to the Caddy Canyon Quartzite, and is ~1200 m thick in the Deep Creek Range. Members B and C consist of phyllite and fine-grained quartzite with minor carbonate, and are interpreted to be correlative with the Inkom Formation. The members are ~200–400 m thick in the Deep Creek Range, but thicken farther west (Misch and Hazzard, 1962). Members D to G contain quartzite, phyllite, and pebbly quartzite with conglomeratic lenses, have a total thickness of ~800–1000 m, and are correlated with the Mutual Formation. Member G also contains minor carbonate. Member H is only locally developed and consists of well-sorted quartzite, which is tentatively correlated with the sandstone member of the Browns Hole Formation. Strata that likely correlate with the McCoy Creek Group are exposed in the hanging wall of the Basin-Elba fault in the Raft River–Albion area (Miller, 1983). Correlative strata, however, are not exposed in the Basin-Elba footwall, possibly due to omission across low-angle normal faults.

DZ spectra are similar through the interval with abundant 1.0–1.3 and 1.3–1.5 Ga grains, plus some 1.7–1.8 Ga grains (J8709E, J8710C, J8710D; Fig. 6F). Patterns are similar to those in the lower Brigham Group and record distal sources and wide dispersal of mature siliciclastic sediment across a broad basin.

4.5. Stage 4—upper variably immature siliciclastic and volcanic package

The start of stage 4 is marked by an influx of feldspathic, coarse-grained sediment within basal parts of the Prospect Mountain, Geertsen Canyon, and Camelback Mountain formations of the western region to hinterland, and within basal parts of the Tintic Quartzite in the eastern region (Figs. 4, 5G). Thin basalt flows are present in lower part of these formations and in the underlying Brown Hole Formation that contains 580 Ma trachytic basalt (Stewart, 1972; Sorensen and Crittenden, 1979). The main parts of these formations consist of subfeldspathic sandstone with interbeds of argillite. Trace fossils in upper parts of the formations include *Skolithus* and rare *Plagiogmus*, indicating an Early Cambrian age (Peterson and Clarke, 1974; Link et al., 1987). The formations are overlain by fossiliferous Middle Cambrian shale and limestone deposited over a wide region during the Sauk transgression (Rigo, 1968).

4.5.1. Eastern region

The Tintic Quartzite is exposed in the Provo to Antelope Island areas where the basal decollement of the Sevier thrust belt ramped down westward; correlative rocks are not exposed farther E where the basal decollement lies within Middle Cambrian shale (Royse, 1993). The basal part of the formation consists of interlayered conglomerate, feldspathic sandstone, and micaceous siltstone that were deposited across dissected paleotopography and have a total thickness of 0–100 m. Conglomerate and sandstone are moderately to poorly sorted and contain subrounded to angular clasts of quartzite, chert, and granitic material. Conglomerate and sandstone lenses are laterally discontinuous, display channels and trough cross beds, and record deposition in fluvial to shallow marine environments. The main part of the formation is 200–400 m thick and consists of mostly subfeldspathic, fine- to coarse-grained, moderately to well-sorted, well-cemented sandstone. Sandstone forms laterally continuous layers with widespread tabular to trough cross-beds that record overall NW-directed paleocurrents. Abundance and thickness of argillite interbeds increase upwards in the formation, recording a transition to lower energy, offshore marine environments. Basalt flows are present near the base of the Tintic Quartzite in the south-central Wasatch Range (Fig. 6A). Petrographic and geochemical characteristics of basalt are described later.

The basal part of the Tintic Quartzite in the Ogden area contains 2.45 Ga DZ grains derived from local basement sources (01AY09; Fig. 6B). The main part of the formation contains abundant 1.7–1.8 Ga DZ grains along with smaller 1.4 Ga and 1.1 Ga peaks (20CD10 in Fig. 6A; 17AY11, WT12-8 in Fig. 6B), reflecting sources from the

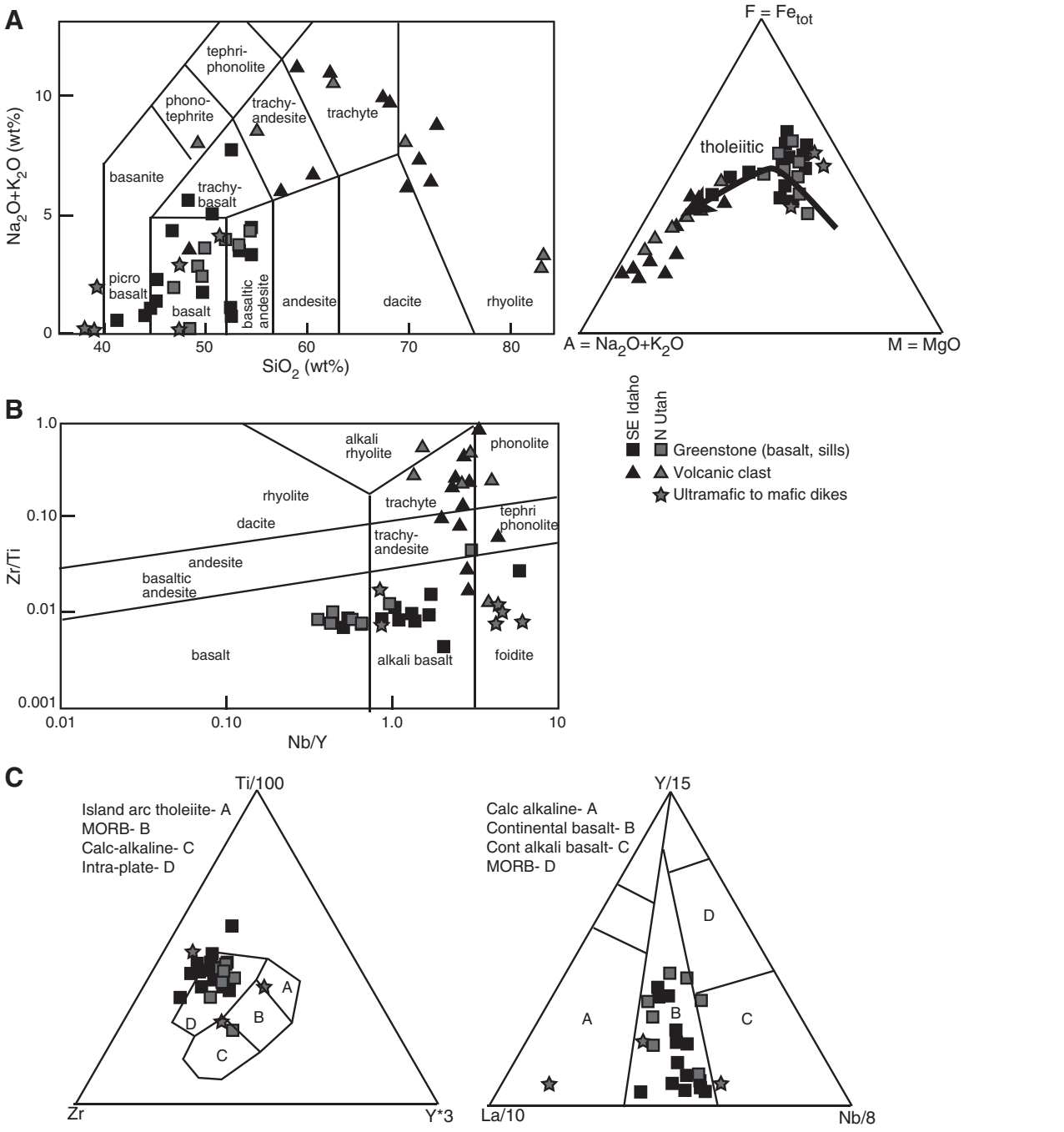

Fig. 10. Geochemistry of greenstone and volcanic clasts in diamictite for early (stage 2) igneous activity. A. Weight percent $Na_2O + K_2O$ and SiO_2 values indicate less altered greenstone samples are basaltic and volcanic clasts are trachytic to rhyolitic. Greenstone and volcanic clasts define a tholeiitic trend on an AFM diagram. B. Trace element Zr/Ti and Nb/Y ratios indicate greenstone samples are subalkaline to alkali basalts and volcanic clasts are trachyte to alkali rhyolite. C. Trace element ratios for greenstone and mafic dike samples plotted on petro-tectonic discrimination diagrams indicate an intraplate/rift setting. Zr–Ti–Y diagram from Pearce and Norry (1979). La–Y–Nb diagram from Cabanis and Lecolle (1989).

Yavapai–Mazatzal provinces and granitic plutons that intruded the southwestern U.S.

4.5.2. Western region and hinterland

The Prospect Mountain, Geertsen Canyon, and Camelback Mountain formations have similar lithologies and thicken westward. The basal part of these formations consists of ~50–300 m of interlayered conglomerate with quartzite and chert pebbles, moderately to poorly sorted, feldspathic sandstone, and micaceous siltstone, which were deposited across paleotopography that marks a sequence boundary (Link et al., 1987; Link and Christie-Blick, 2011). Laterally discontinuous lenses display trough cross beds and are interpreted to reflect fluvial to shallow marine deposition with overall NNE-directed, margin-parallel paleocurrents (Fig. 7), possibly along fault-controlled paleovalleys. The main part of these formations is ~600–1000 m thick and consists mostly of subfeldspathic, moderately to well sorted sandstone. Layers of quartz pebble conglomerate and pebble lags are locally present. Sandstone layers are laterally continuous and display tabular to trough cross-beds that record overall NW-directed paleocurrents, but with dispersion partly related to tidal and long-shore currents (Fig. 7). Argillite beds increase in abundance and thickness upwards, recording a transition to lower energy, offshore environments. Interbedded argillite and quartzite in the upper part of the package contain Early Cambrian fossils (Link et al., 1987).

Basalt flows are present near the base of the Prospect Mountain Formation from central Utah to E Nevada (Stewart, 1972). Basalt contains small, partly altered plagioclase and pyroxene phenocyrsts (Fig. 9C). Some flows preserve cryptic pillows and hyaloclastic material consistent with submarine eruptions (Fig. 5H). In northern Utah, basalt flows, agglomerate, and hematite-rich sandstone are present in the underlying Browns Hole Formation. Agglomerate contains pebble- to cobble-size clasts of basalt to trachyte with plagioclase, clinopyroxene, and hornblende phenocrysts (Fig. 9D). Hornblende from trachytic basalt in the Huntsville area has a K–Ar age of 580 ± 7 Ma (Crittenden and Wallace, 1973), but ages of basalt flows in the basal Prospect Mountain Formation are only bracketed as early Cambrian or older. Within SE California, the correlative upper Stirling to lower Woods Canyon formations contain late Ediacaran to basal Cambrian fossils (Corsetti and Hagadorn, 2000), display unconformities, and have similar changes in lithology and DZ patterns, but the exact position of the sequence boundary here is debated (Fedo and Cooper, 2001; Hogan et al., 2011). Thus later rifting, represented by a regional unconformity and basal part of stage 4, is taken to span 570–540 Ma.

The basal part of the Prospect Mountain and correlative formations displays variable DZ patterns with abundant 1.7–1.8 Ga grains in central Utah derived from local sources in the Yavapai province along the basin margin (35CD10; Fig. 6C), abundant 2.6–2.8 Ga and 1.7–1.8 Ga grains in northern Utah from the nearby Wyoming and Yavapai provinces (66CD10; Fig. 6D), and a mix of 1.7–1.8 Ga and Mesoproterozoic grains in SE Idaho (05Z08, Fig. 6E). The main part of the Prospect Mountain and correlative formations contains abundant 1.7–1.8 Ga DZ grains (34CD10 in Fig. 6C; 20AY11 in Fig. 6D; 09JK08 in Fig. 6E; J8709I, J8710A in Fig. 6F), interpreted to reflect sources mostly from the Yavapai province to the SE, along with possible recycling of grains from the upper part of Belt basin strata to the NE. Less abundant 1.3–1.5 Ga DZ grains may reflect sources from granitic plutons in the SW U.S. The scarcity of distal 1.0–1.3 Ga grains, which were abundant in underlying strata, may reflect disruption of regional drainage patterns during early uplift of the Transcontinental Arch. The upper part of the quartzite of Clarks Basin in the Raft River–Albion area also contains 1.7–1.8 Ga DZ grains and may be correlative to the main part of this package (GC1, 120PL02; Fig. 6G).

4.6. Late rift-related igneous geochemistry

Basalt flows across the region consist of plagioclase (now albite) and clinopyroxene phenocrysts in a groundmass of fine-grained albite, sericite, and chlorite (Fig. 9C). Basalts have broadly alkaline compositions based on major elements and display Fe-enrichment trends (Fig. 11A). However, alkali contents may have been altered, and thus trace element ratios are also used to interpret rock types. Zr/Ti and Nb/Y ratios confirm lavas are mostly alkali basalts (Fig. 11B). Most samples plot in fields related to intra-plate settings on petro-tectonic discrimination diagrams (Fig. 11C). Volcanic clasts in agglomerate of the Browns Hole Formation include plagioclase-phyric basalt and trachyte with alkali amphibole and titaniferous clinopyroxene phenocrysts (Fig. 9D). Clasts have high total alkalis and display a range of silica contents (Fig. 11A). Zr/Ti and Nb/Y also indicate a range of rock types from alkali basalt to trachyte (Fig. 11B), consistent with a rift setting. Early-phase (stage 2) and late-phase (stage 4) igneous rocks share similarities, including subalkaline to alkaline basalts, trachyte clasts in associated strata, and trace element patterns consistent with an intraplate rift setting. However, the volume of volcanic material erupted during stage 4 is less, rhyolite clasts are absent, and young zircon grains are very rare.

4.7. Stage 5—carbonate-rich package

Middle Cambrian to Devonian carbonate-rich strata with lesser amounts of fine-grained siliciclastic rocks were deposited in mostly shallow marine environments. Although different formation names are applied from Utah, Idaho, and Nevada, these strata share similarities. Middle to Late Cambrian strata deposited during the Sauk transgression consist of interlayered shale and micritic to oolitic limestone, overlain by dolostone with a thin unit of quartzose sandstone (Worm Creek Quartzite) that contains abundant 500 Ma DZ grains (Todt and Link, 2013; Fig. 7) likely sourced from igneous rocks in the Lemhi arch to the north (Lund et al., 2010). Lower to Middle Ordovician silty carbonate is capped by a distinctive interval of quartzose sandstone and shale (Swan Peak Formation and Eureka Quartzite), which was deposited during regression and contains abundant 1.8–2.1 Ga DZ grains (Fig. 7) likely sourced from Trans-Hudson basement exposed along the Peace River Arch farther NE (Gehrels et al., 1995; Gehrels and Pecha, 2014). Late Ordovician to Silurian dolostone was deposited during the Tippecanoe transgression, followed by regression and development of a regional unconformity. Overlying Devonian strata comprise a mix of silty carbonate and quartzose sandstone that record initial diruption of the margin.

5. Discussion

Neoproterozoic to early Paleozoic strata in Utah, Nevada, and SE Idaho record protracted rifting and tumultuous climatic events during development of the North American Cordilleran margin. Lithologic characteristics of sedimentary rocks, geochemical signatures of volcanic rocks, and DZ patterns, including young grains that bracket depositional ages, are first integrated to develop a chronostratigraphic framework and series of interpretive paleogeographic reconstructions. Next, stratigraphic thickness-age relations across the study area are combined with constraints on lithospheric structure to estimate subsidence patterns and evaluate rift processes. Finally, implications for Rodinia reconstructions and Neoproterozoic glacial models are discussed.

5.1. Chronostratigraphic framework and paleogeographic evolution

5.1.1. Stage 1

Siliciclastic strata of the Uinta Mountain Group (UMG) and Big Cottonwood Formation (BCF) are correlated based on lithology, stratigraphic position, and consistent DZ patterns (Fig. 6A). Rare young zircon grains in the lower UMG and microfossils in the upper UMG indicate depositional ages from *ca.* 770 to 740 Ma (Dehler et al., 2010). The UMG and BCF were deposited within an intracratonic basin, bounded to the N by an east-striking fault system, that may have been partly connected with the Chuar and Pahrump basins to the SW (Fig. 12A; Kingsbury-Stewart et al., 2013). Sediments were sourced from local basement uplifts to the N, and from distal areas to the SE, including recycling of material from the Grenvillian clastic wedge (Rainbird et al., 2012), with transport via a transcontinental river system. Magmatic activity was limited, with rare 770–780 Ma DZ grains in the UMG, Chuar Group, and middle Pahrump Group (Dehler et al., 2010; Mahon et al., 2014) likely related to early plume activity and intrusion of the 780 Ma Gunbarrel dikes (Harlan et al., 2003). The upper Chuar Group also contains a 742 Ma tuff (Karlstrom et al., 2000).

5.1.2. Stage 2A

The lower Perry Canyon Formation, Otts Canyon Formation, and lower Trout Creek sequence are correlated based on lithology, position, and consistent DZ patterns (Figs. 6, 7). The lower part of the interval contains feldspathic to quartzose strata that were deposited in an overall N–S-trending basin system during onset of extension (Fig. 12B). The basin system appears to have been narrower and deflected around the older Belt basin that may have acted as a stronger block. The middle part includes pebbly diamictite with quartzite clasts, interpreted to record an older glacial episode that may be correlative with 716 Ma glacial deposits in NW Canada (Macdonald et al., 2010). The upper part of the interval contains slate and fine-grained quartzite deposited as turbidites. DZ patterns record a combination of local and distal sources,

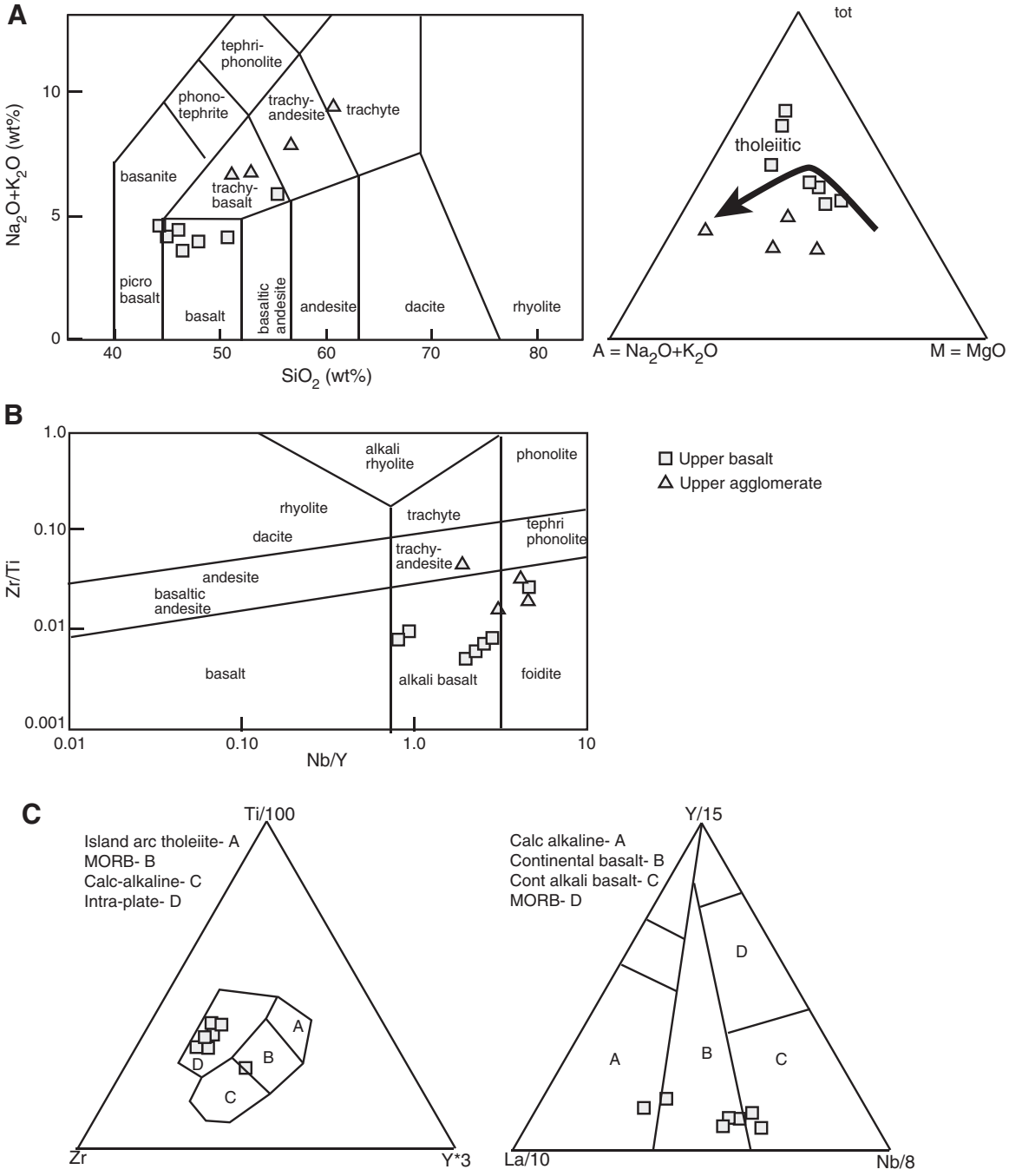

Fig. 11. Geochemistry of basalt flows and agglomerate clasts for late (stage 4) igneous activity. A. Weight percent $Na_2O + K_2O$ and SiO_2 values indicate samples are basalt to trachyte. Basalt flow samples define a tholeiitic trend on an AFM diagram. B. Trace element Zr/Ti and Nb/Y ratios indicate flows and clasts are alkali basalt to foidite. C. Trace element ratios plotted on petrotectonic discrimination diagrams indicate an intraplate/rift setting.

along with possible recycling from the UMG. These strata postdate the ~740 Ma top of the UMG and predate ~700 Ma initiation of widespread igneous activity recorded by mafic volcanic rocks and reworked volcanic zircon grains in overlying strata. The nature of the northern and western margins of the basin system is uncertain as stage 2A strata are only locally exposed.

5.1.3. Stage 2B

Mafic volcanic rocks (now greenstone) exposed in multiple sections have similar geochemical signatures and record widespread igneous activity during regional rifting (Fig. 10). Overlying polymict diamictites in the upper Perry Canyon, Mineral Fork, Dutch Peak, upper Trout Creek, and Pocatello formations display distinctive DZ patterns that record basement sources along the rift margin and reworking of felsic volcanic material (Figs. 6, 7). Maximum depositional ages for lower to upper parts of the polymict diamictite are ~700–670 Ma, and tuffaceous diamictite in SE Idaho has a zircon U–Pb TIMS age of 685.5 ± 0.4 Ma (Keeley et al., 2013), similar to a SHRIMP age of 685 ± 5 Ma for rhyolite associated with diamictite of the Edwardsburg Formation in central Idaho (Lund et al., 2003). Polymict diamictite was deposited over a wide region, contains rare dropstones and faceted clasts, and records a younger glacial episode (Fig. 12C). Interstratified conglomerate, wacke, and argillite in some sections indicate a dynamic environment with locally open water conditions. Variably preserved cap dolostone with negative $\delta^{13}C$ values and distinctive sedimentary structures records rapid deglaciation (Dehler et al., 2011; Hayes, 2013). Igneous

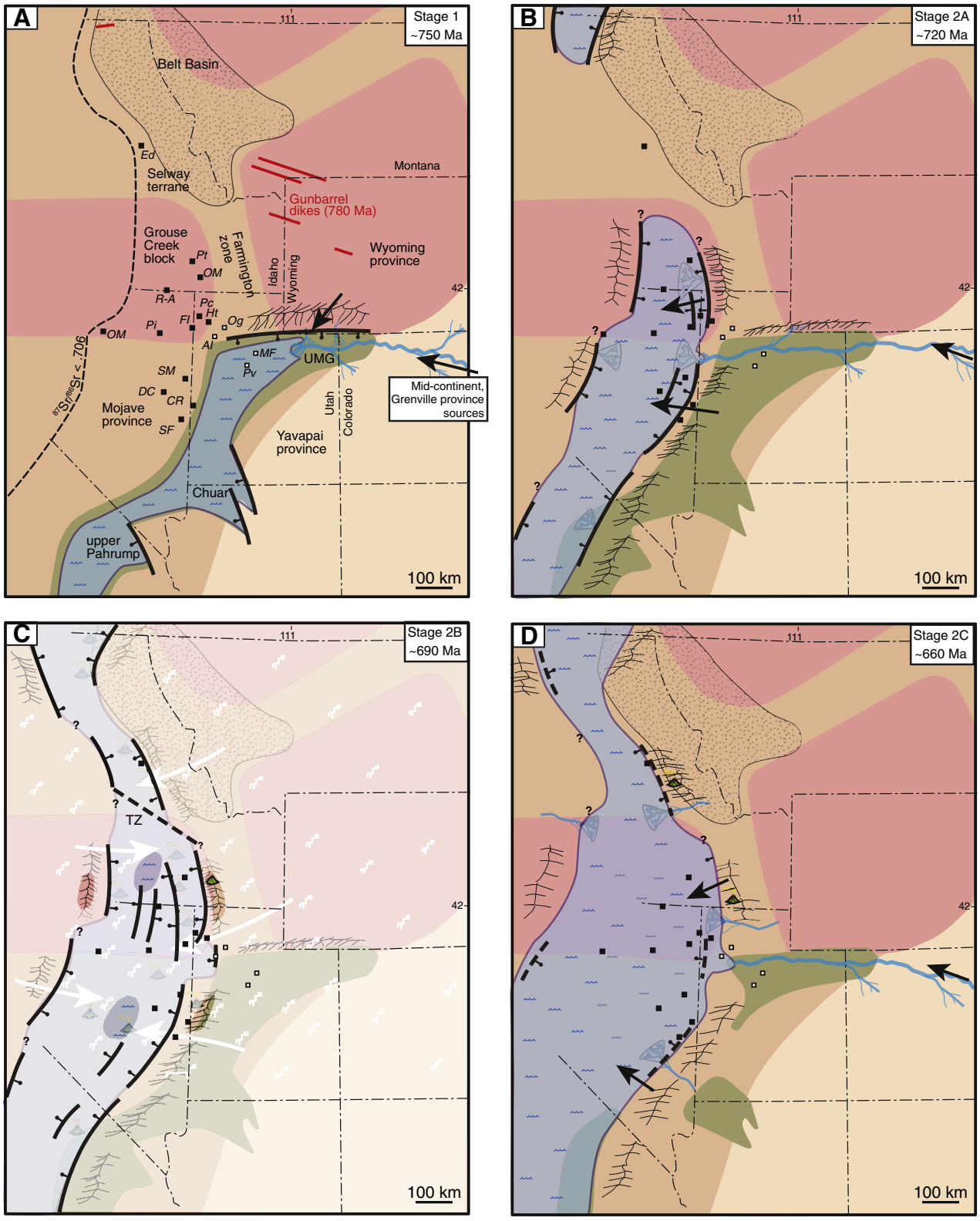
A
Stage 1
~750 Ma
Belt Basin
Ed
Selway terrane
Montana
Gunbarrel dikes (780 Ma)
Grouse Creek block
Pt
OM
Farmington zone
Idaho
Wyoming
Wyoming province
R-A
Pc
Ht
Pi
Fl
Og
Al
MF
Pv
UMG
SM
DC
CR
SF
Mojave province
Yavapai province
Utah
Colorado
Mid-continent, Grenville province sources
Chuar
upper Pahrump
100 km
B
Stage 2A
~720 Ma
C
Stage 2B
~690 Ma
TZ
D
Stage 2C
~660 Ma
mountains/ uplift
marine water
submarine fan
fault
volcanic source
glacial ice
fluvial system
paleocurrent
sediment source
Hinterland
DC- Deep Creek Range
Pi- Pilot Range
R-A- Raft River-Albion ranges
Ed- Edwardsburg
Os - Osgood Mountain
Western
Pt- Pocatello
OM- Oxford Mountain
Ht- Huntsville
PC- Perry Canyon
Fl- Fremont Island
SM- Sheeprock Mountains
SF- San Franscisco Mountains
Eastern
Og- Ogden
Al- Antelope Island
UM- Uinta Mountains
BC- Big Cottonwood
restored areas

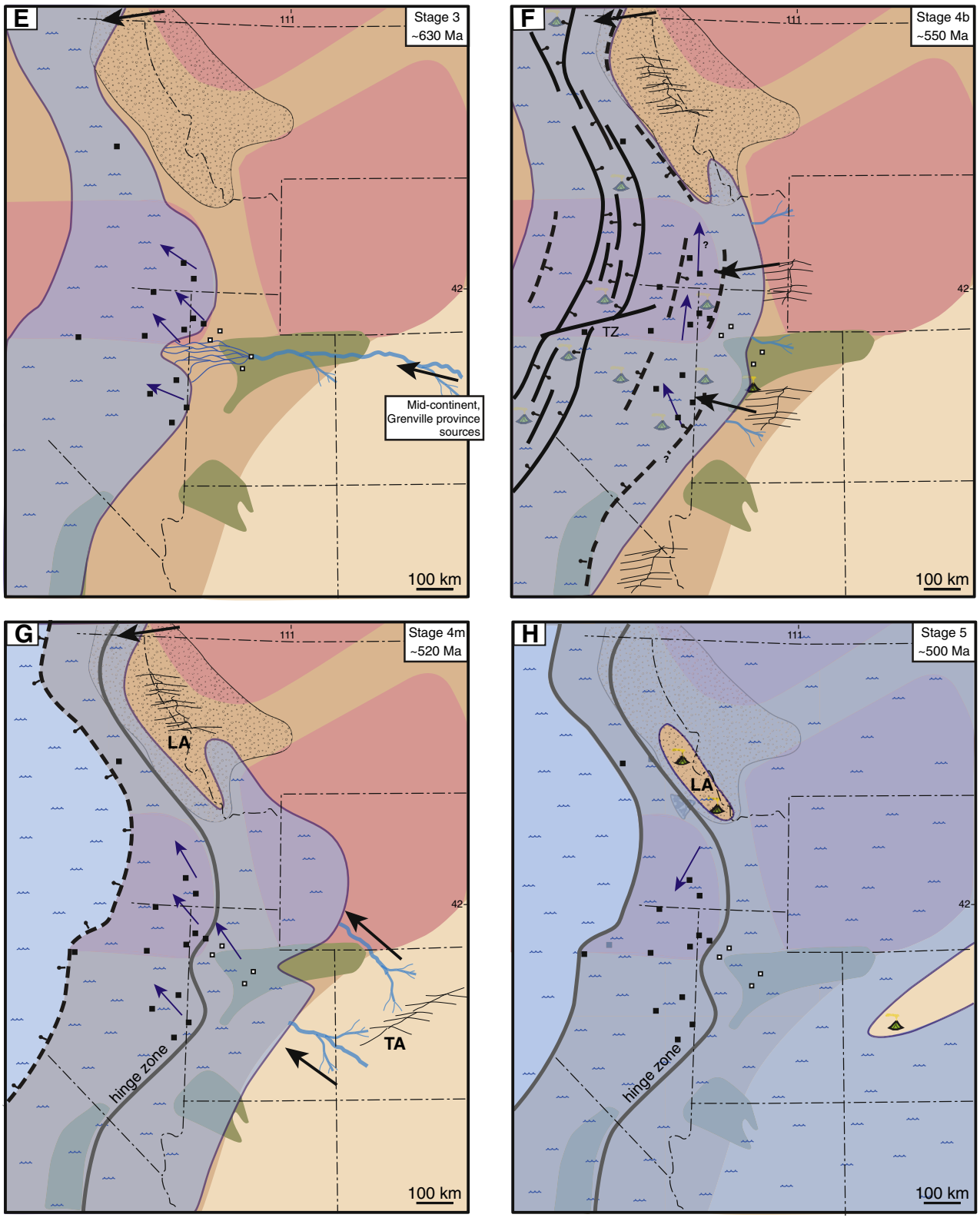

Fig. 12. Paleogeographic maps show interpreted sediment sources, depositional environments, schematic fault geometry (TZ—inferred transfer zone), and restored locations of study areas, along with Osgood Mountain (OM) in central Nevada and Edwardsburg (Ed) in central Idaho. Basement rocks are: Wyoming province and Grouse Creek block (pink), Farmington zone, Mojave province, and Selway terrane (salmon), and Yavapai province (light yellow-orange). Uinta Mountain Group (UMG, greenish brown) also shown. Stage 1—deposition of UMG in intracratonic basin. Stage 2A—deposition of turbidites in basin system during initial extension, which was followed by deposition of pebbly diamictite during the older glacial episode. Stage 2B—volcanism and deposition of polymict diamictite during the younger glacial episode, regional extension, and uplift of rift flanks. Stage 2C—deposition of fine-grained siliciclastics as volcanic activity wanes and basin system subsides. Stage 3—deposition of mature siliciclastics during subsidence along a failed rift. Stage 4 basal—deposition of immature siliciclastics and renewed volcanism during final rifting with concentrated extension to the west. Stage 4 upper—transition to drift and deposition of siliciclastics with sources from Transcontinental arch (TA). Stage 5—deposition of carbonate-rich strata along passive margin and onto craton during Sauk transgression, with local alkali igneous activity in the Lemhi arch (LA).

activity and basement uplift along the rift margin continued during deposition of overlying volcaniclastic wacke, which contains a 667 ± 5 Ma tuffaceous bed in SE Idaho (Fanning and Link, 2004).

5.1.4. Stage 2C

Argillite and fine-grained quartzite of the Kelley Canyon, uppermost Trout Creek, and upper Pocatello formations form a distinctive regional marker with similar DZ patterns (Figs. 6, 7). Strata were deposited during decreasing igneous activity and transition to regional subsidence with increasing input of sediment from distal sources (Fig. 12D). Water depth initially increased following early rifting, but then decreased as sedimentation exceeded subsidence, transitioning into deposition of fine-grained quartzite with syneresis cracks.

5.1.5. Stage 3

Mature siliciclastic rocks of the lower Brigham and McCoy Creek groups are correlated based on consistent lithologies and DZ patterns that record distal sources (Figs. 6, 7). Sediment may have been delivered via a transcontinental river system that crossed the now subdued margin of the former rift system, with strata deposited in mostly shallow marine to local fluvial environments across a broad, slowly subsiding basin (Fig. 12E). Paleocurrent data indicate a range of W- to N-directed offshore to longshore transport that mixed sediment in the basin. Incised valleys near the base of the Inkom Formation are interpreted to represent sea-level drawdown during Marinoan (635–650 Ma) glaciation (Levy et al., 1994), with overlying argillite deposited during deglaciation and sea-level rise. Renewed mafic volcanic activity at 580 Ma (Browns Hole Formation) and an increase in local basement sediment sources at the top of the interval mark the transition to stage 4.

5.1.6. Stage 4

The Prospect Mountain, Geertsen Canyon, and Camelback Mountain formations are correlated based on similar lithology and DZ patterns (Figs. 6, 7). The basal part of these formations is marked by an erosional unconformity, overlain by coarse-grained, feldspathic sediments derived from local basement sources and by associated basalt flows that record final rifting (Fig. 12F). Paleocurrent data indicate local NNE-directed sediment transport along the rift margin. The main part of these formations contains subfeldspathic sandstone with interbeds of argillite that increase in abundance upward, recording lower energy marine environments and transition to drift. Paleocurrent data indicate overall W- to N-directed offshore to longshore transport. Abundant 1.7–1.8 Ga DZ grains record basement sources along the developing Transcontinental Arch to the SE, along with possible recycling of grains from upper levels of the Mesoproterozoic Belt basin to the NE (Fig. 12G). Increases in sedimentary thickness from eastern to western areas may reflect cryptic normal faulting and extension by lower crustal flow, with faulting focused farther W near the $^{87}Sr/^{86}Sr = .706$ line that marked the final rifted margin of western Laurentia (Armstrong et al., 1977). Neoproterozoic to Cambrian strata deposited near the $^{87}Sr/^{86}Sr = .706$ line are locally exposed at Osgood Mountain in central Nevada (Rowell et al., 1979), and include lower strata with similar DZ patterns as the upper McCoy Creek Group (Linde et al., 2012), feldspathic strata with abundant 1.7–1.8 Ga DZ grains similar to the Prospect Mountain Formation (Stewart et al., 2001), and overlying deep water Cambrian mudstone and chert deposited along the continental slope.

5.1.7. Stage 5

Middle to Late Cambrian carbonate-rich strata accumulated in shallow waters of an expansive epicontinental sea as siliciclastic sources were mostly covered during the Sauk transgression. The Lemhi arch to the N had alkaline igneous activity and was a local sediment source (Todt and Link, 2013; Fig. 12H). Siliciclastic strata were deposited again during the middle Ordovician, with sources farther NE in the Peace River arch (Gehrels et al., 1995). Upper Ordovician to Silurian dolostone was deposited during the Tippecanoe transgression, followed by sea level drop and development of a widespread unconformity. Devonian strata were deposited during renewed transgression, followed by early disruption of the passive margin.

Broadly similar stratigraphic patterns are present in other regions along the North America Cordilleran margin (Fig. 2). Middle Neoproterozoic intracratonic basin strata (stage 1) are also present in SE California (Pahrump Group; Mahon et al., 2014) and NW Canada (Coates Lake Group; Rainbird et al., 1996), recording localized extension that overlapped with intrusion of the Gunbarrel and Franklin dike swarms. Diamictite- and volcanic-bearing strata form a distinctive package (stage 2) along the length of the margin, including the Kingston Peak Formation in SE California, Toby Formation and Irene Volcanics in SW Canada, and the Rapitan Group in NW Canada (Fig. 2). Many sections contain two diamictite intervals, similar to the study region, but geochronologic constraints are limited. A lower diamictite-bearing interval in NW Canada contains a 716 Ma tuff (Macdonald et al., 2010) and is overlain by black shale with a Re–Os age of 662 Ma (Rooney et al., 2014). A 685 Ma rhyolite associated with diamictite in central Idaho (Lund et al., 2003) is similar in age to the upper (polymict) diamictite in Utah to SE Idaho. A thick package of mature siliciclastic and minor carbonate strata (stage 3) overlies the diamictite-bearing interval along the length of the margin. Compared to the study region, this package is finer grained and thicker north of the Canadian border, likely indicating a wider, deeper basin (Ross et al., 1995). Overlying feldspathic, coarse-grained strata with local angular unconformities and basalts, including the Hamill Group and a 570 Ma basalt flow in SW Canada (Colpron et al., 2002), are interpreted to record final rifting (base of stage 4). A change to drift is marked by regionally extensive deposition of Middle Cambrian to Devonian carbonate-rich strata (stage 5) (Bond and Kominz, 1984; Levy and Christie-Blick, 1991). Although general stratigraphic patterns are broadly similar along the Cordilleran margin, DZ data indicate along-strike differences in source areas for some strata, with sources mostly from the Canadian shield to the north, and abundant Grenville and Yavapai–Mazatzal sources to the south, separated by a high in the area of the former Belt basin (Gehrels and Pecha, 2014). Ordovician strata display consistent DZ patterns along the length of the margin (Fig. 7).

5.2. Temporal and spatial patterns of subsidence and extension

Accumulation of thick Neoproterozoic to Devonian strata in the west-central U.S. reflects generation of accommodation space from a combination of sea level change, syndepositional faulting, regional subsidence from crustal thinning, and regional uplift to subsidence from mantle lithosphere thinning to subsequent cooling. Tectonic subsidence, Y, was estimated from stratigraphic thickness-age data, corrected for sediment loading, compaction, changes in sea level, ΔSL, and water depth, Wd, using the back-stripping relation

$$Y = \Phi * [S_d(\rho_m - \rho_{sd})/(\rho_m - \rho_w) - \Delta SL * (\rho_m)/(\rho_m - \rho_w)] + (Wd - \Delta SL) \quad (1)$$

where Φ is a basement response function related to flexural loading (local Airy compensation is used here, with Φ set to 1), S_d is sediment thickness corrected for compaction, and ρ_m, ρ_w, and ρ_{sd} are specific gravities for mantle, water, and mean of decompacted strata (Bond and Kominz, 1984; Angevine et al., 1990). Sea level changes during the Paleozoic were taken from Haq and Schutter (2008). Glacio-eustatic changes during the Neoproterozoic have large uncertainties and units used for subsidence analysis were chosen to span pre- to post-glacial strata. Decompacted thickness, S_d, was calculated using relations for porosity, θ, as a function of depth, z, following

$$S_d * (1-\theta) = S_0 * (1-\theta_0) = S_f; \theta = \theta_0 * \exp(-z/h_0) \quad (2)$$

where S_f is final (measured) stratigraphic thickness, S_0 is initial sediment thickness, θ_0 is initial porosity, and h_0 is a depth scaling factor; values of

θ_0 and h_0 depend on lithology and were based on the minimum compaction model of Bond and Kominz (1984) and assuming sediment cement was locally derived. Stratigraphic units were progressively added from oldest to youngest, with porosities integrated over burial depths to estimate S_d, θ, and ρ_{sd} of units for each time step. Uncertainties in estimated tectonic subsidence, Y, are related to measurement errors and local variations in final stratigraphic thicknesses (~±100 m for a 1000 m thick unit), changes in water depths (<100 m for shallow marine strata), and departure from the assumed compaction model.

Tectonic subsidence patterns are compared with relations predicted from simple models for pure-shear thinning of crust and mantle lithosphere followed by cooling (McKenzie, 1978; Royden and Keen, 1980; Cochran, 1983). For rapid extension (time <20 m.y.), initial model subsidence, S_0, from tectonic thinning is given by:

$$S_0 \approx [(\rho_m - \rho_c)/(\rho_m - \rho_w)] * Z_c * (1 - 1/\beta_c) - [\rho_m/(\rho_m - \rho_w)] * (\alpha_v * T_a/2) * Z_m * (1 - 1/\beta_m) \quad (3)$$

where Z_c and Z_m are pre-rift thicknesses of the crust and mantle lithosphere (taken respectively as 40 km and 160 km based on geophysical imaging of non-rifted lithosphere preserved to the east Obrebski et al., 2011); ρ_m, ρ_c, and ρ_w are specific gravities for mantle, crust, and water (respectively 3.3, 2.8, and 1.0); T_a is temperature at the top of the asthenosphere (1300 °C); α_v is the coefficient of thermal expansion ($3 \times 10^{-5}\ K^{-1}$); and β_c and β_m are thinning factors for crust and mantle lithosphere ($\beta = h_i/h_f$, the ratio of initial to final thickness of a layer, which for plane strain is equal to the extensional stretch; Royden and Keen, 1980). Subsequent thermal subsidence, S_T, for conductive cooling with constant thermal diffusivity is approximated by:

$$S_T \approx \left[4 * Z_L * \alpha_v * T_a/\pi^2 * \rho_m/(\rho_m \rho \rho_w) * (\beta_L/\pi) * \sin(\pi/\beta_L)\right] * (1 - \exp(-t/\tau)) \quad (4A)$$

where Z_L is initial lithosphere thickness, t is time since cessation of rifting, β_L is an effective thinning factor for crust and mantle lithosphere, and $\tau = (Z_l)^2/\kappa$ is a time factor related to length scale and thermal diffusivity ($\kappa = 32\ km^2$/m.y.). For slow rifting, subsidence is given by

$$S_T = [4 * Z_L * \alpha_v * T_a/\pi^2 * \rho_m/(\rho_m - \rho_w) * \textstyle\sum_{n=1,\infty} A_n * \sin(n\pi/Z_L)] * (\exp(-t/\tau)) \quad (4B)$$

where A_n are Fourier series coeficients for the appropriate boundary conditions (Cochran, 1983; Karner et al., 1997). Eqs. (4A) and (4B) predict concave-up shaped subsidence curves, which can be compared with observed stratigraphic thickness-age relations to give first-order estimates of extension timing and magnitude. Thickness-age curves for the western region display two concave-up segments that followed rifting concentrated at ~700–670 Ma and 570–540 Ma. Details of synrift subsidence/uplift depend on thinning histories; for the first-order model presented here, thinning rates were taken as constant in 10 m.y. time steps, except for minor thermal thinning from 570 to 560 Ma to simulate development of a regional unconformity.

Localized subsidence along the UMG basin (stage 1,~770–740 Ma) was related to local faulting that had a different spatial pattern compared to subsequent rifting. Intrusion of the ~780 Ma Gunbarrel dikes and ~720 Ma Franklin dikes to the N may reflect mantle plume activity with associated thermal uplift that set the stage for future extension (Harlan et al., 2003; Ernst and Bleeker, 2010).

Onset of extension along a N–S (present day coordinates) basin system is recorded by local deposition of up to 1000 m of siliciclastic strata of the lower Perry Canyon and correlative formations during stage 2A (~720–700 Ma). Lateral variations in lithology, thickness changes, and local unconformities suggest syndepositional faulting, but evidence for volcanic activity is limited. Early, localized uplift is reflected in DZ patterns with a mix of local and distal sources. Early rifting, igneous activity, and glacio-eustatic sea level changes are recorded by deposition of up to 1000 m of diamictite- and volcanic-bearing strata of the upper Perry Canyon and correlative formations during stage 2B (~700–670 Ma). DZ patterns record local sources and uplift of the rift margin. Transition to thermal subsidence is recorded by deposition of up to 800 m of fine-grained strata of the Kelley Canyon and correlative formations during stage 2C. Continued subsidence is recorded by deposition of 2000–3000 m of mature siliciclastic strata of the lower Brigham and McCoy Creek groups during stage 3 (broadly bracketed from 660 to 580 Ma). The inactive rift margin had limited topography based on DZ patterns with distal sources, and igneous activity was minimal during this stage. Subsidence patterns for stages 2 to 3 are consistent with ~25–40% crustal and mantle lithosphere thinning in the western region ($\beta_c \sim \beta_m \sim 1.3$–$1.7$), followed by thermal subsidence (Fig. 13).

Renewed rifting is recorded by development of a regional unconformity followed by influx of coarse-grained, feldspathic sediment and mafic volcanism in the basal Prospect Mountain and correlative formations during early stage 4 (~570–540 Ma), conistent with a component of initial thermal uplift (with model $\beta_m = 1.05$ from 570 to 560 Ma to simulate the regional unconformity). Westward increases in sedimentary thickness likely reflect crustal thinning, but evidence for surface normal faulting is limited. The main part of the Prospect Mountain and correlative formations records a transition to drift. Thermal subsidence along a passive margin (stage 5) is recorded by deposition of up to 5000 m of Middle Cambrian to Devonian, mostly shallow marine, carbonate-rich strata in the western region. Sedimentation was approximately balanced by subsidence and eustatic sea level rise, with local unconformities and influx of siliciclastic material during episodic regressions. Corresponding strata are <2000 m thick in the region east of the Wasatch hinge zone (Hintze and Kowallis, 2009), where deposition was partly related to sea level rise, sediment loading, and flexural subsidence. Subsidence patterns for stages 4 to 5 are consistent with an additional ~15–35% crustal and mantle lithosphere thinning in western areas ($\beta_c \sim 1.2$–1.5 and total $\beta_m \sim 1.4$–1.6; Fig. 13). Extension was concentrated farther west near the $^{87}Sr/^{86}Sr = .706$ line that marked the rifted margin of western Laurentian. Note, comparison of model β values to estimated tectonic subsidence based on local Airy compensation may lead to overestimates of extension toward the basin margin where isostatic flexure contributed to subsidence over a broader area.

In summary, stratigraphic thickness-age relations, igneous activity, and changes in DZ patterns indicate two episodes of rifting concentrated at *ca.* 700–670 Ma and 570–540 Ma. Early rifting was incomplete and followed by thermal subsidence and deposition of mature siliciclastic rocks. Final rifting involved additional thermal thinning and regional extension, followed by deposition of a thick package of carbonate-rich strata along a passive margin. Thickness-age relations in the study region are similar to relations for other areas along the North American Cordilleran margin documented by previous studies (Bond and Kominz, 1984; Bond et al., 1984, 1985; Levy and Christie-Blick, 1991). However, crustal thinning values estimated herein ($\beta_c \sim 1.2$–1.5) during final (~570–540 Ma) rifting are less than values given in these previous studies, reflecting contributions of early rifting, compaction of underlying strata, and Cambrian eustatic sea level rise incorporated into this analysis. The numeric age of 540 Ma for transition to drift estimated herein is slightly younger than in these previous studies, reflecting changes in the geologic time scale; previous studies also placed the drift transition near the basal Cambrian.

5.3. Rift processes

Patterns of subsidence, upper crustal faulting, and lithospheric thinning along rifts provide a partial record of tectonic processes. Previously proposed models for rifts in general and the North American Cordilleran margin in particular include: (1) uniform pure shear extension of crust

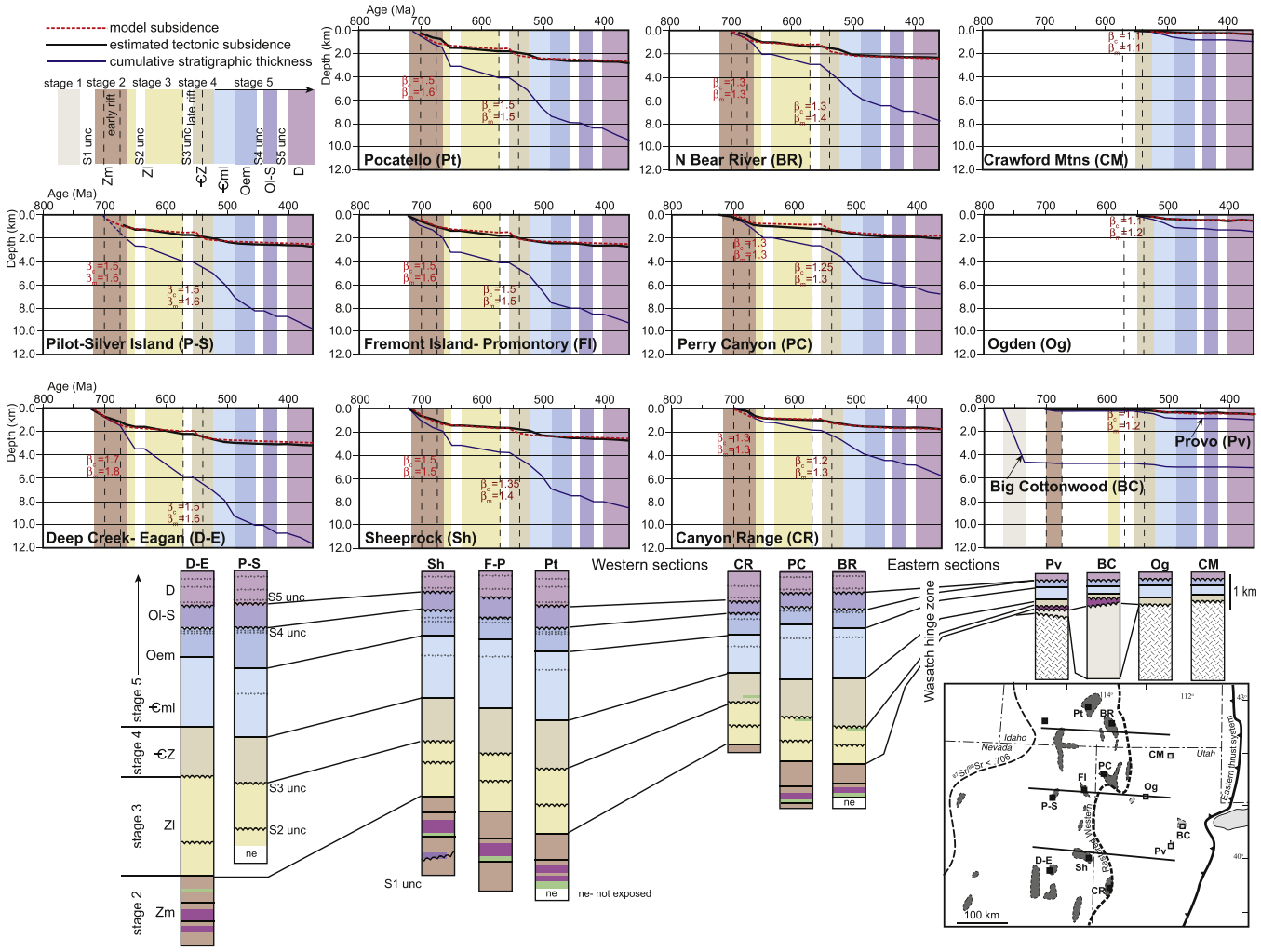

Fig. 13. Cumulative stratigraphic thickness, estimated tectonic subsidence, and model subsidence for early and final rifting intervals (dashed lines) each followed by thermal relaxation. Inset map shows locations of stratigraphic sections. Model subsidence calculated using method of Royden and Keen (1980) and Cochran (1983) with crustal and mantle lithosphere thinning values (β_c and β_m) that fit data listed for each stratigraphic section. Model subsidence/uplift during rifting intervals calculated using 10 m.y. time steps with constant thinning rates, except for $\beta_c = 1$ and $\beta_m = 1.05$ for 570–560 Ma to simulate thermal thinning and development of the S3 unconformity. Patterns for western sections are consistent with 25–40% extension during early rifting and subsidence (stages 2 and 3), and 20–35% additional extension during final rifting followed by thermal subsidence along a passive margin (stages 4 and 5). Major unconformities and sequence boundaries S1 to S5 indicated.

and lithospheric mantle (McKenzie, 1978), which was applied by Bond and Kominz (1984) and Bond et al. (1984, 1985) to estimate early Paleozoic subsidence patterns along the Cordilleran margin; (2) concentrated simple shear and extension along a lithospheric-scale, low-angle detachment zone (Lister et al., 1986), which was applied by Lund (2008) to interpret changes in rift characteristics along the Cordilleran margin; and (3) depth-dependent extension and necking of crust and lithospheric mantle (Braun and Beaumont, 1989; Davis and Kusznir, 2004), which is predicted by thermo-mechanical models (Huismans and Beaumont, 2008).

Model 1 predicts uniform crustal and mantle lithosphere thinning and extension with initial subsidence, followed by thermal subsidence as mantle lithosphere cools and thickens (Fig. 14A). Continued extension leads to development of a new ocean basin with symmetric passive margins. Igneous processes may accompany tectonic extension and modify subsidence patterns (Fig. 14B; Buck, 2004). Dike intrusion decreases lithospheric strength and partly accommodates extension, resulting in less crustal thinning, which combined with thermal thinning of mantle lithosphere may lead to initial uplift rather than subsidence. Parts of rift zones have extensive volcanic deposits and widespread dike intrusions (White and McKenzie, 1989), whereas other parts may lack widespread surface volcanic rocks but still have dikes present at depth that contribute to reduced lithospheric strength during rifting (Buck, 2004).

Model 2 predicts spatially decoupled crustal and mantle lithosphere extension across low-angle detachment and associated listric normal faults, with initial subsidence where crust is extended and initial uplift where mantle lithosphere is attenuated, followed by spatially variably thermal subsidence (Fig. 14C). The dip and shear sense of the detachment may change across transfer zones along the length of a rift. Continued extension leads to development of an asymmetric "lower plate" margin with highly thinned crust and tilted half grabens above normal mantle, and an "upper plate" margin with slightly thinned crust above highly attenuated mantle lithosphere. This model predicts paired margins with opposite asymmetry. However, some paired margins have "upper plate" characteristics (limited upper crustal extension) on both sides of ocean basins, indicating other processes may lead to decoupled crust and mantle lithosphere extension (Driscoll and Karner, 1998; Davis and Kusznir, 2004).

Model 3 incorporates depth-dependent rheology and decoupling of crust and mantle lithosphere extension, which give rise to a variety of rift styles (Fig. 14D; Buck, 1991; Davis and Kusznir, 2004). Variations in rift styles are related to: initial crust and mantle lithosphere thicknesses; rheology that depends on thermal state and fluids; topography;

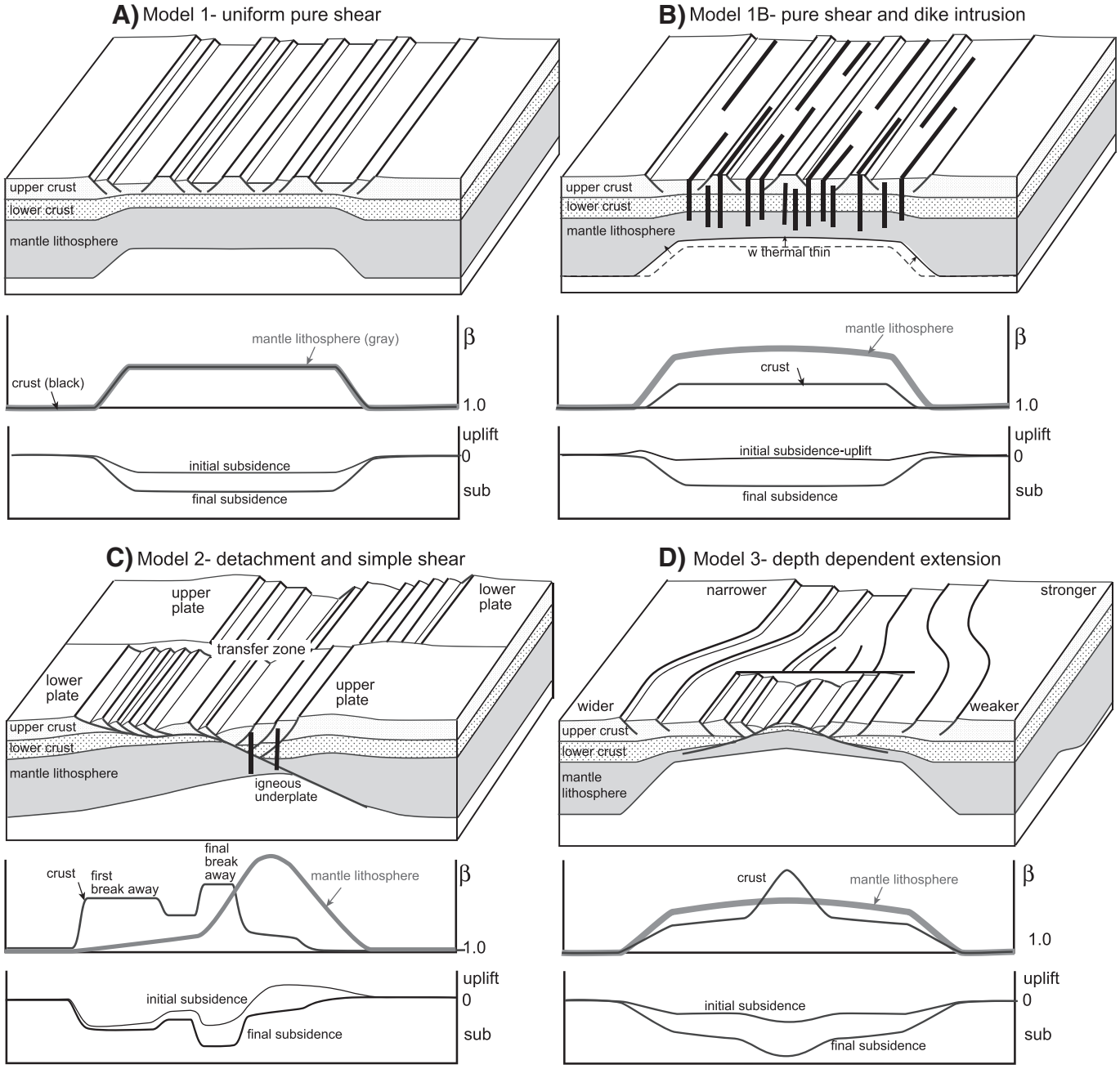

Fig. 14. Block diagrams illustrate idealized kinematic models of rifting. Initial tectonic and final thermal subsidence patterns are schematically indicated. A. Uniform pure shear thinning of crust and mantle lithosphere based on McKenzie (1978). B. Minor thinning of crust, thermal thinning of mantle lithosphere, and intrusion of dikes that partly accommodate extension based on Buck (2004). C. Simple shear concentrated along a lithospheric detachment based on Lister et al. (1986). Areas of highly thinned crust and mantle are decoupled across the detachment, with asymmetric extension and thermal subsidence in "upper plate" and "lower plate" blocks. Asymmetry may change across a transfer zone. D. Depth-dependent crust and mantle lithosphere thinning with localized necking based on Davis and Kusznir (2004). Rift zone width may vary, with narrower rift in stronger lithosphere.

boundary conditions and associated driving forces; and igneous activity (Buck et al., 1999; Frederiksen et al., 2001; Cloetingh et al., 2003; Buck, 2004; Huismans and Beaumont, 2008). Narrow (~100 km wide) rift zones with pure shear extension are favored by initially strong, thick lithosphere (similar to model 1). Low-angle detachment faults and decoupled extension are favored by initially thick, weak crust (similar to model 2).

Subsidence patterns, igneous activity, and constraints on lithosphere thermal state in the study region are combined to develop a simple, interpretive model of evolving rift processes and lithosphere strength. The thermal state of pre-rift lithosphere in the region is constrained by characteristics of non-rifted lithosphere preserved to the east. Geophysical (Schmandt and Humphreys, 2010; Obrebski et al., 2011) and isotopic data (Livaccari and Perry, 1993) indicate Archean to Paleoproterozoic mantle lithosphere to the east has thickness of ~200 km, and xenolith data (Glebovitsky et al., 2004) indicate a low mantle geothermal gradient of ~6 °C/km (and basal heat flow of ~18 mW m^{-2} for mantle thermal conductivity k = 3 W m^{-1} K^{-1}). Thermochronologic data from basement rocks in Wyoming (Peyton et al., 2012) indicate a long-term, upper crustal geothermal gradient of ~18 °C/km (and surface heat flow of ~45 mWm^{-2} for crustal k = 2.5 W m^{-1} K^{-1}). A pre-rift geotherm, calculated using these values and internal heat production rates of 1.0 and 0.4 μW m^{-3} for upper and lower crustal thicknesses of 20 km each, indicates an initially cool, thick lithosphere (Fig. 15A). A simple rheology model for these thermal conditions and a low strain rate of ~10^{-17} s^{-1} prior to rifting, constructed using the

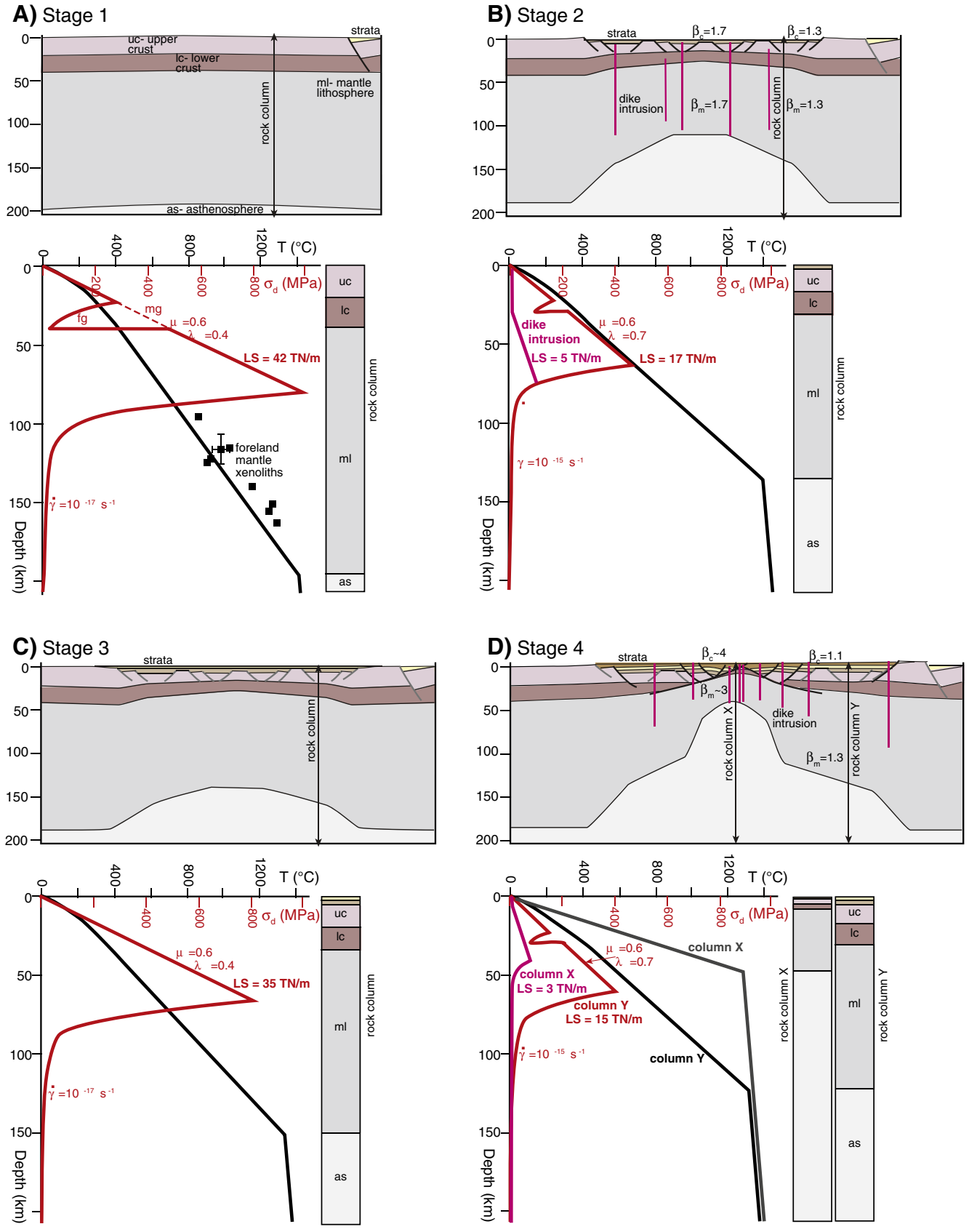

Fig. 15. Schematic lithospheric cross sections, geotherms (solid), and differential stress (dashed) profiles during stages 1 to 4. The initial geotherm is constrained by mantle xenolith data preserved to the east. Stress profiles are based on: normal fault failure given by $\sigma_s = \mu(\sigma_n - P_f)$, where σ_s is resolved shear stress, $\mu = 0.6$ is the friction coefficient, σ_n is resolved normal stress, and P_f is fluid pressure with $\lambda = 0.4$ to 0.7 being the fluid- to lithostatic-pressure ratio for hydrostatic to elevated fluid pressure; power law creep given by $\dot{\gamma} = A \exp(-Q/[RT])\, \tau^n$, where $\dot{\gamma}$ is strain rate, A is a constant, Q is activation energy, T is absolute temperature, τ is maximum shear stress, and n is the power law stress (values for quartz, feldspar, and olivine used respectively for the upper crust, lower crust, and mantle from Kohlstedt et al., 1995); and dike injection (Buck, 2004). Integrated lithospheric strength (LS) values are listed. Lithosphere is initially thick and strong (stage 1). Early rifting leads to thinned lithosphere with lower strength related to dike intrusion (stage 2). Lithosphere partly regains strength and thickens during stage 3. Renewed dike intrusion, weakening, and necking instabilities leads to final rifting (stage 4).

approach of Kohlstedt et al. (1995), indicates strong lithosphere with an integrated strength of ~40 TN/m (Fig. 15A), similar to values estimated for other cratonic areas, but substantially greater than forces of ~3–5 TN/m thought to be available to drive whole-lithosphere extension (Kusznir and Park, 1987; Lynch and Morgan, 1987; Buck, 2004).

Onset of mantle plume activity and intrusion of dike swarms across parts of Rodinia may have set the stage for initial extension (Li et al., 1999). Igneous activity can substantially decrease strength, with differential stress for through going dikes related to density differences between magma and wallrock (Buck, 2004). Intrusion of the Gunbarrel dikes at ~780 Ma in western Laurentia was followed by development of intracratonic basins. However, early plume activity here does not appear to have resulted in long-term weakening of the lithosphere; rather once dikes solidified stresses needed for continued extension exceeded the available driving force. Intrusion of the Franklin dike swarm at ~720 Ma may have led to more widespread weakening that facilitated onset of regional rifting (Ernst and Bleeker, 2010).

The early rift stage in Utah, Nevada, and SE Idaho involved widespread mafic and felsic igneous activity from 700 to 670 Ma and modest extension (~25–40%) across the western region (stage 2B, Fig, 15B). Lack of distinctly tilted strata is interpreted to reflect overall pure shear extension, similar to model 1, consistent with initially strong lithosphere. Dike intrusion and enhanced plastic flow from increased thermal gradients during thinning likely weakened the lithosphere, with estimated integrated strength dropping to ~5–20 TN/m. Early rifting, however, was incomplete as dikes solidified and weaker lower crust was replaced by stronger uppermost mantle during slow extension. Alternatively, Lund (2008) interpreted Utah, Nevada, and SE Idaho to be in the lower plate of a low-angle detachment, similar to model 2.

The early rift phase was followed by thermal subsidence from ~660 to 580 Ma (stage 3, Fig. 15C). Although the lithosphere in the western region partly cooled, it remained weaker and thinner compared to cratonic lithosphere preserved to the east. Final rifting was associated with renewed mafic volcanism. Compared to early rifting, this final phase operated on lithosphere of moderate thickness and strength. Crustal extension was modest in the western region (~15–35%) and likely partly accommodated by lower crustal flow, with concentrated extension farther west leading to final break up along the $^{87}Sr/^{86}Sr = .706$ line. Concentrated extension may have resulted from necking instabilities as the uppermost mantle thinned and warmed, strain rates increased, and dike intrusion decreased total strength, possibly to <5 TN/m (stage 4, Fig. 15D). Although details have been obscured by younger geologic events, regional stratigraphic relations, DZ patterns, volcanism, and thickness-age data of Neoproterozoic to early Paleozoic rocks across the study region are consistent with protracted rifting that included early extension of initially strong lithosphere (similar to model 1), followed by later extension of partly weakened lithosphere (similar to model 3). Broadly similar histories have been interpreted for other regions, such as the Atlantic and South China passive margins (Mosar et al., 2002; Davis and Kusznir, 2004; Clark et al., 2013; Peron-Pinvidic et al., 2013). The western region and zone along the $^{87}Sr/^{86}Sr = .706$ line are interpreted to correspond respectively to the proximal continental stretching and necking domains of Peron-Pinvidic et al. (2013); the nature of the distal to oceanic domains farther west has been obscured by younger geologic events.

5.4. Implications for Rodinia reconstructions

The geometry and timing of Rodinia rifting continue to be debated (e.g., Li et al., 2008). Various models place different continental blocks on the western margin of Laurentia, including East Antarctica (SWEAT model; Moores, 1991; Dalziel, 1991; Hoffman, 1991), Australia (AUSWUS model; Karlstrom et al., 2001; Burrett and Berry, 2000), South China (Missing-Link model; Li et al., 1995), and Siberia (Sears and Price, 2003). Furthermore, significantly different ages have been proposed for rift timing, with some models showing separation of crustal blocks from western Laurentia prior to 750 Ma (Meert and Torsvik, 2003; Cawood, 2005; Li et al., 2008), whereas stratigraphic relations suggest final rifting and transition to drift at ~550 Ma (Bond et al., 1984; Colpron et al., 2002; this study). Such discrepancies in Rodinia models reflect differing interpretations of limited paleomagnetic data, correlations of basement and cover rocks, and fits of continental margins, each of which has uncertainties. An integrated model with protracted separation of E Antarctica–Australia from W Laurentia is illustrated in Fig. 16, based on published data and new data in this paper as briefly summarized below.

Paleomagnetic data indicate Laurentia was located at low paleo-latitudes and rotated with respect to its current orientation from 780 to 720 Ma, prior to fragmentation of Rodinia (Harlan et al., 1997; Weil et al., 2004, 2006; Denyszyn et al., 2009). Laurentia was also at low paleo-latitudes from 530 to 510 Ma, but may have been at higher latitudes during the Ediacaran (Murthy et al., 1992; Torsvik et al., 1996; Kirschvink et al., 1997). Australia was at low paleo-latitudes from ~800 to 510 Ma, but underwent changes in paleo-declination. Additionally, geologic and paleomagnetic evidence indicate counterclockwise vertical-axis rotation of N Australia relative to S Australia (Giles et al., 2004; Li and Evans, 2011), likely during the 600–530 Ma Petermann orogeny (Raimondo et al., 2010). Paleomagnetic data are lacking for E Antarctica, but it was likely tied to S Australia based on similar geologic histories.

Correlation of basement rocks with 2.0–2.3 Ga Nd model ages, 1.7 Ga metamorphic ages, and 1.4 Ga A-type granitic plutons suggests connection of E Antarctic to SW Laurentia (Goodge et al., 2008). Overlying Neoproterozoic strata in E Antarctica contain abundant Paleoproterozoic and Mesoproterozoic DZ grains, and are associated with 670 Ma volcanic rocks (Goodge et al., 2004), similar to patterns in the west-central U.S. General similarities of Archean cratons bounded by Paleoproterozoic mobile belts and locally overlain by Mesoproterozoic sedimentary basins suggest connection of E Australia to NW Laurentia. Diamictite-bearing strata in SE Australia contain 660 and 580 Ma volcanic rocks (Fanning and Link, 2008; Calver et al., 2013), similar to the patterns along W Laurentia.

Paleo-continental margins have been modified by subsequent deformation and accretion, leading to uncertainties in reconstructions. The Neoproterozoic margin of E Australia is conservatively taken as the boundary between the eastern limit of Precambrian basement, based partly on magnetic signatures, and the Ross-Delamerian orogenic belt that contains deformed Neoproterozoic to earliest Cambrian rift-related strata (Goodge et al., 2004; Foden et al., 2006). The Neoproterozoic margin of W Laurentia is conservatively taken as the current $^{87}Sr/^{86}Sr = .706$ line. However, actual paleo-margins may have been located significantly further outboard, as subsequent contractional orogenesis shifted material inboard. Additionally, rifted continental fragments were subsequently accreted to North America, including: the eastern Klamath terrane that contains 560–580 Ma mafic igneous rocks of the Trinity complex and Ediacaran quartzite with DZ grains likely sourced from Laurentia (Scherer et al., 2010); and the Peninsular and Wrangellia terranes that contain Paleoproterozoic basement (Bacon et al., 2012), Cambrian arc-like rocks with similarities to the Ross-Delamerian belt, and early Paleozoic strata with DZ patterns suggestive of Australian source areas (Gehrels et al., 1996).

Paleomagnetic data and correlation of basement rocks are consistent with connection of E Antarctica–Australia to W Laurentia at ~780–740 Ma (stage 1, Fig. 16A). Paleomagnetic data, with 1σ uncertainties ±5° in paleo-latitude and declination, indicate the paleo-margins of NE Australia to NW Laurentia were separated by a narrow to wide (~500 to >1000 km) gap, depending on how subsequent deformation along the margins is restored. A narrow gap could have been filled with continental fragments, such as the Klamath, Peninsular, and Wrangellia terranes. Alternatively, a wide gap may have been filled by the South China block (Missing Link model; Li et al., 2008). South China drifted northward to middle paleo-latitudes by 720 Ma (Evans

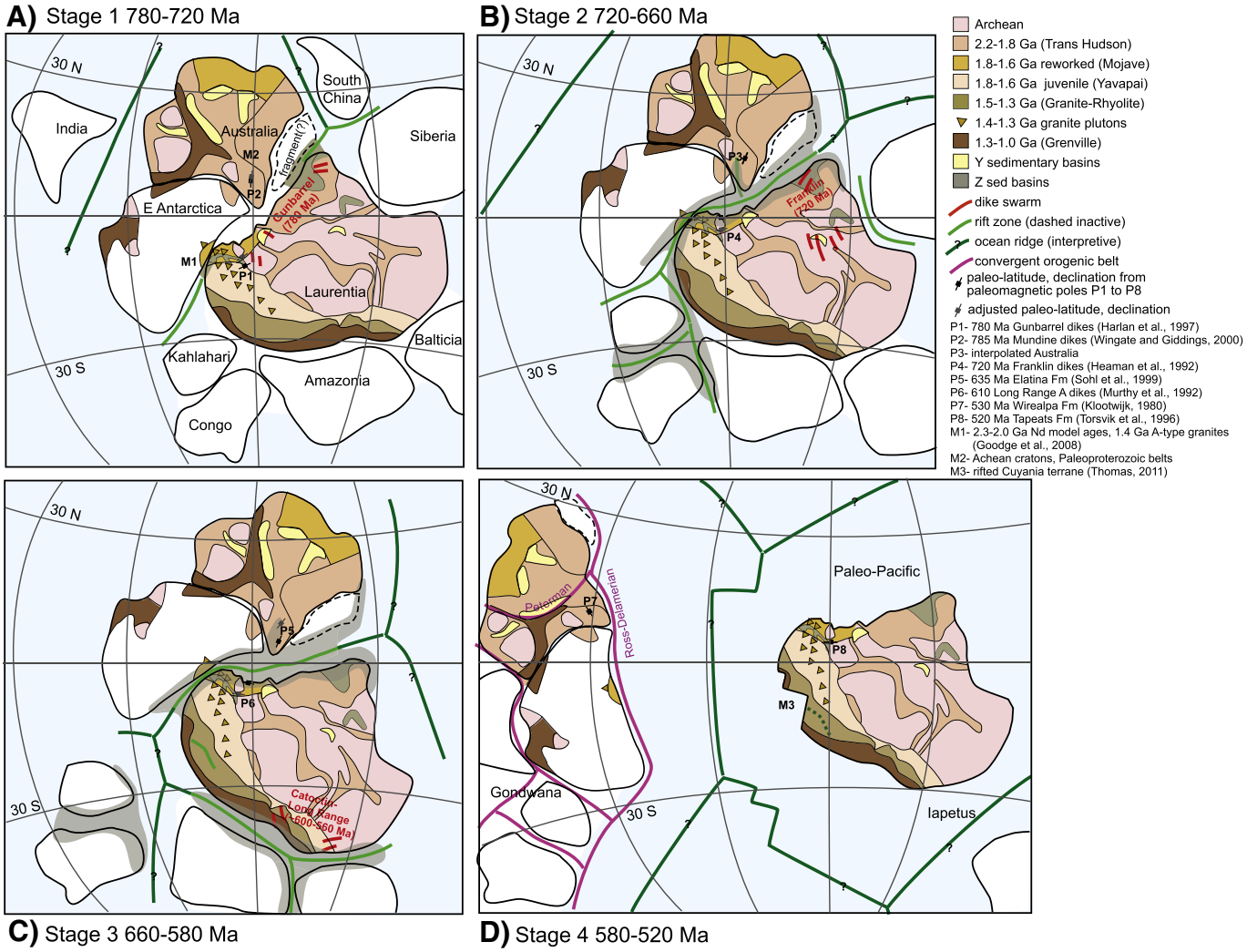

Fig. 16. Plate reconstruction model shows protracted rifting and final separation of Australia-E Antarctica from western Laurentia during stages 1 to 4. Reference paleo-latitudes and declinations for Utah in Laurentia and Adelaide in Australia blocks are indicated for paleomagnetic pole references P1 to P8 (Harlan et al., 1997; Wingate and Giddings, 2000; Heaman et al., 1992; Sohl et al., 1999; Murthy et al., 1992; Torsvik, 1996). Margin fits are based on listed references M1 to M3 (Goodge et al., 2008; Thomas, 2011). Figure constructed with aid of GMAP software of Torsvik (2012).

et al., 2000), whereas Laurentia stayed at low latitudes, which requires early rift timing. However, significant extension and igneous activity along W Laurentia did not begin until after 720 Ma, inconsistent with the Missing Link model, and thus the narrow gap reconstruction is preferred. Neoproterozoic dike swarms, including the 780 ± 1 Ma Gunbarrel and 717 ± 2 Ma Franklin swarms in W Laurentia (Harlan et al., 2003; Macdonald et al., 2010), 827 ± 6 Ma Gairdner, 824 ± 4 Ma Amata, and 755 ± 3 Ma Mundine Well swarms in Australia (Wingate et al., 1998; Wingate and Giddings, 2000), and 820–780 Ma swarms in the South China block likely record plume activity that presaged break up of Rodinia (Li et al., 1999).

Early rifting from ~720 to 660 Ma resulted in development of regional extensional basins along E Antarctica–Australia and W Laurentia (stage 2, Fig. 16B). Limited paleomagnetic data during this time span suggest continued low paleo-latitudes. Correlation of similar age diamictite- and volcanic-bearing stratigraphic sections in E Antarctica, SE Australia, and W Laurentia suggest a connected rift system (Goodge et al., 2004).

Following early, incomplete rifting, thick, mostly marine siliciclastic and minor carbonate strata were deposited during thermal subsidence within an elongate basin system that was wider and deeper along NW Laurentia (stage 3, Fig. 16C). Marinoan (~635 Ma) glacial strata were deposited along parts of the margin (Calver et al., 2013). Localized igneous activity initiated along parts of the Mississippi Valley graben system, E Laurentia, and Baltica (Murthy et al., 1992; Torsvik et al., 1996).

Final rifting and associated volcanism led to final separation and transition to drift from 570–520 Ma with opening of ocean basins between W Laurentia and E Antarctica–Australia, and between E Laurentia, Baltica, and Amazonia (stage 4, Fig. 16D). Thick passive margin strata were deposited along the margins of Laurentia. A complex system of convergent orogenic belts developed along margins of western Australia–E Antarctica, India, Congo, Kahlahari, Amazonia, and other blocks, with continued rapid convergence from ~570 to 500 Ma leading to assemblage of Gondwana (Meert, 2003; Cawood, 2005; Gray et al., 2008) and development of the ~520–500 Ma Ross-Delamarian belt along eastern Australia–E Antarctica (Boger and Miller, 2004).

The interpretive model illustrated in Fig. 16 shows slow rates of plate motion during much of the Neoproterozoic, with development of partly failed rift basins during protracted break up of Rodinia. The paucity of major convergent margins prior to 700 Ma suggests limited sea floor spreading and associated heat loss by mantle convection, which may have been partly compensated by plume activity. Continued rifting and thermal weakening culminated in final break up of Rodinia with development of extensive sea-floor spreading centers, rapid plate motion (typical rates ~15 cm/yr), development of multiple convergent orogenic belts, and eustatic sea level rise, synchronous with major evolutionary

shifts to the biosphere (Torsvik et al., 1996; Dalziel, 1997). Maximum sea level rise is expected to lag behind development of extensive seafloor spreading centers by ~50 m.y., as younger oceanic crust is created and older crust is subducted (Bond et al., 1984), consistent with Late Cambrian to Early Ordovician flooding of much of the Laurentian craton.

5.5. Implications for Snowball Earth model

Multiple models have been proposed to explain the presence of globally distributed Neoproterozoic diamictite-bearing packages, including the Snowball Earth model that predicts long duration, globally synchronous glacial episodes, followed by rapid changes to greenhouse conditions with deposition of cap carbonates (Hoffman and Schrag, 2002; Halverson et al., 2005; Fairchild and Kennedy, 2007; Hoffman, 2011). The ages and extents of glacial episodes, however, remain debated, with Hoffman and Li (2009) proposing that two major intervals of glaciation from 660–720 Ma and 635–650 Ma, referred to respectively as the Sturtian and Marinoan. Along W Laurentia, wide geographic distribution of diamictites, exotic clast compositions, and presence of rare striated clasts and dropstones record two or more glacial episodes (Ojakangas and Matsch, 1980; Christie-Blick, 1983; Macdonald et al., 2010). Within Utah, two diamictite-bearing intervals are interpreted to record two Sturtian glaciation episodes (Fig. 8; Crittenden et al., 1983). The older diamictite contains mostly quartzite clasts, is less extensive, and lacks a cap carbonate. The younger diamictite contains large basement clasts likely delivered via ice sheets that flowed across uplifted rift flanks, and is locally overlain by a cap dolostone with negative $\delta^{13}C$ and distinctive sedimentary structures (Dehler et al., 2011). DZ data from associated volcaniclastic material suggest deposition of the younger diamictite and cap carbonate from ~700 to 670 Ma (Fig. 7), similar to ages of 660 ± 5 Ma for tuffaceous siltstone from the upper part of the type Sturtian section in Australia (Fanning and Link, 2008). The younger diamictite package also contains evidence for locally open marine conditions, supporting a model of dynamic, waxing and waning ice sheets during the Sturtian (Allen and Etienne, 2008; Le Heron et al., 2011). Marinoan glaciation and sea-level fall in Utah to Idaho may be represented by regionally incised valleys near the base of the Inkom Formation, which were infilled by conglomerate (Levy et al., 1994). The apparent lack of Marinoan diamictite here may reflect limited glacial development across subdued topography. However, diamictites and cap carbonates with similar features in other parts of W Laurentia have been interpreted as Marinoan (Prave, 1999; Hoffman, 2011), based on global lithostratigraphic correlations with other diamictite-cap carbonate intervals dated at 635 to 636 Ma in the Namibia, South China, and Australia blocks (Hoffmann et al., 2004; Condon et al., 2005; Calver et al., 2013). Widespread development of early rift basins with deposition of carbonates and carbonaceous mudstones during enhanced weathering and uplift of low-latitude continental fragments may have decreased atmospheric CO_2 and set the stage for Snowball glaciations (Donnadieu et al., 2004). However, glacial ice cover may not have been complete, with low latitude basins, such as along W Laurentia, providing protected areas with locally open waters, as predicted in thin-ice climate models (Pollard and Kasting, 2005). Significant uncertainties remain and additional geochronologic and geochemical data are needed to test models of global to regional glaciations and relations of paleoclimate to Rodinia rifting.

6. Conclusions

1. Neoproterozoic to early Paleozoic sedimentary and volcanic rocks in the west-central U.S. record protracted rifting leading to development of a passive margin. Sedimentologic characteristics and DZ data record changing depositional patterns and contributions from distal sources to local sources along an evolving rift system.
2. Strata are divided into stages related to rift history. Stage 1 strata (Uinta Mountain Group) record initial development of intracratonic basins from ~770–740 Ma. Stage 2 rocks (Perry Canyon, Pocatello, and correlative formations) record early rifting along a N–S basin system from ~720 to 660 Ma, which overlapped with mafic to silicic volcanism and two episodes of glaciation. Variations in sediment thickness and lithology reflect syndepositional faulting. Stage 3 strata (McCoy Creek and lower Brigham groups) record broad subsidence and deposition of mature siliciclastic rocks during lithospheric cooling following early extension. Stage 4 rocks (Prospect Mountain and correlative formations) record later rifting and transition to drift from ~570 to 520 Ma, with volcanism and influx of immature sediments at the base. Extension was concentrated to the west, culminating in a rift to drift transition. Stage 5 carbonate-rich strata were deposited along a passive margin.
3. Sediment thickness-age relations are consistent with two periods of rifting, each followed by thermal subsidence. Estimated crust the mantle lithosphere thinning values within the western region are ~25–40% during early rifting and ~20–35% during final rifting.
4. Pre-rift lithosphere was thick and strong, with minor uplift and weakening related to early dike intrusion. Early rifting was slow and incomplete, likely related to strain hardening and waning igneous activity. Renewed extension, dike intrusion, and thermal weakening during later rifting likely led to necking instabilities, concentrated extension, and final separation.
5. Two diamictite-bearing intervals are interpreted to record older (~715 Ma) and younger (~700–670 Ma) glacial episodes. Locally interstratified conglomerate, wacke, and mudstone in the intervals support a model of episodically open marine conditions and dynamic ice sheets.
6. Available paleomagnetic data, global correlations of basement rocks and Neoproterozoic strata, and fits of paleo-continental margins are consistent with early linkage of E Antarctica–Australia to Laurentia, followed by protracted rifting and final separation.

Supplementary data to this article can be found online at http://dx.doi.org/10.1016/j.earscirev.2014.05.004.

Acknowledgments

Funding was provided by National Science Foundation grants EAR-0819759 (Link) and EAR-0819810 (Yonkee). Constructive reviews by W.V. Priess, Michelle Kominz, and Associate Editor Andre Strasser improved the paper. We are grateful for use of the NSF-supported Arizona LaserChron Center and for help from George Gehrels, Mark Pecha, Clayton Loehn, and Nicky Giesler. Spencer Pantone, Jens Gibbs, Sara Yearsley, and Dave Richey helped with field work. Dave Rodgers shared his knowledge of the Deep Creek Range.

References

Allen, P.A., Etienne, J.L., 2008. Sedimentary challenge to Snowball Earth. Nat. Geosci. 1, 817–825.
Angevine, C., Heller, P., Paola, C., 1990. Quantitative sedimentary basin modeling. American Association of Petroleum Geologists Continuing Education Course Notes #32 (132 pp.).
Armstrong, R.L., 1968. Mantled gneiss domes in the Albion Range, southern Idaho. Geol. Soc. Am. Bull. 79, 1295–1314.
Armstrong, R.L., Taubeneck, W.H., Hales, P.O., 1977. Rb–Sr, K–Ar geochronometry of Mesozoic granitic rocks and their Sr isotopic composition, Oregon, Washington, Idaho. Geol. Soc. Am. Bull. 88, 397–411.
Bacon, C.R., Vazquez, J.A., Wooden, J.L., 2012. Peninsular terrane basement ages recorded by Paleozoic and Paleoproterozoic zircon in gabbro xenoliths and andesite from Redoubt volcano, Alaska. Geol. Soc. Am. Bull. 124, 24–34.
Balgord, E.A., 2011. Stratigraphic, geochronologic and geochemical analysis of the Neoproterozoic Formation of Perry Canyon, northern Utah: Implications for Rodinian rifting and snowball earth. (MS thesis) , Idaho State University, Pocatello, ID.
Balgord, E.A., Yonkee, W.A., Link, P.K., Fanning, C.M., 2013. Stratigraphic, geochronologic, and geochemical record of the Cryogenian Perry Canyon Formation, northern Utah: implications for Rodinian rifting and Snowball Earth glaciation. Geol. Soc. Am. Bull. 125, 1442–1467.
Bennett, C., DePaolo, D.J., 1987. Proterozoic crustal history of the western United States as determined by neodymium isotopic mapping. Geol. Soc. Am. Bull. 99, 674–685.

Bickford, M.E., Van Schmus, W.R., Zietz, I., 1986. Proterozoic history of the midcontinent region of North America. Geology 15, 492–496.
Bickford, M.E., Mueller, P.A., Kamenov, G.D., Hill, B.M., 2008. Crustal evolution of southern Laurentia during the Paleoproterozoic: insights from zircon Hf isotopic studies of ca. 1.75 Ga rocks in central Colorado. Geology 36, 555–558.
Blick, N.H., 1979. Stratigraphic, structural and paleogeographic interpretation of Upper Proterozoic glaciogenic rocks in the Sevier Orogenic belt, Northwestern Utah. (PhD dissertation) , University of California, Santa Barbara.
Boger, S.D., Miller, J. McL, 2004. Terminal suturing of Gondwana and the onset of the Ross-Delamerian orogeny: the cause and effect of an Early Cambrian reconfiguration of plate motions. Earth Planet. Sci. Lett. 219, 35–48.
Bond, G.C., Kominz, M.A., 1984. Construction of tectonic subsidence curves for the early Paleozoic miogeocline, southern Canadian Rocky Mountains: implications for subsidence mechanisms, age of breakup and crustal thinning. Geol. Soc. Am. Bull. 95, 155–173.
Bond, G.C., Nickeson, P.A., Kominz, M.A., 1984. Breakup of a supercontinent between 625 Ma and 555 Ma: new evidence and implications for continental histories. Earth Planet. Sci. Lett. 70, 325–345.
Bond, G.C., Christie-Blick, N., Kominz, M.A., Devlin, W.J., 1985. An early Cambrian rift to post-rift transition in the Cordillera of western North America. Nature 114, 742–745.
Bradley, M.D., Bruhn, R.L., 1988. Structural interactions between the Uinta Arch and the overthrust belt, north-central Utah; implications of strain trajectories and displacement modeling. In: Schmidt, C.J., Perry, W.J. (Eds.), Interaction of the Rocky Mountain Foreland and the Cordilleran thrust belt. Geological Society of America Memoir, 171, pp. 431–445.
Braun, J., Beaumont, C., 1989. A physical explanation of the relation between flank uplifts and the breakup unconformity at rifted continental margins. Geology 17, 760–764.
Bryant, B., 1988. Geology of the Farmington Canyon complex, Wasatch Mountains, Utah. U.S. Geological Survey Professional Paper 1476 (54 pp.).
Buck, W.R., 1991. Modes of continental lithospheric extension. J. Geophys. Res. 96, 20,161–20,178.
Buck, W.R., 2004. Consequences of asthenospheric variability on continental rifting. In: Karner, G.D., Taylor, B., Driscoll, N.W., Kohlstedt, D.L. (Eds.), Rheology and Deformation of the Lithosphere at Continental Margins. Columbia University Press, New York, pp. 1–30.
Buck, W.R., Lavier, L.L., Poliakov, A.N.B., 1999. How to make a rift wide. Philos. Trans. R. Soc. Lond. A 357, 671–693.
Burrett, C., Berry, R., 2000. Proterozoic Australia–Western United States (AUSWUS) fit between Laurentia and Australia. Geology 28, 103–106.
Cabanis, B., Lecolle, M., 1989. Le diagramme La/10-Y/15-Nb/8: Un outfi l pour la discrimination de series volcaniques et la mise en evidence des processus de mélange et/ou de contamination crustale. CR Acad. Sci. Paris 309, 2023–2029.
Calver, C.R., Crowley, J.L., Wingate, M.T.D., Evans, D.A.D., Raub, T.D., Schmitz, M.D., 2013. Globally synchronous Marinoan deglaciation indicated by U–Pb geochronology of the Cottons Breccia, Tasmania, Australia. Geology 41, 1127–1130.
Cawood, P.A., 2005. Terra Australis orogen: Rodinia breakup and development of the Pacific and Iapetus margins of Gondwana during the Neoproterozoic and Paleozoic. Earth-Sci. Rev. 69, 249–279.
Christie-Blick, N., 1982. Upper Proterozoic and Early Cambrian rocks of the Sheeprock Mountains, Utah: regional correlation and significance. Geol. Soc. Am. Bull. 93, 735–750.
Christie-Blick, N., 1983. Glacial-marine and subglacial sedimentation, Upper Proterozoic Mineral Fork Formation, Utah. In: Molnia, B.F. (Ed.), Glacial Marine Sedimentation. Plenum Press, New York, pp. 703–776.
Clark, S.A., Glorstad-Clark, E., Faleide, J.I., Schmid, D., Hartz, E.H., Fjeldskaar, W., 2013. Southwest Barrents Sea rift basin evolution: comparing results from backstripping and time-forward modeling. Basin Res. 25, 1–17.
Cloetingh, S., Spadini, G., Van Wees, J.D., Beekman, F., 2003. Thermo-mechanical modeling of Black Sea Basin deformation. Sediment. Geol. 156, 169–184.
Cochran, J.R., 1983. Effects of finite rifting times on the development of sedimentary basins. Earth Planet. Sci. Lett. 66, 289–302.
Colpron, M., Logan, J.M., Mortensen, J.K., 2002. U–Pb zircon age constraint for late Neoproterozoic rifting and initiation of the lower Paleozoic passive margin of western Laurentia. Can. J. Earth Sci. 39, 133–143.
Compton, R.R., 1972. Geologic map of the Yost Quadrangle, Box Elder County, Utah, and Cassia County, Idaho. U.S. Geological Survey Map I-672, scale 1:31680.
Compton, R.R., Todd, V.R., Zartman, R.E., Naeser, C.W., 1977. Oligocene and Miocene metamorphism, folding, and low-angle faulting in northwestern Utah. Geol. Soc. Am. Bull. 88, 1237–1250.
Condie, K.C., 1967. Petrology of the late Precambrian tillite(?) association in northern Utah. Geol. Soc. Am. Bull. 78, 1317–1343.
Condon, D.J., Bowring, S.A., 2011. A user's guide to Neoproterozoic geochronology. In: Arnaud, E., Halverson, G., Shields, G.A. (Eds.), The Geological Record of Neoproterozoic Glaciations. Geological Society of London Memoir, 36, pp. 135–149.
Condon, D.J., Zhu, M., Bowring, S.A., Wang, W., Yang, A., Jin, Y., 2005. U–Pb ages from the Neoproterozoic Doushantuo Formation, China. Science 308, 95–98.
Corsetti, F.A., Hagadorn, J.W., 2000. Precambrian–Cambrian transition: Death Valley, United States. Geology 28, 299–302.
Corsetti, F.A., Link, P.K., Lorentz, N., 2007. $\delta^{13}C$ chemostratigraphy of the Neoproterozoic succession near Pocatello, Idaho, U.S.A.: implications for glacial chronology and regional correlations. In: Link, P.K., Lewis, R. (Eds.), Proterozoic Geology of Western North America and Siberia. SEPM Special Publication No, 86, pp. 193–205.
Crittenden Jr., M.D., 1972. Willard thrust and the Cache allochthon, Utah. Geol. Soc. Am. Bull. 83, 2871–2880.
Crittenden, M.D., Jr., 1988. Bedrock geologic map of the Promontory Mountains, Box Elder County, Utah. U.S. Geological Survey Open-File Report 88-646, scale 1:100,000.
Crittenden Jr., M.D., Sorensen, M.L., 1980. The Facer Formation, a new early Proterozoic unit in northern Utah. U.S. Geological Survey Bulletin 1482-F.
Crittenden Jr., M.D., Wallace, C.A., 1973. Possible equivalents of the Belt Supergroup in Utah. Belt Symposium Volume 1. Moscow, Idaho, Idaho Bureau of Mines and Geology, pp. 116–138.
Crittenden Jr., M.D., Sharp, B.J., Calkins, F., 1952. Geology of the Wasatch Mountains east of Salt Lake City, Parleys Canyon to Traverse Range. In: Marsell, R.E. (Ed.), Geology of the central Wasatch Mountains. Utah Geological Survey Guidebook, 8, pp. 1–37.
Crittenden Jr., M.D., Schaeffer, F.E., Trimble, D.E., Woodward, L.A., 1971. Nomenclature and correlation of some upper Precambrian and basal Cambrian sequences in western Utah and southeastern Idaho. Geol. Soc. Am. Bull. 82, 581–602.
Crittenden Jr., M.D., Christie-Blick, N., Link, P.K., 1983. Evidence for two pulses of glaciation during the Late Proterozoic in northern Utah and southeastern Idaho. Geol. Soc. Am. Bull. 94, 437–450.
Dalziel, I.W.D., 1991. Pacific margins of Laurentia and East Antarctica–Australia as a conjugate rift pair: evidence and implications for an Eocambrian supercontinent. Geology 19, 598–601.
Dalziel, I.W.D., 1997. Neoproterozoic–Paleozoic geography and tectonics: review, hypothesis, and environmental speculation. Geol. Soc. Am. Bull. 109, 16–42.
Davis, M., Kusznir, N., 2004. Depth-dependent lithospheric stretching at rifted continental margin. In: Karner, G.D., Taylor, B., Driscoll, N.W., Kohlstedt, D.L. (Eds.), Rheology and Deformation of the Lithosphere at Continental Margins. Columbia University Press, New York, pp. 92–137.
DeCelles, P.G., 2004. Late Jurassic to Eocene evolution of the Cordilleran thrust belt and foreland basin system, western U.S.A. Am. J. Sci. 304, 105–168.
DeCelles, P.G., Coogan, J.C., 2006. Regional structure and kinematic history of the Sevier fold-and-thrust belt, central Utah. Geol. Soc. Am. Bull. 118, 841–864.
Dehler, C.M., Elrick, M.E., Karlstrom, K.E., Smith, G.A., Crossey, L.J., Timmons, M.J., 2001. Neoproterozoic Chuar Group (~800–742 Ma), Grand Canyon: a record of cyclic marine deposition during global cooling and supercontinent rifting. Sediment. Geol. 141–142, 465–499.
Dehler, C.M., Fanning, C.M., Link, P.K., Kingsbury, E.M., Rybcynski, D., 2010. Maximum depositional age and provenance of the Uinta Mountain Group and Big Cottonwood Formation, northern Utah: paleogeography of rifting western Laurentia. Geol. Soc. Am. Bull. 122, 1686–1699.
Dehler, C.M., Anderson, K., Nagy, R., 2011. New descriptions of the cap dolostone and associated strata, Neoproterozoic Pocatello Formation, southeastern Idaho, U.S.A. Geol. Soc. Am. Field Guide 21, 181–192.
Dehler, C.D., Yonkee, W.A., Hayes, D., Nagy, R., Link, P.K., Balgord, E., Keeley, J., 2012. The Cryogenian–Ediacaran(?) tectono-stratigraphic, paleoenvironmental, and biologic record of northern Utah and southeastern Idaho. Geological Society of London International Symposium—The Neoproterozoic era, evolution, glaciation and oxygenation, Fermor, vol. 12, pp. 153–154.
Denyszyn, S.W., Davis, D.W., Halls, H.C., 2009. Paleomagnetism and U–Pb geochronology of Franklin dykes in High Arctic Canada and Greenland: a revised age and paleomagnetic pole constraining block rotations in the Nares Strait region. Can. J. Earth Sci. 46, 155–167.
Devlin, W.J., Brueckner, H.K., Bond, G.C., 1988. New isotopic data and a preliminary age for volcanics near the base of the Windermere Supergroup, northeastern Washington, U.S.A. Can. J. Earth Sci. 25, 1906–1911.
Donnadieu, Y., Goddéris, Y., Ramstein, G., Nédélec, A., Meert, J., 2004. A snowball Earth's climate triggered by continental break-up through changes in runoff. Nature 428, 303–306.
Driscoll, N., Karner, G., 1998. Lower crustal extension across the northern Camarvon basin, Australia: evidence for an eastward dipping detachment. J. Geophys. Res. 103, 4975–4990.
Ehlers, T.A., Chan, M.A., 1999. Tidal sedimentology and estuarine deposition of the Proterozoic Big Cottonwood Formation, Utah. J. Sediment. Res. 69, 1169–1180.
Elison, M.W., Speed, R.C., Kistler, R.W., 1990. Geologic and isotopic constraints on the crustal structure of the northern Great Basin. Geol. Soc. Am. Bull. 102, 1077–1092.
Eriksson, K.A., Campbell, I.H., Palin, J.M., Allen, C.M., 2003. Predominance of Grenvillian magmatism recorded in detrital zircons from modern Appalachian rivers. J. Geol. 111, 707–717.
Ernst, R., Bleeker, W., 2010. Large igneous provinces (LIPs), giant dyke swarms, and mantle plumes: significance for breakup events within Canada and adjacent regions from 2.5 Ga to the Present. Can. J. Earth Sci. 47, 695–739.
Evans, D.A.D., 2000. Stratigraphic, geochronological, and paleomagnetic constraints upon the Neoproterozoic climatic paradox. Am. J. Sci. 300, 347–433.
Evans, D.A.D., Li, Z.X., Kirschvink, J.L., Wingate, M.T.D., 2000. A high-quality mid-Neoproterozoic paleomagnetic pole from South China, with implications for ice ages and the breakup configuration of Rodinia. Precambrian Res. 100, 313–334.
Eyles, N., Januszczak, N., 2004. 'Zipper-rift': a tectonic model for Neoproterozoic glaciations during the breakup of Rodinia after 750 Ma. Earth-Sci. Rev. 65, 1–73.
Fairchild, I.J., Kennedy, M.J., 2007. Neoproterozoic glaciation in the Earth System. J. Geol. Soc. Lond. 164, 895–921.
Fan, M., DeCelles, P.G., Gehrels, G.E., Dettman, D.L., Quade, J., Peyton, S.L., 2011. Sedimentology, detrital zircon geochronology, and stable isotope geochemistry of the lower Eocene strata in the Wind River Basin, central Wyoming. Geol. Soc. Am. Bull. 123, 979–996.
Fanning, C.M., Link, P.K., 2004. U–Pb SHRIMP ages of Neoproterozoic (Sturtian) glaciogenic Pocatello Formation, southeastern Idaho. Geology 32, 881–884.
Fanning, C.M., Link, P.K., 2008. Age constraints for the Sturtian Glaciation; data from the Adelaide Geosyncline, South Australia and Pocatello Formation, Idaho, USA. In: Gallagher, S.J., Wallace, M.W. (Eds.), Neoproterozoic extreme climates and the origin of early metazoan life. Geological Society of Australia Extended Abstracts, 91, pp. 57–62.

Farmer, G.L., Ball, T.T., 1997. Sources of middle Proterozoic to Early Cambrian siliciclastic sedimentary rocks in the Great Basin: a Nd isotope study. Geol. Soc. Am. Bull. 109, 1193–1205.
Fedo, C.M., Cooper, J.D., 2001. Sedimentology and sequence stratigraphy of Neoproterozoic and Cambrian units across a craton-margin hinge zone, southeastern California, and implications for the early evolution of the Cordilleran margin. Sediment. Geol. 141–142, 465–499.
Foden, J., Elburg, M.A., Dougherty-Page, J., Burtt, A., 2006. The timing and duration of the Delamerian orogeny: correlation with the Ross orogeny and implications for Gondwana assembly. J. Geol. 114, 189–210.
Foster, D.A., Mueller, P.A., Mogk, D.W., Wooden, J.L., Vogl, J.J., 2006. Proterozoic evolution of the western margin of the Wyoming craton: implications for the tectonic and magmatic evolution of the northern Rocky Mountains. Can. J. Earth Sci. 43, 1601–1619.
Frederiksen, S., Nielsen, S.B., Balling, N., 2001. A numerical dynamic model for the Norwegian–Danish Basin. Tectonophysics 343, 165–183.
Frost, C.D., Fruchey, B.L., Chamberlain, K.R., Frost, B.R., 2006. Archean crustal growth by lateral accretion of juvenile supracrustal belts in the south-central Wyoming Province. Can. J. Earth Sci. 43, 1533–1555.
Gehrels, G.E., Pecha, M., 2014. Detrital zircon U–Pb geochronology and Hf isotope geochemistry of Paleozoic and Triassic strata of western North America. Geosphere 10, 49–65.
Gehrels, G.E., Dickinson, W.R., Ross, G.M., Stewart, J.H., Howell, D.G., 1995. Detrital zircon reference for Cambrian to Triassic miogeoclinal strata of western North America. Geology 23, 831–834.
Gehrels, G.E., Butler, R.F., Bazard, D.R., 1996. Detrital zircon geochronology of the Alexander terrane, southeastern Alaska. Geol. Soc. Am. Bull. 108, 722–734.
Gehrels, G.E., Valencia, V.A., Pullen, A., 2006. Detrital zircon geochronology by laser-ablation multicollector ICPMS at the Arizona LaserChron Center. In: Olszewski, T. (Ed.), Emerging Opportunities, Paleontological Society short course. Paleontological Society Papers, 12.
Gehrels, G.E., Valencia, V.A., Ruiz, J., 2008. Enhanced precision, accuracy, efficiency, and spatial resolution of U–Pb ages by laser ablation-multicollector-inductively coupled plasma-mass spectrometry. Geochem. Geophys. Geosyst. 9, Q03017.
Giles, D., Betts, P.G., Lister, G.S., 2004. 1.8–1.5-Ga links between the North and South Australian cratons and the Early-Middle Proterozoic configuration of Australia. Tectonophysics 380, 27–41.
Glebovitsky, A., Nikitina, L.P., Khiltova, Y.V., Ovchinnikov, N.O., 2004. The thermal regimes of the upper mantle beneath Precambrian and Phanerozoic structures up to the thermobarometry data of mantle xenoliths. Lithos 74, 1–20.
Goddéris, Y., Donnadieu, Y., Nédélec, A., Dupré, B., Dessert, C., Grard, A., Ramstein, G., François, L.M., 2003. The Sturtian 'snowball' glaciation: fire and ice. Earth Planet. Sci. Lett. 211, 1–12.
Goodge, J.W., Williams, I.S., Myrow, P., 2004. Provenance of Neoproterozoic and lower Paleozoic siliciclastic rocks of the central Ross orogeny, Antarctica: detrital record of rift-, passive-, and active-margin sedimentation. Geol. Soc. Am. Bull. 116, 1253–1298.
Goodge, J.W., Vervoort, J.D., Fanning, C.M., Brecke, D.M., Farmer, G.L., Williams, I.S., Myrow, P.M., DePaolo, D.J., 2008. A positive test of East Antarctica–Laurentia juxtaposition within the Rodinia supercontinent. Science 321, 235–240.
Gray, D.R., Foster, D.A., Meert, J.G., Goscombe, B.D., Armstrong, R., Trouw, R.A.J., Passchier, C.W., 2008. A Damara orogen perspective on the assembly of southwestern Gondwana. In: Pankhurst, R.J., Trouw, R.A.J., Brito, A.J., Neves, B.B., De Wit, M.J. (Eds.), West Gondwana: Pre-Cenozoic Correlations across the South Atlantic Region. Geological Society of London Publications, 294, pp. 257–278.
Halverson, G.P., Hoffman, P.F., Schrag, D.P., Maloof, A.C., Rice, A.H.N., 2005. Toward a Neoproterozoic composite carbon-isotope record. Geol. Soc. Am. Bull. 117, 1181–1207.
Hansen, W.R., 1965. Geology of the Flaming Gorge area, Utah–Colorado–Wyoming. U.S. Geological Survey Professional Paper 490. 196 pp.
Hansen, V.L., Goodge, J.W., Keep, M., Oliver, D.H., 1993. Asymmetric rift interpretation of the western North America Margin. Geology 21, 1067–1070.
Haq, B., Schutter, S., 2008. A chronology of Paleozoic sea-level changes. Science 322, 64–68.
Harlan, S.S., Geissman, J.W., Snee, L.W., 1997. Paleomagnetic and $^{40}Ar/^{39}Ar$ geochronologic data from Late Proterozoic mafic dikes and sills, Montana and Wyoming. U.S. Geological Survey Professional Paper 1580 (16 pp.).
Harlan, S.S., Heaman, L.W., LeCheminant, A.N., Premo, W.R., 2003. The Gunbarrel mafic magmatic event: a key 780 Ma time marker for Rodinia plate reconstructions. Geology 31, 1053–1056.
Harper, G.D., Link, P.K., 1986. Geochemistry of Upper Proterozoic rift-related volcanics, northern Utah and southeastern Idaho. Geology 14, 864–867.
Hayes, D.S., 2013. Two Scenes from Utah's Stratigraphic Record: Neoproterozoic Snowball Earth, Before and After. (PhD dissertation) , Utah State University, Logan, UT.
Heaman, L.M., LeCheminant, A.N., Rainbird, R.H., 1992. Nature and timing of Franklin igneous events Canada; implications for a late Proterozoic mantle plume and the break-up of Laurentia. Earth Planet. Sci. Lett. 109, 117–131.
Hintze, L.F., Davis, F.D., 2002. Geologic map of the Wah Wah Mountains North 30′ × 60′ quadrangle and part of the Garrison 30′ × 60′ quadrangle, southwest Millard County and part of Beaver County, Utah. Utah Geological Survey Map 182, scale 1:100,000.
Hintze, L.F., Kowallis, B.J., 2009. Geologic History of Utah. Brigham Young University Geology Studies Special Publication 9.
Hodges, K.A., Walker, J.D., 1992. Extension in the Cretaceous Sevier orogen, North American Cordillera. Geol. Soc. Am. Bull. 104, 560–569.
Hoffman, P.F., 1991. Did the breakout of Laurentia turn Gondwanaland inside out? Science 252, 1409–1412.
Hoffman, P.F., 2011. Strange bedfellows: glacial diamictite and cap carbonate from the Marinoan (635 Ma) glaciation in Namibia. Sedimentology 58, 57–119.
Hoffman, P.F., Li, Z., 2009. A paleogeographic context for Neoproterozoic glaciations. Palaeogeogr. Palaeoclimatol. Palaeoecol. 277, 158–177.
Hoffman, P.F., Schrag, D.P., 2002. The snowball Earth hypothesis: testing the limits of global change. Terra Nova 14, 129–155.
Hoffman, P.F., Kaufman, A.J., Halverson, G.P., Schrag, D.P., 1998. A Neoproterozoic Snowball Earth. Science 281, 1342–1346.
Hoffmann, K.H., Condon, D.J., Bowring, S.A., Crowley, J.L., 2004. U–Pb zircon date from the Neoproterozoic Ghaub Formation Namibia: constraints on Marinoan glaciation. Geology 32, 817–820.
Hogan, E.G., Fedo, C.M., Cooper, J.D., 2011. Reassessment of the basal Sauk supersequence boundary across the Laurentian craton-margin hing zone, southeastern California. J. Geol. 119, 661–685.
Huismans, R.S., Beaumont, C., 2008. Complex rifted continental margins explained by dynamical models of depth-dependent lithospheric extension. Geology 36, 163–166.
Isakson, V.H., 2012. Constraining the origin and evolution of the basement rocks in the Raft-River–Albion–Grouse Creek core complex, northwestern Utah and southern Idaho. (MS thesis) , Washington State University (94 pp.).
Karner, G.D., Driscoll, N.W., McGinnis, J.P., Brumbaugh, W.D., Cameron, N.R., 1997. Tectonic significance of syn-rift sediment packages across the Gabon–Cabinda continental margin. Mar. Pet. Geol. 14, 973–1000.
Karlstrom, K.E., Bowring, S.A., Dehler, C.M., Knoll, A.H., Porter, S.M., Des Marais, D.J., Weil, A.B., Sharp, Z.D., Geissman, J.W., Elrick, M.B., Timmons, J.M., Crossey, L.J., Davidek, K.L., 2000. Chuar Group of the Grand Canyon: record of breakup of Rodinia, associated change in the global carbon cycle, and ecosystem expansion by 740 Ma. Geology 28, 619–622.
Karlstrom, K.E., Ahall, K.-I., Harlan, S.S., 2001. Long lived (1.8–1.0 Ga) convergent orogen in Southern Laurentia, its extensions to Australia and Baltica, and implications for refining Rodinia. Precambrian Res. 111, 5–30.
Keeley, J.A., Link, P.K., Fanning, C.M., Schmitz, M.D., 2013. Pre- to synglacial rift-related volcanism in the Neoproterozoic (Cryogenian) Pocatello Formation, SE Idaho: New SHRIMP and CA-ID-TIMS constraints. Lithosphere 5, 128–150.
Kingsbury-Stewart, E.M., Osterhout, S.L., Link, P.K., Dehler, C.M., 2013. Sequence stratigraphy and formalization of the Middle Uinta Mountain Group (Neoproterozoic), central Uinta Mountains, Utah: a closer look at the western Laurentian Seaway at ca. 750 Ma. Precambrian Res. 236, 65–84.
Kirschvink, J.L., 1992. Late Proterozoic low-latitude global glaciation: the snowball earth. In: Klein, C., Schopf, J.W. (Eds.), The Proterozoic Biosphere. Cambridge University Press, pp. 51–52.
Kirschvink, J.L., Ripperdan, R.L., Evans, D.A., 1997. Evidence for a large-scale reorganization of Early Cambrian continental masses by inertial interchange true polar wander. Science 277, 541–545.
Knoll, A.H., Blick, N., Awramik, S.M., 1981. Stratigraphic and ecologic implications of late Precambrian microfossils from Utah. Am. J. Sci. 281, 247–263.
Kohlstedt, D.L., Evans, B., Mackwell, S.J., 1995. Strength of the lithosphere: constraints imposed by laboratory experiments. J. Geophys. Res. 100, 17,587–17,602.
Kusznir, N.J., Park, R.G., 1987. Extensional strength of continental lithosphere. In: Coward, M.P., Dewey, J.F., Hancock, P.L. (Eds.), Continental Extensional Tectonics. Geological Society Special Publication, No. 28, pp. 35–52.
Le Heron, D.P., Cox, G., Trundley, A., Collins, A.S., 2011. Two Cryogenian glacial successions compared: aspects of the Sturt and Elatina sediment record of South Australia. Precambrian Res. 186, 147–168.
Levy, M., Christie-Blick, N., 1991. Tectonic subsidence of the early Paleozoic passive continental margin in eastern California and southern Nevada. Geol. Soc. Am. Bull. 103, 1590–1606.
Levy, M., Christie-Blick, N., Link, P.K., 1994. Neoproterozoic incised valleys of the eastern Great Basin, Utah and Idaho: fluvial response to changes in depositional base level. In: Dalrymple, R.W., Boyd, R., Zaitlin, B.A. (Eds.), Incised valley systems: Origin and sedimentary sequences. Society for Sedimentary Geology Special Publication, 51, pp. 369–382.
Li, Z.X., Evans, D.A.D., 2011. Late Neoproterozoic 40° intraplate rotation within Australia allows for a tighter-fitting and longer-lasting Rodinia. Geology 39, 39–42.
Li, Z.X., Zhang, L., Powell, C.M., 1995. South China in Rodinia: part of the missing link between Australia–East Antarctica and Laurentia? Geology 23, 407–410.
Li, Z.X., Li, X.H., Kinny, P.D., Wang, J., 1999. The breakup of Rodinia: did it start with a mantle plume beneath South China? Earth Planet. Sci. Lett. 173, 171–181.
Li, Z.X., Li, X.H., Kinny, P.D., Wang, J., Zhang, S., Zhou, H., 2003. Geochronology of Neoproterozoic syn-rift magmatism in the Yangtze craton South China and correlations with other continents: evidence for a mantle superplume that broke up Rodinia. Precambrian Res. 122, 85–109.
Li, Z.X., Bogdanova, S.V., Collins, A.S., Davidson, A., DeWaele, B., Ernst, R.E., Fitzsimons, I.C.W., Fuck, R.A., Gladkochub, D.P., Jacobs, J., Karlstrom, K.E., Lu, S., Natapov, L.M., Pease, V., Pisarevsky, S.A., Thrane, K., Vernikovsky, V., 2008. Assembly, configuration, and break-up history of Rodinia: a synthesis. Precambrian Res. 160, 179–210.
Linde, G.M., Cashman, P.H., Dickinson, W.R., Trexler, J.H. Jr, 2012. Provenance implications of new U–Pb detrital zircon data from Cambrian passive margin strata of northern Nevada. Geological Society of America Abstracts with Programs 44, no. 7, p. 379.
Link, P.K., 1982. Geology of the upper Proterozoic Pocatello Formation, Bannock Range, southeastern Idaho. (Ph. D. thesis) , University of California Santa Barbara, Santa Barbara, CA.
Link, P.K., 1987. The Late Proterozoic Pocatello Formation; A record of continental rifting and glacial marine sedimentation, Portneuf Narrows, southeastern Idaho. Geological Society of America Field Guide, 1987 Rocky Mountain Section, pp. 139–142.
Link, P.K., Christie-Blick, N., 2011. Neoproterozoic strata of southeastern Idaho and Utah: record of Cryogenian rifting and glaciation. In: Arnaud, E., Halverson, G., Shields, G.A. (Eds.), The Geological Record of Neoproterozoic Glaciations. Geological Society of London Memoir, 36, pp. 425–436.

Link, P.K., Jansen, S.T., Halimdihardja, P., Lande, A., Zahn, P., 1987. Stratigraphy of the Brigham Group (Late Proterozoic–Cambrian), Bannock, Portneuf, and Bear River Ranges, southeastern Idaho. Thirty-eighth Field Conference, Wyoming Geological Association Guidebook, pp. 133–148.
Link, P.K., Christie-Blick, N., Devlin, W.J., Elston, D.P., Horodyski, R.J., Levy, M., Miller, J.M.G., Pearson, R.C., Prave, A., Stewart, J.H., Winston, D., Wright, L.A., Wrucke, C.T., 1993. Middle and Late Proterozoic stratified rocks of the western U.S. Cordillera, Colorado Plateau, and Basin and Range province. In: Reed, J.C., Bickford, M.E., Houston, R.S., Link, P.K., Rankin, D.W., Sims, P.K., Van Schmus, W.R. (Eds.), The Geology of North America. Precambrian: Conterminous U.S. Geological Society of America, vol. C-2, pp. 463–595.
Link, P.K., Fanning, C.M., Lund, K.L., Aleinikoff, J.N., 2007. Detrital zircon populations and provenance of Mesoproterozoic strata of east-central idaho, U.S.A.: correlation with Belt Supergroup of southwest Montana. Society for Sedimentary Geology Special Publication 86, pp. 101–128.
Lister, G.S., Etheridge, M.A., Symonds, P.A., 1986. Detachment faulting and the evolution of passive continental margins. Geology 14, 246–250.
Livaccari, R.F., Perry, F.V., 1993. Isotopic evidence for preservation of Cordilleran lithospheric mantle during the Sevier-Laramide orogeny, western United States. Geology 21, 719–722.
Lorentz, N.L., Corsetti, F.A., Link, P.K., 2004. Seafloor precipitates and C-isotope stratigraphy from the Neoproterozoic Scout Mountain Member of the Pocatello Formation, southeast Idaho: implications for Neoproterozoic earth system behavior. Precambrian Res. 130, 57–70.
Ludwig, K.R., 2008. Isoplot 3.60. Berkeley Geochronology Center, Special, Publication No. 4.
Lund, K., 2008. Geometry of the Neoproterozoic and Paleozoic rift margin of western Laurentia: implications for mineral deposit settings. Geosphere 4, 429–449.
Lund, K., Aleinikoff, J.N., Evans, K.V., Fanning, C.M., 2003. SHRIMP U–Pb geochronology of Neoproterozoic Windermere Supergroup, central Idaho; implications for rifting of western Laurentia and synchroneity of Sturtian glacial deposits. Geol. Soc. Am. Bull. 115, 349–372.
Lund, K., Aleinikoff, J., Evans, K., Dewitt, E., Unruh, D., 2010. SHRIMP U–Pb dating of recurrent Cryogenian and Late Cambrian–Early Ordovician alkalic magmatism in central Idaho: Implications for Rodinian rift tectonics. Geol. Soc. Am. Bull. 122, 430–453.
Lynch, H.D., Morgan, P., 1987. Tensile strength of the lithosphere. In: Coward, M.P., Dewey, J.F., Hancock, P.L. (Eds.), Continental Extensional Tectonics. Geological Society Special Publication, 28, pp. 53–65.
Macdonald, F.A., Schmitz, M.D., Crowley, J.L., Roots, C.F., Jones, D.S., Maloof, A.C., Strauss, J.V., Cohen, P.A., Johnston, D.T., Schrag, D.P., 2010. Calibrating the Cryogenian. Science 327, 1241–1243.
Macdonald, F.A., Prave, A.R., Petterson, R., Smith, E.F., Pruss, S.B., Oates, K., Waechter, F., Trotzuk, D., Fallick, A.E., 2013. The Laurentian record of Neoproterozoic glaciation, tectonism, and eukaryotic evolution in Death Valley, California. Geol. Soc. Am. Bull. 125, 1203–1223.
Mahon, R.C., Dehler, C.M., Link, P.K., Karlstrom, K.E., Gehrels, G.E., 2014. Geochronologic and stratigraphic constraints on the Mesoproterozoic and Neoproterozoic Pahrump Group, Death Valley, California: a record of the assembly, stability and breakup of Rodinia. Geol. Soc. Am. Bull 126, 652–664.
McKenzie, D., 1978. Some remarks on the development of sedimentary basins. Earth Planet. Sci. Lett. 49, 25–32.
Meert, J.G., 2003. A synopsis of events related to the assembly of eastern Gondwana. Tectonophysics 362, 1–40.
Meert, J.G., Torsvik, T.H., 2003. The making and unmaking of a supercontinent: Rodinia revisited. Tectonophysics 375, 261–288.
Miller, D.M., 1983. Allochthonous quartzite sequence in the Albion Mountains, Idaho, and proposed Proterozoic Z and Cambrian correlatives in the Pilot Range, Utah and Nevada. In: Miller, D.M., Todd, V.R., Howard, K.A. (Eds.), Tectonic and Stratigraphic Studies in the Eastern Great Basin. Geological Society of America Memoir, 157, pp. 191–213.
Misch, P., Hazzard, J.C., 1962. Stratigraphy and metamorphism of late Precambrian rocks in central northeastern Nevada and adjacent Utah. AAPG Bull. 46, 289–343.
Moores, E.M., 1991. Southwest U.S.–East Antarctic (SWEAT) connection: a hypothesis. Geology 19, 425–428.
Mosar, J., Eide, A.E., Osmundsen, P.T., Sommarugo, A., Torsvik, T.H., 2002. Greenland–Norway separation: a geodynamic model for the North Atlantic. Nor. J. Geol. 82, 281–298.
Mueller, P.A., Frost, C.D., 2006. The Wyoming Province: a distinctive Archean craton in Laurentian North America. Can. J. Earth Sci. 43, 1319–1397.
Mueller, P.A., Heatherington, A.C., Kelly, D.M., Wooden, J.L., Mogk, D.W., 2002. Paleoproterozoic crust within the Great Falls tectonic zone: implications for the assembly of southern Laurentia. Geology 30, 127–130.
Mueller, P.A., Burger, H., Wooden, J.L., Brady, J., Cheney, J., Harms, T., Heatherington, A.C., Mogk, D.W., 2005. Age and tectonic implications of Paleoproterozoic metamorphism in the northern Wyoming Province. J. Geol. 113, 169–179.
Mueller, P.A., Wooden, J.L., Mogk, D.W., Foster, D.A., 2011. Paleoproterozoic evolution of the Farmington zone: implications for terrane accretion in southwestern Laurentia. Lithosphere 3, 401–408.
Mukul, M., Mitra, G., 1998. Finite strain and strain variation analysis in the Sheeprock thrust sheet: an internal thrust sheet in the Provo salient of the Sevier fold-and-thrust belt, central Utah. J. Struct. Geol. 20, 385–405.
Murthy, G., Tubrett, G.M., Patcold, R., 1992. Paleomagnetism of Eocambrian Long Range dykes and Double Mer Formation from Labrador, Canada. Can. J. Earth Sci. 29, 1224–1234.
Nelson, S.T., Hart, G.L., Frost, C.D., 2011. A reassessment of Mojavia and new Cheyenne Belt alignment in the eastern Great Basin. Geosphere 7, 513–527.
Obrebski, M., Allen, R.M., Pollitz, F., Hung, S.H., 2011. Lithosphere–asthenosphere interaction beneath the western United States from the joint inversion of body-wave travel times and surface-wave phase velocities. Geophys. J. Int. 185, 1003–1021.
Ojakangas, R.W., Matsch, C.L., 1980. Upper Precambrian (Eocambrian) Mineral Fork Tillite of Utah: a continental glacial and glaciomarine sequence. Geol. Soc. Am. Bull. 91, 495–501.
Oldow, J.S., Bally, A.W., Ave Lallemant, H.G., Leeman, W.P., 1989. Phanerozoic evolution of the North American Cordillera, United States and Canada. In: Bally, A.W., Palmer, A.R. (Eds.), The Geology of North America—An overview, Geological Society of America, The Geology of North America A, pp. 139–232.
Pearce, J.A., Cann, J.R., 1973. Tectonic setting of basic volcanic rocks determined using trace element analyses. Earth Planet. Sci. Lett. 19, 290–300.
Pearce, J.A., Norry, M.J., 1979. Petrogenetic implications of Ti, Zr, Y, and Nb variations in volcanic rocks. Contrib. Mineral. Petrol. 69, 33–47.
Peron-Pinvidic, G., Manatschal, G., Osmundsen, P.T., 2013. Structural comparison of archetypal Atlantic rifted margins: a review of observations and concepts. Mar. Pet. Geol. 43, 21–47.
Peterson, D.O., Clarke, D.L., 1974. Trace fossils *Plagiogmus* and *Skolithus* in the Tintic Quartzite of Utah. J. Paleontol. 48, 766–768.
Petterson, R., Prave, A.R., Wernicke, B.P., Fallick, A.E., 2011. The Neoproterozoic Noonday Formation, Death Valley region, California. Geol. Soc. Am. Bull. 123, 1317–1330.
Peyton, S.L., Reiners, P.W., Carrapa, B., DeCelles, P.G., 2012. Low-temperature thermochronology of the northern Rocky Mountains, Western U.S.A. Am. J. Sci. 312, 145–212.
Pollard, D., Kasting, J.F., 2005. Snowball Earth: a thin-ice solution with flowing sea glaciers. J. Geophys. Res. 110, C07010.
Poole, F.G., Steward, J.H., Palmer, A.R., Sandberg, C.A., Madrid, R.J., Ross, R.J., Hintze, L.F., Miller, D.M., Wrucke, C.T., 1992. Latest Precambrian to latest Devonian time, development of a continental margin. In: Burchfiel, B.C., Lipman, P.W., Zoback, M.L. (Eds.), The Cordilleran orogen Conterminous U.S., Geological Society of America, The Geology of North America G-3, pp. 9–56.
Prave, A.R., 1999. Two diamictites, two cap carbonates, two δ13C excursions, two rifts: the Neoproterozoic Kingston Peak Formation, Death Valley, California. Geology 27, 339–342.
Raimondo, T., Collins, A.S., Hand, M., Walker-Hallam, A., Smithies, R.H., Evins, P.M., Howard, H.M., 2010. The anatomy of a deep intracratonal orogeny. Tectonics TC4024.
Rainbird, R.H., Jefferson, C.W., Young, G.M., 1996. The early Neoproterozoic sedimentary Succession B of northwestern Laurentia: correlations and paleogeographic significance. Geol. Soc. Am. Bull. 108, 454–470.
Rainbird, R.H., Cawood, P., Gehrels, G., 2012. The great Grenvillian sedimentation episode: record of supercontinent Rodinia's assembly. In: Busby, C., Azor, A. (Eds.), Tectonics of Sedimentary Basins: Recent Advances. Wiley, Ch, p. 29.
Rigo, R.J., 1968. Middle and Upper Cambrian Stratigraphy in the Autochthon and Allochthon of Northern Utah. 15, Brigham Young University Geology Studies pp. 31–66 (part 1).
Rodgers, D., 1984. Stratigraphy, correlation, and depositional environments of Upper Proterozoic and Lower Cambrian rocks of the southern Deep Creek Range, Utah. Geology of Northwest Utah, Southern Idaho and Northeast Nevada, Utah Geological Association Guidebook, pp. 79–92.
Rooney, A.D., Macdonald, F.A., Strauss, J.V., Dudas, F.O., Hallmann, C., Selby, D., 2014. Re–Os geochronology and coupled Os–Sr isotope constraints on the Sturtian snowball Earth. Proc. Natl. Acad. Sci. 111, 51–56.
Ross, G.M., 1991. Tectonic setting of the Windermere Supergroup revisited. Geology 19, 1125–1128.
Ross, G.M., Bloch, J.D., Krouse, H.R., 1995. Neoproterozoic strata of the southern Canadian Cordillera and the isotopic evolution of seawater sulfate. Precambrian Res. 78, 70–99.
Rowell, A.J., Rees, M.N., Suczek, C.A., 1979. Margin of the North America continent in Nevada during Late Cambrian time. Am. J. Sci. 279, 1–18.
Royden, L., Keen, C.E., 1980. Rifting process and thermal evolution of the continental margin of eastern Canada determined from subsidence curves. Earth Planet. Sci. Lett. 51, 343–361.
Royse, F., 1993. An overview of the geologic structure of the thrust belt in Wyoming, northern Utah, and eastern Idaho. In: Snoke, A.W., Steidtmann, J.R., Roberts, S.M. (Eds.), Geology of Wyoming. Geological Survey of Wyoming Memoir, 5, pp. 272–311.
Scherer, H.H., Ernst, W.G., Wooden, J.L., 2010. Regional detrital zircon provenance of exotic metasandstone blocks, eastern Hayfork terrane, western Paleozoic and Triassic belt, Klamat Mountains, California. J. Geol. 118, 641–653.
Schmandt, B., Humphreys, E., 2010. Complex subduction and small-scale convection revealed by body-wave tomography of the western United States upper mantle. Earth Planet. Sci. Lett. 297, 435–445.
Sears, J.W., Price, R.A., 2003. Tightening the Siberian connection to western Laurentia. Geol. Soc. Am. Bull. 115, 943–953.
Shufeldt, O.P., Karlstrom, K.E., Gehrels, G.E., Howard, E., 2010. Archean detrital zircons in the Proterozoic Vishnu Schist of the Grand Canyon, Arizona: implications for crustal architecture and Nuna supercontinent reconstructions. Geology 38, 1099–1102.
Smith, L.H., Kaufman, A.J., Knoll, A.H., Link, P.K., 1994. Chemostratigraphy of predominantly siliciclastic Neoproterozoic successions: a case study of the Pocatello Formation and lower Brigham Group, Idaho, USA. Geol. Mag. 131, 301–314.
Sohl, L.E., Christie-Blick, N., Kent, D.V., 1999. Paleomagnetic polarity reversals in Marinoan (ca 600 Ma) glacial deposits of Australia: implications for the duration of low-latitude glaciation in Neoproterozoic time. Geol. Soc. Am. Bull. 111, 1120–1139.
Sorensen, M.L., Crittenden, M.D., Jr., 1979. Geologic map of the Huntsville quadrangle, Weber and Cache counties, Utah. U.S. Geological Survey Map GQ-1503, scale 1:24,000.
Stewart, J.H., 1972. Initial deposits of the Cordilleran geosyncline: evidence of a late Precambrian (<850 m.y.) continental separation. Geol. Soc. Am. Bull. 83, 1345–1360.

Stewart, J.H., 1991. Latest Proterozoic and Cambrian rocks of the western United States—An overview. In: Cooper, J.D., Stevens, C.H. (Eds.), Paleozoic paleogeography of the western United States-II, volume 1. Los Angeles, Pacific Section, Society of Economic Paleontologists and Mineralogists, Book 67, pp. 13–38.
Stewart, J.H., Gehrels, G.E., Barth, A.P., Link, P.K., Christie-Blick, N., Wrucke, C.T., 2001. Detrital zircon provenance of Mesoproterozoic to Cambrian arenites in the western United States and northwestern Mexico. Geol. Soc. Am. Bull. 113, 1343–1356.
Strickland, A., Miller, E.L., Wooden, J.L., 2011. The timing of Tertiary metamorphism and deformation in the Albion–Raft River–Grouse Creek metamorphic core complex, Utah and Idaho. J. Geol. 119, 185–206.
Thomas, W.A., 2011. The Iapetan rifted margin of southern Laurentia. Geosphere 7, 97–120.
Todt, M.K., Link, P.K., 2013. Sedimentary provenance of the Upper Cambrian Worm Creek Quartzite, Idaho, using U–Pb and Lu–Hf Isotopic analysis of zircon grains. Northwest Geol. 42, 293–298.
Torsvik, T.H., 2012. GMAP 2012. Web site http://www.earthdynamics.org/Bugs/whnjs.htm.
Torsvik, T.H., Smethurst, M.A., Meert, J.G., Van der Voo, R., McKerrow, W.S., Brasier, M.D., Sturt, B.A., Walderhaug, H.J., 1996. Continental break-up and collision in the Neoproterozoic and Paleozoic—a tale of Baltica and Laurentia. Earth-Sci. Rev. 40, 229–258.
Weil, A.B., Geissman, J., Van der Voo, R., 2004. Paleomagnetism of the Neoproterozoic Chuar Group, Grand Canyon Supergroup, Arizona: implications for Laurentia's Neoproterozoic APWP and Rodinia break-up. Precambrian Res. 129, 71–92.
Weil, A.B., Geissman, J., Ashby, J.M., 2006. A new paleomagnetic pole for the Neoproterozoic Uinta Mountain supergroup, Central Rocky Mountain States, USA. Precambrian Res. 147, 234–359.
Wells, M.L., 1997. Alternating contraction and extension in the hinterlands of orogenic belts: an example from the Raft River Mountains, Utah. Geol. Soc. Am. Bull. 109, 107–126.
Wells, M.L., Hoisch, T.D., Peters, M.T., Miller, D.M., Wolff, E.D., Hanson, L.M., 1998. The Mahogany Peaks fault, a Late Cretaceous-Paleocene(?) normal fault in the hinterland of the Sevier orogen. J. Geol. 106, 623–634.
White, R., McKenzie, D., 1989. Magmatism at rift zones: the generation of volcanic continental margins and flood basalt. J. Geophys. Res. 94, 7685–7729.
Whitmeyer, S.J., Karlstrom, K.E., 2007. Tectonic model for the Proterozoic growth of North America. Geosphere 3, 220–259.
Williams, I.S., 1998. U–Th–Pb geochronology by ion microprobe. In: McKibben, M.A., Shanks, W.C., Ridley, W.I. (Eds.), Applications of Microanalytical Techniques to Understanding Mineralizing Processes. Reviews in Economic Geology, 7, pp. 1–35.
Wingate, M.T.D., Giddings, J.W., 2000. Age and paleomagnetism of the Mundine Well dyke swarm, Western Australia: implications for an Australia–Laurentia connection at 755 Ma. Precambrian Res. 100, 335–357.
Wingate, M.T.D., Campbell, I.H., Compston, W., Gibson, G.M., 1998. Ion microprobe U–Pb ages for Neoproterozoic-basaltic magmatism in south-central Australia and implications for the breakup of Rodinia. Precambrian Res. 87 (1), 35–159.
Woodward, L.A., 1963. Late Precambrian metasedimentary rocks of Eagan Range, Nevada. AAPG Bull. 47, 814–822.
Woodward, L.A., 1967. Stratigraphy and correlation of late Precambrian rocks of Pilot Range, Elko County, Nevada, and Box Elder County, Utah. AAPG Bull. 51, 235–243.
Yonkee, W.A., 2005. Strain patterns within part of the Willard thrust sheet, Idaho–Utah–Wyoming thrust belt. J. Struct. Geol. 27, 1315–1343.
Yonkee, W.A., Willis, G.C., Doelling, H.H., 2000. Proterozoic and Cambrian sedimentary and low-grade metasedimentary rocks on Antelope Island, Utah. In: King, J.K., Willis, G.C. (Eds.), The Geology of Antelope Island. Davis County, Utah, Utah Geological Survey Miscellaneous Publication, 2000-1, pp. 37–47.
Yonkee, W.A., Czeck, D.M., Nachbor, A.C., Barszewski, C., Pantone, S., Balgord, E.A., Johnson, K.R., 2013. Strain accumulation and fluid–rock interaction in a naturally deformed diamictite, Willard thrust system, Utah (USA): implications for crustal rheology and strain softening. J. Struct. Geol. 50, 91–118.
Young, C.M., 2002. Geochemical investigation of a Neoproterozoic glacial unit: the Mineral Fork Formation in the Wasatch Range, Utah. Geol. Soc. Am. Bull. 114, 387–399.